



HAL
open science

How specific classes of retinal cells contribute to vision: a computational model

Evgenia Kartsaki

► **To cite this version:**

Evgenia Kartsaki. How specific classes of retinal cells contribute to vision: a computational model. Bioinformatics [q-bio.QM]. Université Côte d'Azur, Inria, France; Newcastle University, 2022. English. NNT: . tel-03869570v1

HAL Id: tel-03869570

<https://inria.hal.science/tel-03869570v1>

Submitted on 31 May 2022 (v1), last revised 24 Nov 2022 (v3)

HAL is a multi-disciplinary open access archive for the deposit and dissemination of scientific research documents, whether they are published or not. The documents may come from teaching and research institutions in France or abroad, or from public or private research centers.

L'archive ouverte pluridisciplinaire **HAL**, est destinée au dépôt et à la diffusion de documents scientifiques de niveau recherche, publiés ou non, émanant des établissements d'enseignement et de recherche français ou étrangers, des laboratoires publics ou privés.

THÈSE DE DOCTORAT

Comment des classes spécifiques de
cellules rétiniennes contribuent à la vision:
un modèle computationnel

Evgenia KARTSAKI

INRIA Sophia Antipolis

**Présentée en vue de l'obtention
du grade de docteur en Informatique
d'Université Côte d'Azur
et d'Université de Newcastle**

Dirigée par : Bruno Cessac / Evelyne Sernagor
/ Gerrit Hilgen

Soutenue le : 17/03/2022

Devant le jury, composé de :

Mathieu Desroches, Chargé de recherche,
Université Côte d'Azur, Inria
Matthias Hennig, Reader, University of
Edinburgh

Anya Hurlbert, Professeure, Newcastle
University

Olivier Marre, Directeur de recherche, INSERM

DOCTORAL THESIS

How specific classes of retinal cells contribute to vision: a computational model

Evgenia KARTSAKI

INRIA Sophia Antipolis

**Presented in fulfilment of the requirements
for the degree of Doctor of Philosophy in the
Biosciences Institute, Faculty of Medical
Sciences, Newcastle University and the
University of Côte d'Azur**

Supervised by : Bruno Cessac / Evelyne
Sernagor / Gerrit Hilgen

Submitted : 12/2021

Defended on : 17/03/2022

In front of the jury, composed of :

Mathieu Desroches, Associate Research
Professor, Université Côte d'Azur, Inria
Matthias Hennig, Reader, University of
Edinburgh

Anya Hurlbert, Professor, Newcastle University
Olivier Marre, Research Director, INSERM

Comment des classes spécifiques de cellules rétiniennes contribuent à la vision: un modèle computationnel

Jury :

Président du jury

Olivier Marre, Directeur de recherche, INSERM

Rapporteurs

Matthias Hennig, Reader, University of Edinburgh

Anya Hurlbert, Professeure, Newcastle University

Examineurs

Mathieu Desroches, Chargé de recherche, Université Côte d'Azur, Inria

Olivier Marre, Directeur de recherche, INSERM

'The real challenge of human biology, beyond the task of finding out how genes orchestrate the construction and maintenance of the miraculous mechanism of our bodies, will lie ahead as we seek to explain how our minds have come to organise thoughts sufficiently well to investigate our own existence.'

J.C. Venter

Abstract

The human brain can recreate images by combining parallel streams of information emitted by about one million retinal ganglion cells (RGCs). RGCs exhibit an astonishing functional, anatomical, and molecular diversity and their preference for particular features of the visual scene (contrast, motion, etc.) can be attributed to synaptic connectivity patterns from upstream retinal circuits as well as intrinsic characteristics (such as gene expression, morphological features, membrane properties). However, how these different attributes give rise to distinct functional groups is still largely unknown. In this thesis, we investigated the functional properties of specific RGCs subgroups, sharing gene expression, by applying experimental and theoretical approaches to control their neuronal activity using pharmacogenetics. We hypothesised that modifying their activity may not only affect their individual response but also their concerted activity, thereby elucidating their role in population encoding of visual scenes.

To explore this hypothesis, we worked on three main axes:

1. General response characterisation of RGCs in control condition and when their activity is altered through pharmacogenetics.
2. Development of a mathematical model, constrained by empirical data, to unravel the circuit wiring underlying functional diversity.
3. Large-scale simulations of the model on Macular, a novel simulation platform, to explore retinal behaviour to complex stimuli.

In this context, we analysed light responses recorded from mouse RGCs and we identified distinct cell types that respond in diverse patterns when their activity is pharmacologically modified. We hypothesised that these various response patterns may arise from lateral interactions between the different RGC types. We tested this hypothesis by means of model definition, mathematical analysis, and numerical simulations and illustrated the role of connectivity patterns in the behaviour of the system. Taken together, our work suggests possible physiological mechanisms underlying the variability of RGCs responses with an emphasis on the role of lateral connectivity on the retinal response.

Keywords : Retina, modelling, simulations, connectivity.

Résumé

Le cerveau humain peut recréer des images en combinant des flux parallèles d'informations émis par environ un million de cellules ganglionnaires rétiniennes (RGCs). Les RGCs présentent une étonnante diversité fonctionnelle, anatomique et moléculaire et leurs préférences pour des caractéristiques particulières d'une scène visuelle (contraste, mouvement, etc.) peuvent être attribuées aux modèles de connectivité synaptique des circuits rétiniens amont ainsi que des caractéristiques intrinsèques (telles que l'expression des gènes, les caractéristiques morphologiques, les propriétés membranaires). Cependant, la manière dont ces différents attributs donnent naissance à des groupes fonctionnels distincts est encore largement inconnue. Dans cette thèse, nous avons étudié les propriétés fonctionnelles de sous-groupes spécifiques de RGCs, partageant l'expression de certains gènes, en appliquant des approches expérimentales et théoriques pour contrôler leur activité neuronale en utilisant la pharmacogénétique. Nous avons émis l'hypothèse que la modification de leur activité peut non seulement affecter leur réponse mais aussi leur activité collective, soulignant ainsi leur rôle dans le codage de scènes visuelles effectué au niveau de populations neuronales.

Pour explorer cette hypothèse, nous avons travaillé sur trois axes principaux :

1. Caractérisation générale de la réponse des RGCs en condition de contrôle et lorsque leur activité est altérée par la pharmacogénétique.
2. Développement d'un modèle mathématique, contraint par des données empiriques, pour explorer la structure des circuits sous-tendant la diversité fonctionnelle.
3. Simulations à grande échelle du modèle sur Macular, une nouvelle plate-forme, dont le but est d'explorer le comportement rétinien à travers des stimulations visuelles complexes.

Dans ce contexte, nous avons analysé les réponses lumineuses enregistrées à partir des RGCs de souris et nous avons identifié des cellules des types distincts qui répondent de diverses manières lorsque leur activité est pharmacologiquement modifiée. Nous avons émis l'hypothèse que ces divers modèles de réponse peuvent résulter d'interactions latérales entre les différents types de RGCs. Nous avons testé cette hypothèse au moyen de la définition du modèle, de l'analyse mathématique, et des simulations numériques et avons illustré le rôle des modèles de connectivité dans le comportement du système. Nos travaux suggèrent des mécanismes physiologiques possibles sous-tendant la variabilité des réponses des RGC en mettant l'accent sur le rôle de la connectivité latérale sur la réponse rétinienne.

Mots clés : Rétine, modélisation, simulations, connectivité.

Acknowledgements

Pursuing a PhD resembles running a marathon in many aspects; both are long, gruelling, lonely endeavours, yet crossing the finish line makes all the effort so worth it! Sharing the challenge with a team of running partners definitely alleviates the whole process, and it even makes it more enjoyable. For this reason, I would like to thank all the people that supported me on every km along the way of this journey, one way or another, and pushed me across the finish line.

First of all, I would like to thank my advisors, Bruno Cessac, Evelyne Sernagor and Gerrit Hilgen, for their guidance, invaluable advice, immense knowledge and all the nice moments we shared during these years. Their unique, yet complementary, set of skills and plentiful experience were vital in making this thesis a reality. Bruno, thank you for your tremendous support, constant encouragement and patience on every step of this bumpy journey. Evelyne, thank you for introducing me to the experimental world and for sharing your enthusiasm and knowledge. Gerrit, thank you for your engagement and excellent guidance through the learning process of the experimental aspects of this thesis.

I am very grateful to Prof. Anya Hurlbert and Matthias Hennig for accepting to be examiners for this thesis. A special thanks to Matthias, for helping me with the analysis of the experimental data and the insightful discussions.

I would also like to thank all the members of the Biovision team, including the members that have left during my PhD and those that recently joined the team, for a cherished time spent together in the lab, and in social settings. During these years, I have been lucky enough to have not one but three awesome office mates that made every day at work a little bit brighter and a whole lot of fun. Dora, for being an inspiration in so many ways, Selma, my partner in crime, and Simone, my running buddy, you are the best office mates I could ask for!

I would also like to thank the people at SED, not only for the great collaboration during this thesis, but also for welcoming me as I pursue the next steps in my career.

My gratitude extends to the Leverhulme Trust for funding this work, and also to the University of Newcastle and Inria Sophia Antipolis for the additional financial support.

Last but not least, thank you to all my friends and family for all their assistance and support. To the friends that became family in Côte d'Azur, Fay, Maria and Arshak, for all the moments we shared in France and abroad, and for always being there for me. To my best friends who became my sisters, Marilena and Antonia, for encouraging me and motivating me to become a better version of myself. To Alex, for all preceding reasons, plus those that do not need to be written.

Contents

1	Introduction	1
2	Background	4
2.1	Overview of the Early Visual System	5
2.2	The Retina	5
2.2.1	A multi-layered architecture	6
2.2.2	General functional characterisation	9
2.2.3	Computational models of neural encoding	11
2.3	From the Retina to the Brain: Retinal Ganglion Cells	11
2.3.1	Why so many?	12
2.3.2	RGCs classification: a contemporary challenge	13
3	Experimental Data Analysis	15
3.1	Introduction	16
3.2	Experimental Materials and Methods	17
3.3	Analytical Methods	24
3.3.1	Modelling light responses : The Linear-Nonlinear model	24
3.3.2	Characterising neuronal activity at the single-cell level	28
3.4	Results	30
3.4.1	Cell classification	31
3.4.2	General response characterisation	32
3.5	Summary and Discussion	45
4	Towards a Large-Scale Retina Model: Definition and Analysis	50
4.1	Introduction	52
4.1.1	Neural models of retinal cells	52
4.2	General Structure of the Model	53
4.2.1	Conception of the model	53
4.2.2	Mathematical framework	55
4.2.3	Model assumptions	57
4.2.4	Retinal mosaics	59
4.3	Bipolar cells layer	60
4.3.1	Receptive field and stimulus integration	60

4.3.2	Bipolar cells voltage	62
4.4	Amacrine cells layer	62
4.4.1	Synaptic connections with BCs	63
4.4.2	Amacrine cells voltage	63
4.4.3	CNO effect on ACs	64
4.5	Ganglion cells layer	64
4.5.1	Synaptic inputs to ganglion cells	64
4.5.2	Ganglion cells response	65
4.5.3	CNO effect on RGCs	65
4.6	Model overview/summary	66
4.6.1	Joint dynamics	66
4.6.2	Connectivity patterns	66
4.7	A mathematical analysis of model dynamics	67
4.7.1	Dynamical system	67
4.7.2	Linear approximation	68
4.7.3	Linear analysis	69
4.8	Numerical results	71
4.8.1	Physiological reproductions	71
4.8.2	Role of ACs lateral connectivity	72
4.8.3	CNO effect on the retinal network	73
4.9	Summary and Discussion	77
5	Probing Retinal Function with a Multi-layered Simulator	81
5.1	Introduction	82
5.1.1	Yet another simulator?	83
5.1.2	Developing Macular	83
5.1.3	How do we use Macular in the context of this thesis?	85
5.1.4	Software development	85
5.1.5	Contributions	87
5.2	Software Architecture	87
5.2.1	Core concepts	88
5.2.2	Workspaces	93
5.3	Usage Scenario	96
5.4	Simulation Results	98
5.4.1	Physiological reproductions	98
5.4.2	Complex stimuli	101
5.5	Summary and Discussion	108
6	Conclusion	110

List of Figures

2.1	Structure of the human visual system	5
2.2	The structure of the retina	6
2.3	Neuronal diversity in the retina	8
2.4	Schematic drawing of connections between the basic cell classes	12
2.5	Parallel processing in the retina	13
3.1	Designer Receptor Exclusively Activated by Designer Drugs	17
3.2	Wholemout micrographs of the selected genetic models	18
3.3	A model experiment using the Cre-lox system	19
3.4	Basic principles of Immunohistochemistry	19
3.5	Large-scale, high-density multielectrode array recordings and light stimulation setup	20
3.6	Light stimuli	22
3.7	Potential scenarios of DREADD activation	23
3.8	Linear-Nonlinear model	25
3.9	Spike-Triggered Average	26
3.10	Spatio-temporal profile and response nonlinearity for ON and OFF cells	27
3.11	Estimating spatio-temporal response properties	29
3.12	Estimating the biphasic index of the temporal profile	30
3.13	Estimating the parameters of the nonlinearity	31
3.14	Spatio-temporal profiles and non-linearities of the selected ganglion cells	33
3.15	Number of RGCs per functional type in Grik4 and Scnn1a retinas	34
3.16	Change of RGCs polarity in CTL and CNO conditions	34
3.17	Assessing the average temporal responses of Grik4 ON and OFF cell types in CTL and CNO conditions	35
3.18	Assessing the average temporal responses of Scnn1a ON and OFF cell types in CTL and CNO conditions	36
3.19	Investigating the temporal properties of Grik4 cells in CTL and CNO conditions	38
3.20	Investigating the temporal responses of Scnn1a cells in CTL and CNO conditions	39
3.21	Temporal profiles of three Grik4 ON monophasic cells exhibiting diverse effects under CNO activation	40
3.22	Temporal profiles of three Grik4 ON biphasic cells exhibiting diverse effects under CNO activation	40

3.23	Temporal profiles of four Scnn1a ON biphasic cells exhibiting diverse effects under CNO activation	41
3.24	Temporal profiles of two ON monophasic cells exhibiting diverse effects under CNO activation	41
3.25	Population distribution of the RF sizes per functional type	42
3.26	Investigating the spatial characteristics of Grik4 cells in CTL and CNO conditions	43
3.27	Investigating the spatial characteristics of Scnn1a cells in CTL and CNO conditions	44
3.28	Assessing the nonlinear properties of Grik4 cell types in CTL and CNO conditions	45
4.1	Translation of the retinal circuit to a computational network model	56
4.2	α -function to model the postsynaptic activity in a chemical synapse	58
4.3	Spatio-temporal linear filter that models the receptive field of a neuron	61
4.4	Model simulation of a Grik4 ON-monophasic RGC's response to a spatially uniform flashed stimulus	73
4.5	Model simulation of a Grik4 ON-biphasic RGC's response to a spatially uniform flashed stimulus	74
4.6	Simulating the variation of the characteristic time constant of ACs for a Grik4 ON-monophasic cell	75
4.7	Simulating the variation of the characteristic time constant of ACs for a Grik4 ON-biphasic cell	76
4.8	Model simulation of a Grik4 ON-monophasic RGC's response to a spatially uniform flashed stimulus	78
4.9	Model simulation of a Grik4 ON-biphasic RGC's response to a spatially uniform flashed stimulus	79
5.1	General Diagram of Macular architecture	88
5.2	Graph generator workspace	95
5.3	Simulator workspace visualisation	96
5.4	Simulator workspace in action	97
5.5	Physiological reproductions with Macular	99
5.6	CNO effect at the individual cell level	100
5.7	ON monophasic cell's response to Chirp stimulus	101
5.8	ON biphasic cell's response to Chirp stimulus	102
5.9	Network role and CNO effect on the response peak time	104
5.10	Time shift	105
5.11	Network role and CNO effect on the response trough time	106
5.12	Network role and CNO effect on the response peak amplitude	107
5.13	Network role and CNO effect on the response trough amplitude	108

Chapter 1. Introduction

Philosophers have likened the eyes to windows to the soul long before scientists realised that they are also windows to the brain (London et al., 2013). Eyes offer us the gift of sight, one of the most fundamental amongst our senses: it is estimated that 80% of what we perceive comes through the sense of sight. They enable us to perceive colours, shapes, patterns and movements, thereby becoming windows to the world around us. The first steps in the process of vision start in the retina, which receives the light that the cornea and lens have captured from different parts of the visual scene, converts it into electrical signals in the form of action potentials (spikes), and transmits these signals to the brain visual areas. Amazingly, the human brain can recreate images from combining and interpreting the fireworks of about one million retinal ganglion cells (RGCs), the sole retinal output neurons. This ability is partially due to the astonishing functional, anatomical and molecular diversity of the RGCs, with each cell type extracting a particular feature of the visual scene, such as contrast, motion, colour, etc. (Wässle, 2004; Masland, 2012a).

It has been proposed that at the heart of the observed response diversity in RGCs lies a dynamic balance of synaptic excitation and inhibition, originating from the interactions of upstream neurons (Demb et al., 2015). Previous studies have thus attempted to investigate how the inner retinal neurons are organised into parallel circuits across different cell types and converge onto RGCs (Wässle, 2004; Gollisch et al., 2010). This has been studied extensively at the level of bipolar cells, leading to a fairly good understanding of their function (Euler et al., 2014). Other studies have investigated the functional role of amacrine cell (ACs) types in retinal processing (Asari et al., 2012; Franke et al., 2017a; Diamond, 2017), suggesting either specific functions such as direction selectivity (starburst ACs) or more general computations, like motion anticipation (Berry et al., 1999; Souihel et al., 2021). Nevertheless, how exactly the diverse RGC responses emerge from the contributions of the inner neurons, and in particular, how AC types shape the RGC output, is still largely unknown (Baccus, 2007).

Tackling this challenge is the aim of this thesis, carried out as part of the Leverhulme Trust funded project "A novel approach to functional classification of retinal ganglion cells", under the joint supervision of Dr. Cessac (Université Côte d'Azur, Inria, France), Prof. Sernagor (Biosciences Institute, Newcastle University, UK) and Dr. Hilgen (Health & Life Sciences, Northumbria University, UK). It is mainly a computational thesis that revolves around a novel experimental approach based on the ability to pharmacologically control the neural activity in specific subgroups of RGCs, which share gene expression, using pharmacogenetics. Our main hypothesis relies on the fact that RGCs do not only act independently conveying local spatio-temporal information, but they also encode information at a population level, as they interact indirectly via lateral connectivity provided by ACs. Thus, modifying their activity

may not only affect their individual responses but also their concerted activity to different stimuli, thereby impacting the information sent to the brain and shedding light on their role in population encoding of basic and complex visual scenes. Based on this hypothesis, we raised the following question: How does the pharmacological alteration of neural activity of retinal cells affect the retinal response to visual stimuli? The research presented in this thesis attempts to address this question on experimental, modelling and computational grounds, giving different and complementary answers.

First, we analysed the light responses recorded from mouse RGCs and identified distinct cell types on the basis of their responses to diverse stimuli. Then, we employed a simple mathematical model in order to fit the experimental data and compute multiple response characteristics. Finally, we explored the general response properties of these RGCs at the single-cell level and compared them between control conditions and when their activity is altered through pharmacogenetics. Our data analysis highlights the variability of response patterns and implicates the role of lateral interactions between RGCs as a potential underlying mechanism.

Next, we developed a mathematical model of the retina, based on biophysics, which obeys three basic principles: (1) It is simple, yet useful and biologically plausible, to account for a realistic structure and functionality similar to the experimental setup; (2) It is mathematically tractable, to infer potential underlying mechanisms that explain the experimental observations; (3) It is predictive, to anticipate effects and responses to complex stimuli, potentially involving network contributions. The model allows us to design local retinal circuits and connect them laterally (via ACs), thus sharing local information and interacting dynamically. It also accounts for dynamics of different cell types, that are potentially sensitive to pharmacological manipulation. The mathematical analysis of the model's dynamics illustrates the role of the characteristic times and synaptic weights in the behaviour of the system. In addition, model simulations in 1D demonstrate how the lateral connectivity via ACs can induce a variety of response patterns at the output of the retina in different experimental conditions.

Finally, we contributed to the development of Macular, a novel large-scale simulation platform of the response of the early visual system to visual stimuli or electrical stimulation, across a range of scenarios, spanning the healthy, developmental and diseased states. In the context of this thesis, Macular allows us to perform large-scale simulations of our model in 2D, to mimic the experimental setup and reproduce experimental responses to specific stimuli, and ultimately to explore retinal behaviour to complex stimuli. Numerical simulations lay emphasis on the role of connectivity on the retinal output, which manifests itself as a propagating wave of activity to the response to moving stimuli.

Outline

The rest of this thesis is organised as follows: in Chapter 2 we start with an overview of the early visual system and then, we focus on a review of the current knowledge of the retina in terms of structure, functionality and modelling. Afterwards, we inspect the literature about RGCs and their classification challenges.

The next three chapters can be considered stand-alone in the sense that they contain methods and results, yet they mutually rely on each other and each is a piece of the puzzle. Chapter 3 starts with a brief presentation of the experimental pipeline and then, describes the methods used for the experimental data analysis. We end the chapter with observations and questions that will be later addressed on modelling and computational grounds. In Chapter 4, we introduce the retina model we have developed in order to explain the experimental observations and, based on mathematical analysis of its dynamics and simulations, we propose potential underlying mechanisms. In Chapter 5, we introduce Macular, that is used to implement on a large-scale the model presented in the previous chapter and study the retina response to complex 2D stimuli. Finally, we summarise and draw conclusions in Chapter 6.

Chapter 2. Background

The aim of this chapter is to provide the necessary elements for the reader to follow the ideas of this thesis. The chapter starts with a brief description of the early visual system, in order to situate the role of the retina in a wider context of visual processing. Then, section 2 presents the general properties of the retina in terms of architecture, physiology and modelling, followed by a description of the RGCs, the sole output neurons that connect the retina to the brain. Finally, we review the challenges in classifying RGCs.

Contents

2.1	Overview of the Early Visual System	5
2.2	The Retina	5
2.2.1	A multi-layered architecture	6
2.2.2	General functional characterisation	9
2.2.3	Computational models of neural encoding	11
2.3	From the Retina to the Brain: Retinal Ganglion Cells	11
2.3.1	Why so many?	12
2.3.2	RGCs classification: a contemporary challenge	13

2.1 Overview of the Early Visual System

Vision is the most fundamental of our senses and visual processing involves some of the most complex neural networks in the vertebrate central nervous system. "A glance is sufficient to describe the shape, colour, size, texture, and location of objects and, if the objects are moving, their direction and speed, over a broad range of light intensities from the dim starlight to bright sunlight." (Purves et al., 2001). The visual system comprises mainly the eyes, the Lateral Geniculate Nucleus (LGN) and the visual cortex (Fig. 2.1).

The first steps in vision start in the eye, which receives physical stimuli in the form of light and transduces it via the retina into electrical and biochemical signals. Then, these electrical signals, in the form of spike trains, travel through the optic nerve towards the LGN, and then to the primary visual cortex, where they are interpreted in order to construct visual images.

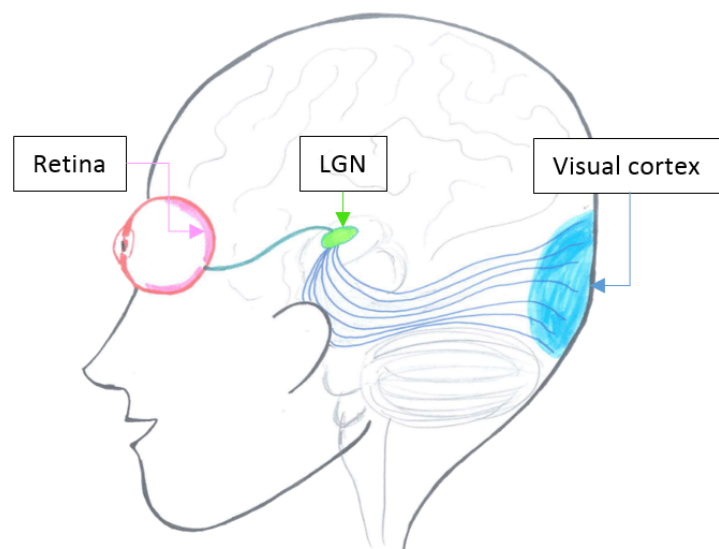


Figure 2.1. Structure of the human visual system. A basic representation of the visual system comprising the retina, the LGN and the visual cortex (Sarrabezolles et al., 2017).

2.2 The Retina

The retina is the main entry point to our visual system, allowing us to perceive the beautiful world around us and mediating most of our learning and cognitive activities. Located at the back of the eye, this thin neural tissue transforms the visual information entering the eye into neural signals that then conveys to various brain regions, via the optic nerve. Besides this basic sensory function, the retina plays an important role in the initial pre-processing of visual information and engages in a great deal of elaborated tasks, from light/contrast adaptation to the selective computation and encoding of specific stimulus features - in contrast to a mere pre-filter, an outdated textbook view of the retina. Many of these computations, such as detection of direction, orientation and object motion just to name a few, emanate from the actual challenges that many

animals face in their natural environments: to detect a moving object and locate it correctly in various light conditions; to predict the future and adapt to varying visual environments (Gollisch et al., 2010). Thus, the downstream areas in the brain receive a collection of features extracted from the visual scene. But how this is achieved by the retina is still a matter of active research.

Over the years, many researchers from various disciplines have been drawn into its spell and try to understand retinal processing and the underlying neural mechanisms. In the following sections, we review the current knowledge of the retina in terms of anatomical structure, physiology (function) and computational modelling. We focus on the vertebrate retina as much of this intricate information is conserved across species, yet we should keep in mind that numerous differences exist.

2.2.1 A multi-layered architecture

The retina is organised in an inverse layout and comprises five major neuronal classes. The cell bodies of these neurons are stacked in three alternating cellular layers interconnected by two synaptic layers. In the outermost layer (Outer Nuclear Layer or ONL), against the pigment epithelium and choroid, lie the photoreceptors, while in the innermost layer (Ganglion Cell Layer or GCL), near the front of the eye, are the ganglion cells (Purves et al., 2001). In between, the Inner Nuclear Layer (INL) hosts the bodies of bipolar, horizontal and amacrine cells. A simplified view of the complex structure of the retina can be seen at Figure 2.2.

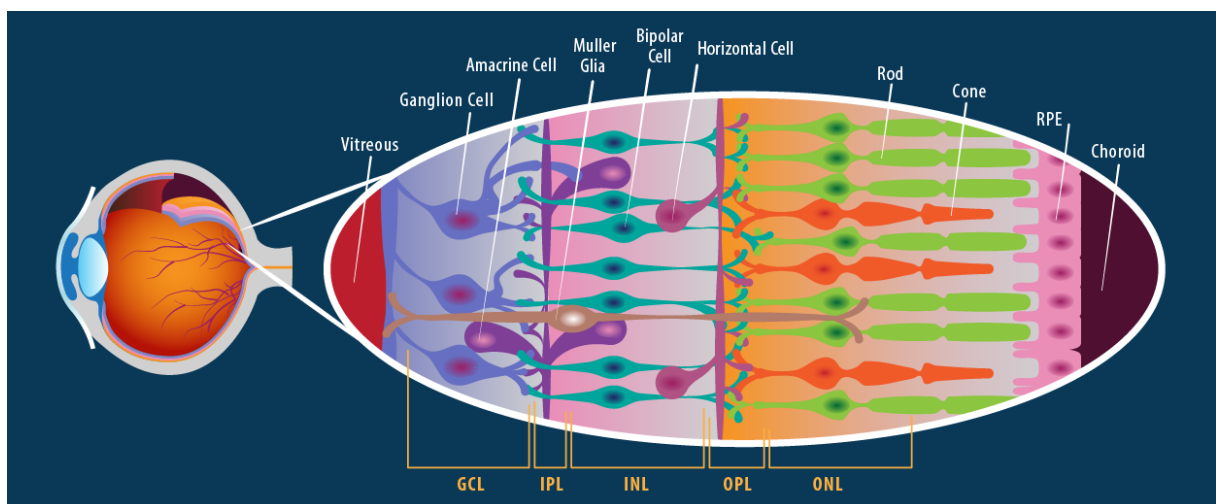


Figure 2.2. The structure of the retina. (Adapted from LifeMap Sciences, Inc. - Discovery)

Light follows a vertical excitatory pathway from photoreceptors to bipolar cells and onwards to ganglion cells. Due to the inverse layout, light must travel through the thickness of the retina before striking and activating the light-sensitive photoreceptors. Subsequently, the absorption of photons by the visual pigment of the photoreceptors initiates a cascade of biochemical and electrical events that is then transmitted to bipolar cells and is modified by the inhibitory feedback of horizontal cells. This takes place in the first synaptic layer, the Outer Plexiform Layer (OPL).

In the second synaptic layer, the Inner Plexiform Layer (IPL), bipolar cells send signals to ganglion cells, and this transmission is modulated by the predominately inhibitory inputs of amacrine cells. The role of amacrine cells is complex as they receive input from bipolar cells and other amacrine cells, and they provide feedback to bipolar cells and ganglion cells. Finally, the feed-forward and lateral flow of the signals in the retina generates multiple neural circuits that operate in parallel and eventually converge onto ganglion cells (Wässle, 2004; Demb et al., 2015; Baden et al., 2018). Hence, ganglion cells receive and integrate signals typically across many different bipolar and amacrine cells. They are the sole output of the retina and unlike the other retinal neurons that communicate via graded potentials, ganglion cells emit action potentials that travel to the brain via their long axons that form the optic nerve.

To unravel the retina, we need to investigate its constituent parts - the cell types from which its complex circuitry is made and understand how their properties and synaptic connections give rise to diverse functions and behaviours. Before presenting the different neuronal classes in more detail, it is interesting to note that each of these cell types can be further divided into multiple sub-types (Fig. 2.3).

Photoreceptors Photoreceptors are light-sensitive neurons that are capable of visual phototransduction, i.e. the process by which light is converted to electrical signals. There are two sub-types of photoreceptors: rods and cones. Rods are sensitive to dim light and thus are specialised in scotopic (night) vision, whereas cones are sensitive to bright light and thus more involved in photopic vision. They are sensitive to colours and the opsin that they contain determines the colour to which they respond. At intermediate light levels, both types are active.

Both rods and cones hyperpolarise when they detect light, releasing the excitatory neurotransmitter glutamate and conversely, they are depolarised in darkness, thereby reducing glutamate release. Basically, glutamate acts as a messenger that transmits signals from photoreceptors to horizontal and bipolar cells.

Horizontal cells Horizontal cells are inhibitory inter-neurons that modulate the signal transmission from photoreceptors to bipolar cells. They have AMPA and glutamate receptors, and thus depolarise in the absence of light, which is triggered by the release of glutamate by photoreceptors. Moreover, they provide inhibitory feedback to photoreceptors, yet it's still not clear whether they also influence bipolar cells directly or they do so via the feedback mechanism onto photoreceptors (Masland, 2012a). They are also thought to play an important role for the surround property of the receptive field of ganglion cells, hence enhancing edge detection (Demb et al., 2015).

Bipolar cells Due to their strategic position, bipolar cells act as a 'turntable' between OPL and IPL (Wohrer et al., 2009). They receive glutamatergic input from photoreceptors, which is

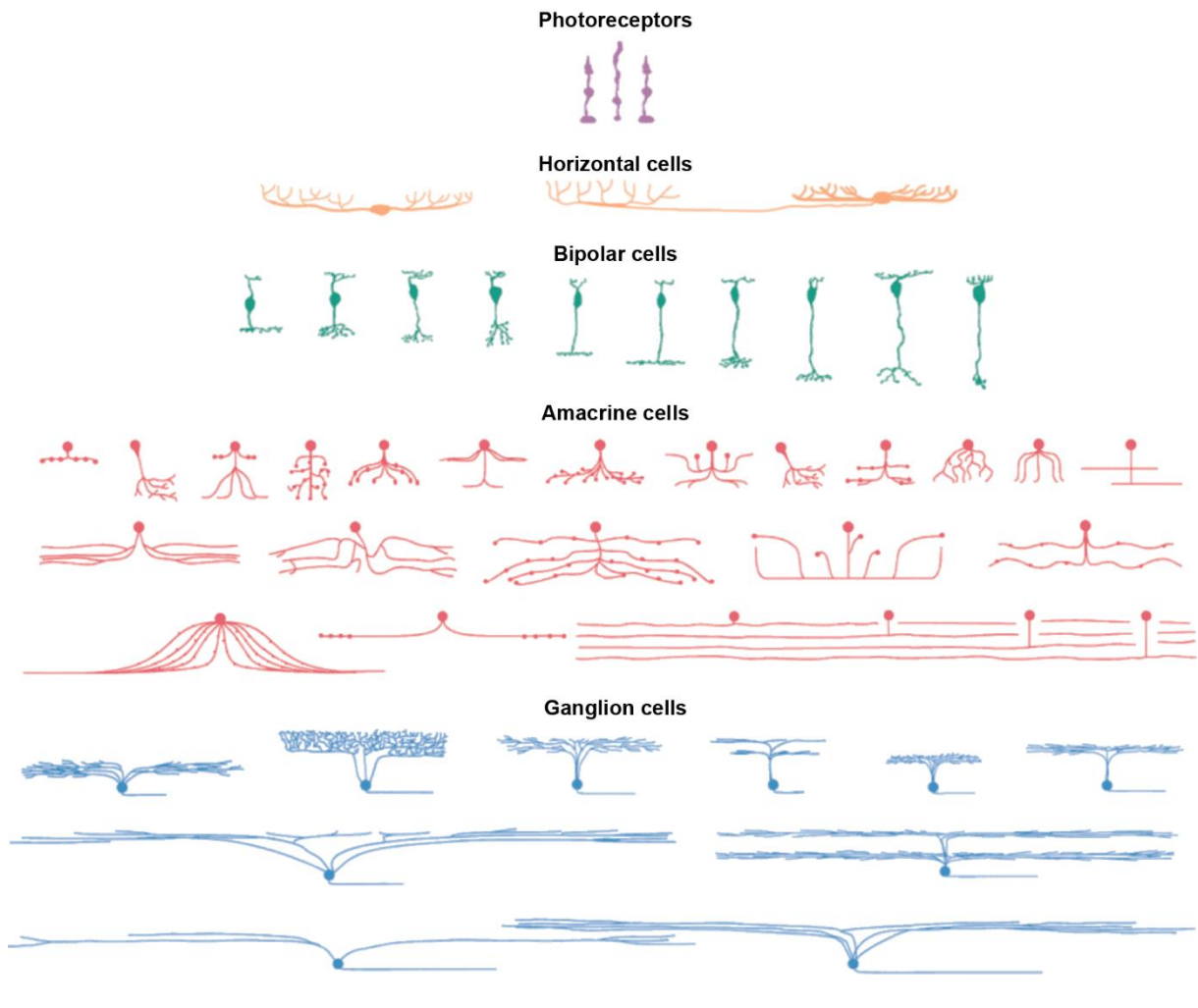


Figure 2.3. Neuronal diversity in the retina. The five major retinal neuronal types and their sub-types. (Schreyer, 2018).

mediated by the inhibitory input from horizontal cells and convey visual information to amacrine and ganglion cells through glutamate release.

Two basic types of bipolar cells can be identified based on the type of photoreceptor to which they connect, rod bipolar cells and cone bipolar cells. Then, depending on the type of receptor they express, cone bipolar cells can be divided into ON and OFF bipolar cells. The former express metabotropic glutamate receptors and hyperpolarise after glutamate binding and the latter express ionotropic glutamate receptors and depolarise after glutamate binding. This means that in the dark, photoreceptors will depolarise and release glutamate, which will inhibit the ON bipolar cells and excite the OFF bipolar cells. On the contrary, the onset of light causes the hyperpolarisation of photoreceptors and the decrease of glutamate release. This initiates a cascade that will finally activate the ON bipolar cells and hyperpolarise the OFF bipolar cells. Bipolar cells can be further subdivided into at least 13 sub-types based on morphology, physiology and synaptic connectivity and each of them forms specific information pathways that encode stimulus properties in parallel (Euler et al., 2014).

Amacrine cells Amacrine cells are inter-neurons that work laterally akin to the horizontal cells and mediate the feed-forward pathway from bipolar to ganglion cells. In particular, their role is manifold: to integrate and modulate the signals from many bipolar cells and other amacrine cells, to provide feedback to bipolar cells and to transmit visual information to ganglion cells. Most of them are inhibitory and release two types of neurotransmitters: GABA and glycine.

Moreover, amacrine cells form the most heterogeneous retinal class, and although little is known about their complex morphology and function, they are considered as one of the main players in the functional diversity of the retinal output (Masland, 2012b). The latest estimation counts up to approximately 60 different types in the mouse retina (Yan et al., 2020).

Ganglion Cells Ganglion cells are the output neurons of the retina and their axons make up the optic nerve. About 1.2 million ganglion cells in the human retina (45,000 in the mouse) integrate the visual signals transmitted by the upstream neurons and carry them to the brain. In particular, ganglion cells receive excitatory glutamatergic input from bipolar cells and primarily inhibitory GABAergic or glycinergic inputs from amacrine cells and encode this information in the form of trains of spikes.

Furthermore, there is remarkable diversity within this neuronal class and different sub-types extract distinct features from the visual scene and project to different sites within the visual system (Sanes et al., 2015). Currently, more than 40 types with unique morphological, functional and genetic properties exist in the mouse retina (Baden et al., 2016).

2.2.2 *General functional characterisation*

In order to understand how such an intricate structure gives rise to an array of diverse functionalities, we need to study the retinal output. Here, we review the general characteristics of retinal filtering, as measured from the recorded light-driven responses of ganglion cells; namely, the response polarity, the receptive field, and the temporal behaviour.

Response polarity

The pioneering work of H.K. Hartline on the electrical recordings of the responses of single ganglion cell axons of the optic nerve revealed diverse patterns of discharges of impulses (Hartline, 1938). Specifically, he found that ganglion cells could be divided in three functional classes: the ON cells that responded to the onset of the light, the OFF cells that responded to the offset of the light, and, the ON-OFF cells that responded both when the light was turned on or off. Later on, Werblin and Downling's work on the recordings of bipolar cells responses in the salamander retina uncovered that bipolar cells also exhibit an ON/OFF polarity (Werblin et al., 1969). Almost a decade later, Famiglietti and Kolb showed that ganglion cells' preference in polarity originates from bipolar cells polarity (Famiglietti et al., 1976). According to their findings, ON ganglion cells receive excitatory inputs from ON bipolar cells, OFF ganglion

cells receive excitatory inputs from OFF bipolar cells and ON-OFF ganglion cells presumably aggregate responses from both ON and OFF bipolar cells.

The receptive field

Another major contribution of H.K Hartline to the study of the retina, was the introduction of the term receptive field. Initially coined by Sherrington (1906) as the area of a dog's skin from which a scratch reflex could be elicited, Hartline extended the term to single neurons from the frog retina and defined it as the region of visual space which must be illuminated to elicit an electrical response in a retinal ganglion cell. As he so eloquently said: "responses can be obtained in a given optic nerve fiber only upon illumination of a certain restricted region of the retina, termed the receptive field of the fiber" (Hartline, 1938). Later on, Kuffler discovered the center-surround antagonistic organisation of the receptive field, by flashing small spots in different regions of the receptive field of ganglion cells (Kuffler, 1953). Depending on the location of the spot within the ganglion cell's receptive field, he recorded ON, OFF or ON-OFF responses, which he attributed to the existence of two regions (central and surrounding) sensitive to the opposite polarity. Barlow extended Kuffler's findings by presenting spots of different sizes to cells and demonstrating how a bigger spot might decrease the response (Barlow, 1953).

The center-surround antagonism arises from the inputs of many upstream neurons both in a feed-forward and lateral manner and allows ganglion cells to transmit information about the differences of the cells responses between the centre and surround of their receptive field. Consequently, ganglion cells are able to detect spatial contrast, such as object edges. The centre region could be attributed to the influence of photoreceptors and bipolar cells, while for the shaping of the surround synaptic interactions in the OPL (via horizontal cells) and in the IPL (via amacrine cells) have been shown to contribute to the phenomenon (Demb et al., 2015).

Temporal behaviour

Not long after Kuffler, Cleland grouped ganglion cells into two classes on the basis of their temporal kinetics: transient cells that respond very briefly to light and sustained cells that respond for longer time (Cleland et al., 1971). Since then, several potential underlying mechanisms have been proposed to account for this phenomenon, such as selective synaptic inputs from bipolar cells, regulation from amacrine cells, or intrinsic cell properties just to name a few, yet the transient/sustained dichotomy is still controversial (Zhao et al., 2017). According to the same study, a unique set of mechanisms for each cell type appears to be responsible for the different temporal behaviour.

2.2.3 Computational models of neural encoding

Even though we now have a relatively good understanding of retina's anatomy and physiology, how exactly the retinal circuitry processes visual information remains poorly understood. Computational neuroscience employs mathematical models, theoretical analysis and simulations to unveil general principles underlying neural information processing. Basically, by placing a problem in a modelling framework we aim at understanding what the nervous systems do, how they function and why they operate in particular ways (Dayan et al., 2001).

Computational models may be broadly classified into three main categories :

- **Descriptive or phenomenological models:** address the "what" question, by attempting to fit large amounts of experimental data in a compact yet accurate manner. Their main objective is to describe phenomena, rather than explaining them and thus can be based loosely on biophysical, anatomical, and physiological elements.
- **Mechanistic models:** address the "how" question and seek to describe the underlying mechanisms of the neural system on the basis of known anatomy, physiology, and circuitry.
- **Interpretive models:** address the "why" question by employing information-theoretic and computational approaches in order to investigate how behaviour and cognition arises from the neural circuitry.

Within each category, one can find a range of models with different levels of abstraction that attempt to capture the response dynamics of neurons from the single-cell level to their contributions via synaptic inputs in larger neural networks (Herz et al., 2006). Most of these models though consider that neurons communicate with each other in the language of action potentials, a quite efficient way of transmitting information over long distances, e.g in the cortex. However, in the retina distances are substantially smaller and thus, retinal neurons, except ganglion cells, interact via smoothly changing membrane potentials rather than spikes. This is quite sufficient for signalling within the retina, but inadequate for conveying information from the retina to the brain. For this reason, ganglion cells finally emit action potentials that travel to the brain via the optic nerve.

2.3 From the Retina to the Brain: Retinal Ganglion Cells

Retinal ganglion cells (RGCs) serve as the bridge between the retina and the brain, conveying highly processed and integrated signals from the upstream retinal neurons to downstream visual processing cortical areas, thereby contributing not only to visual perception, but also to our physiology and circadian behaviour (Baden, 2020). Their axons form the optic nerve and transmit spatio-temporal information about a visual scene in the form of spike trains.

RGC's response is driven by two controllers (Figure 2.4): 1) The output of the bipolar cell that includes both the intrinsic response properties of the bipolar cell (input from photoreceptors)

and the actions of amacrine cells upon the bipolar cell (lateral connectivity between the bipolar cells). 2) The direct input from amacrine cells via chemical synapses or gap junctions, helping spike synchrony between neighbour RGCs (Masland, 2012b). Thus, the spike encoding of a visual scene contains local information, that can be read in the spike emitted by a single RGC (firing rate, latency of the first spike), as well as non-local information provided by lateral connectivity, encoded in the RGCs' spatio-temporal spike correlations deciphered by the brain. How precisely this complexity is encoded in the spike trains produced by the RGCs, strongly depends on their remarkable diversity.

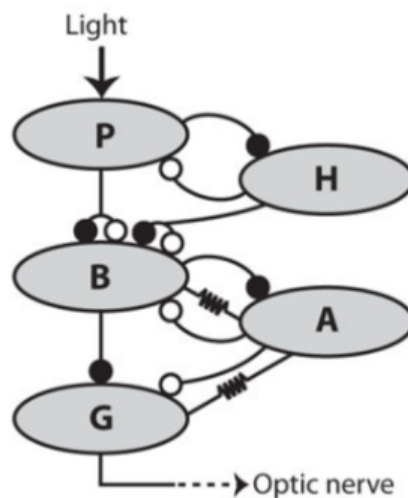


Figure 2.4. Schematic drawing of connections between the basic cell classes. The neurons in the retina are connected through chemical synapses that are either excitatory (closed circles) or inhibitory (open circles). Additionally, cells are electrically coupled via gap junctions across some types of cells (resistor symbol). This general connectivity sets the framework for any specific retinal microcircuit (Gollisch et al., 2010).

2.3.1 Why so many?

RGCs exhibit astounding morphological, functional and genetic diversity. At present, there are at least 40 different sub-types of RGCs in the mouse retina (Baden et al., 2016; Tran et al., 2019). Each sub-type tiles the retinal surface and interprets specific features of the visual scene, thanks to afferent circuits related to specific tasks, such as light intensity or contrast adaptation, motion detection, orientation, motion direction etc. (Masland, 2001; Wässle, 2004; Azeredo da Silveira et al., 2011). Therefore, the brain receives a stream of spikes emitted by almost 1.2 million (in the human retina) of parallel channels, each conveying a piece of information about our external world (Fig. 2.5).

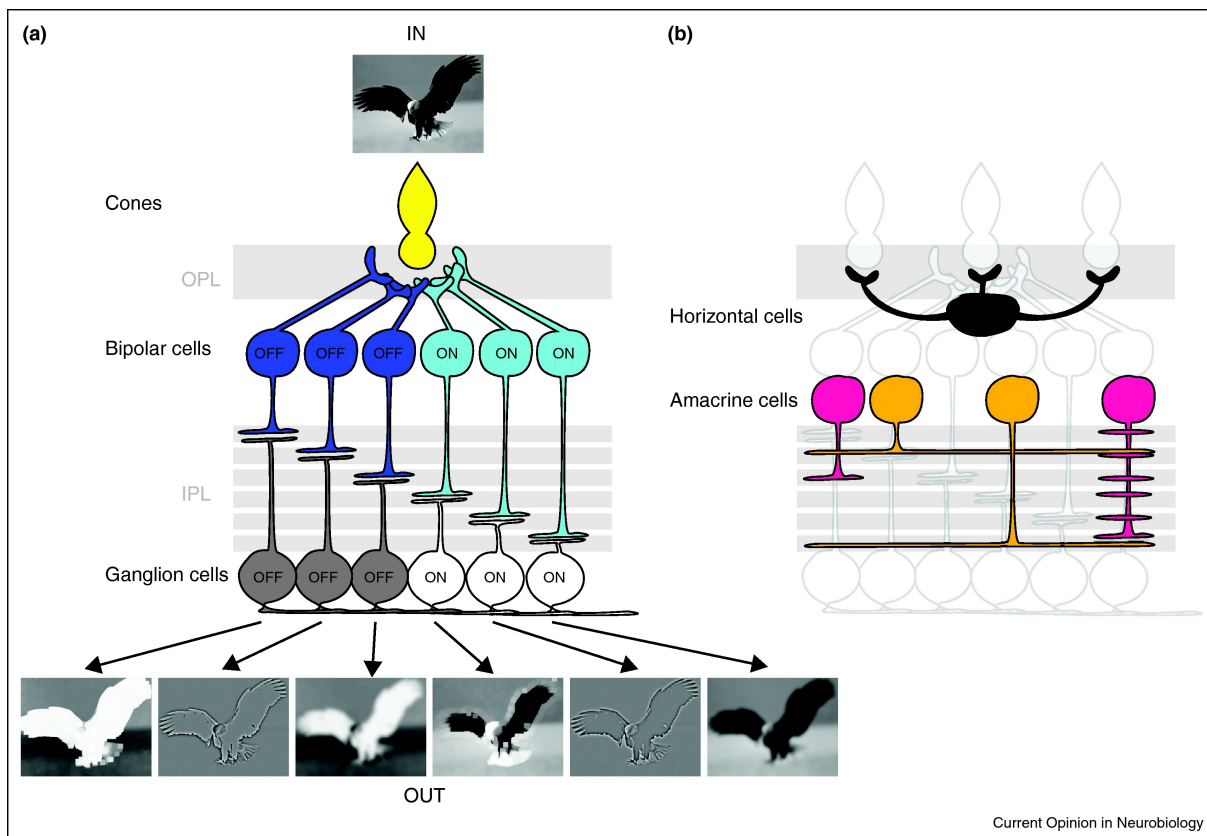


Figure 2.5. Parallel processing in the retina. Each RGC sub-type has an afferent circuit related to a specific task. These circuits involve sub-types from other retinal classes as bipolar and amacrine cells (Azeredo da Silveira et al., 2011).

2.3.2 RGCs classification: a contemporary challenge

A RGC type consists of several neurons that perform a task in a different way from other neurons. However, investigating RGC classification from a functional perspective is a challenging task. Single cell recordings are limited in throughput and calcium imaging techniques improve the yield, but have their own limitations (e.g. barren of temporal resolution to characterise precise information on spike timing). On the other hand, multielectrode arrays allow electrical recordings from many RGCs simultaneously with high temporal resolution.

Basic classification schemes group RGCs based on their responses to light (e.g. ON, OFF or ON-OFF, transient or sustained, see 2.2.2). More sophisticated functional schemes, have identified more than 30 cell types (Vaney et al., 2002; Zhang et al., 2012; Baden et al., 2016; Jouty et al., 2018). Moreover, a RGC type can be further defined upon three criteria: 1) morphology 2) shared gene expression 3) mosaic arrangement (Sanes et al., 2015). Anatomical classifications suggest around 20 cell types (Rockhill et al., 2000; Sun et al., 2002; Kong et al., 2005; Coombs et al., 2006; Völgyi et al., 2009), whereas more recent studies have found up to 50 types on the basis of shared gene expression (Sümbül et al., 2014; Rheaume et al., 2018; Laboissonniere et al., 2019; Tran et al., 2019). Last but not least, there have been efforts to combine multiple

criteria (Wang et al., 2016; Pisano et al., 2017), with the more recent one to identify 24 RGCs' types with dense anatomy and physiology (Bae et al., 2017).

RGCs classification has puzzled researchers for a long time because it is difficult to include all aspects in the same study and requires combining data with high-resolution anatomical, functional and genetic information. (Seung et al., 2014; Sanes et al., 2015).

A novel classification approach

The Leverhulme funded project "A novel approach to functional classification of retinal ganglion cells" intends to tackle the RGCs classification challenge both at an experimental and a computational level, and unravel their role in the encoding of visual scenes, both at the single cell and population level. It proposes a novel, interdisciplinary approach for classifying RGCs into different functional groups on the basis of common gene expression using pharmacogenetics combined with anatomy, large-scale retinal electrophysiology and modelling (Hilgen et al., 2021).

Chapter 3. Experimental Data Analysis

In this chapter, we describe the analysis performed on the light responses recorded from mouse RGCs. First, we briefly provide the essential elements needed to understand the experimental methods. Then, we describe the analytical methods employed in order to investigate and characterise the RGCs responses in various experimental conditions. Finally, we present the results of the data analysis.

Contents

3.1	Introduction	16
3.2	Experimental Materials and Methods	17
3.3	Analytical Methods	24
3.3.1	Modelling light responses : The Linear-Nonlinear model	24
3.3.2	Characterising neuronal activity at the single-cell level	28
3.4	Results	30
3.4.1	Cell classification	31
3.4.2	General response characterisation	32
3.5	Summary and Discussion	45

3.1 Introduction

The retina has long fascinated many researchers who tried to decipher its function and intricate structure, composed of at least 50 distinct cell types (Masland, 2001). Studying the anatomy for more than a century, with Cajal's drawings of this marvellous neural circuit constituting a landmark in the early stages of neuroscience (Cajal, 1893), investigating the physiology for more than half a century and decades of modelling and simulations, have laid the groundwork for better understanding of information processing in the retina (Baccus, 2007). From many perspectives, the retina is an ideal system to probe the information processing mechanisms that underlie its neuronal circuits. It can be isolated and studied on its own, with negligible feedback inputs from other parts of the central nervous system and a complete control of visual stimulation.

Today, the rapid evolution and development of experimental methods enables neuroscientists to perform various tasks, such as recording from hundreds to thousands of retinal ganglion cells (RGCs) simultaneously (in vitro electrophysiology), investigating their morphological properties (immunohistochemistry) and most recently, manipulating the neuronal activity of cells and characterising their physiological properties based on shared gene expression (pharmacogenetics).

Leveraging these techniques aligns with the following objectives of the project I was involved in: (1) Identify distinct neuronal types in the RGC layer, (2) Characterise and reverse-engineer their function, and (3) Shed light on their role in population activity. To achieve these aims, we investigated the functional properties of subgroups of RGCs by applying experimental and theoretical approaches to modify their neural activity using pharmacogenetics. The experimental part introduces a novel approach for RGC classification, targeting (1) and (2), while the theoretical side proposes a model, grounded on experiments, aiming at (2) and (3).

The computational part, which is the main focus of this thesis, revolves around the experimental approach. Therefore, we will first provide the reader with the essential context needed to understand the experimental pipeline (Section 3.2). Next, we will describe the data analysis performed to first explore and assess the diversity of cell responses in different experimental conditions and secondly to extrapolate information that will be later used to constrain our model (Section 3.3 & 3.4).

Personal note During my thesis, I was very lucky to work closely with Prof. Sernagor and Dr. Hilgen, experts in experimental neuroscience. Apart from imparting their knowledge on retinal anatomy and physiology, they also introduced me to the experimental world, by explaining and demonstrating the techniques used, ranging from dissecting the retina and placing it on the device, where action potentials are recorded, to behavioural experiments on live mice. As a computer scientist, I was fascinated by the capabilities of the experiments and I have learned a great deal so as to (1) further my understanding of retinal physiology and anatomy, (2) develop methods to analyse the experimental data (see Sections 3.3, 3.4), (3) propose a model of retinal activity (see Chapter 4), and (4) perform *in silico* experiments on Macular (see Chapter 5). Nevertheless, as

my background is mainly computational I lack the expertise to perform experiments on my own. Therefore, I must clarify that all the experiments have been carried out by Dr. Hilgen at Prof. Sernagor’s lab and that Section 3.2 describes the experimental pipeline.

3.2 Experimental Materials and Methods

Here, we briefly introduce the novel multimodal methodology for RGC classification, based on pharmacogenetics combined with immunohistochemistry and large-scale retinal electrophysiology, as presented in Hilgen et al., 2021.

Pharmacogenetics

Manipulating gene expression in specific cell types in the retina is an invaluable tool for understanding the anatomy and function of neuronal circuits. It is done by modifying or deleting a specific gene, resulting in a phenotypic change linked to the specific protein whose synthesis is normally under the control of that gene. In the context of our project, mice carrying specific genes were engineered so that all cells that express that gene co-express an engineered version of G-protein coupled receptors called DREADDs (Designer Receptor Exclusively Activated by Designer Drugs). DREADDs are designed upon cholinergic muscarinic receptors that do not respond to any endogenous ligands, but only to artificial “designer drugs” with no endogenous receptors in the organism, such as clozapine-N-oxide (CNO) (Urban et al., 2015).

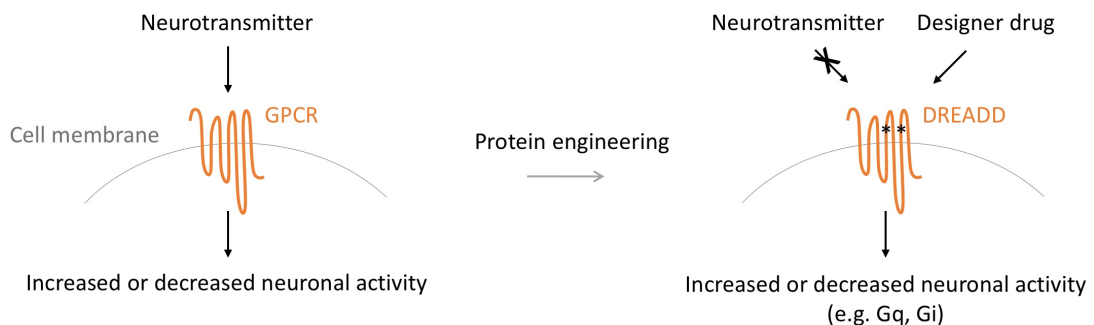


Figure 3.1. Designer Receptor Exclusively Activated by Designer Drugs. *Left.* Neurotransmitters bind to G protein-coupled receptors (GPCRs) of the membrane, which leads to a change in the activity of the neuron. *Right.* An engineered version of GPCRs, called DREADDs, responds only to a specific biologically inert chemical (a designer drug), hence allowing us to control neuronal activity. Source: <https://benchling.com/pub/dreadds>

DREADDs can be excitatory (hM3Dq - release of calcium from organelles leading to increase of intracellular concentration of free calcium, leading to membrane depolarisation and higher neuronal excitability), or inhibitory (hM4Di - opening of potassium channels, leading to membrane hyperpolarisation and neuronal silencing). DREADDs technology is widely used to modulate and control neural activity acutely in groups of cells sharing gene expression, thus

enabling to pharmacologically dissect out the role of specific neuronal cell classes in network activity (Roth, 2016). This powerful technique offers several advantages; namely, it is easy to implement, simply by injecting CNO systemically, which in turn induces a prolonged systemic effect and it is fully reversible, as the effect winds down within a few hours post-injection.

Genetic models

Two mouse lines were used in this project. One line expresses the *Grik4* (Glutamate receptor, ionotropic, kainate subunit 4) and the second one, the *Scnn1a* (non-voltage gated sodium channel, epithelial 1 subunit alpha) gene. These genes were selected on the basis of micrographs available from the Allen Mouse Brain Connectivity Atlas (2011), showing a relatively sparse and non-homogeneous expression across the RGC layer, thereby suggesting area specialisation.

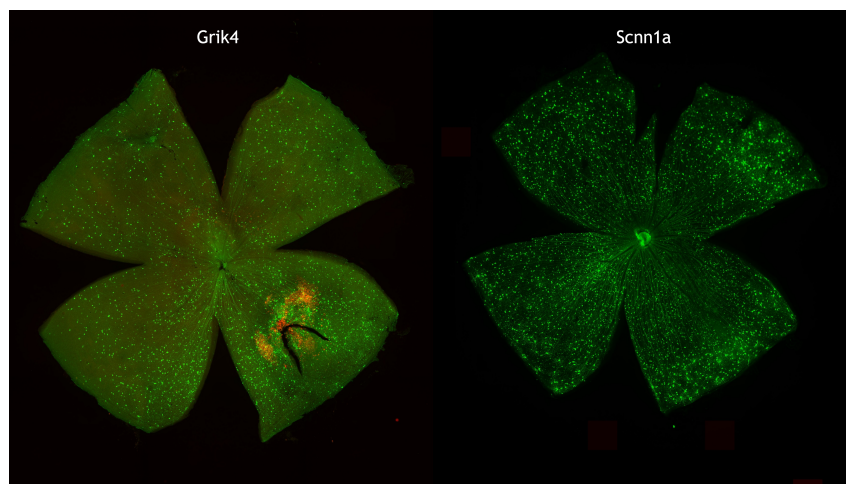


Figure 3.2. Wholemout micrographs of the selected genetic models. Fluorescent RGCs expressing *Grik4* (left) and *Scnn1a* (right) genes. Pictures from the Allen Mouse Brain Connectivity Atlas (2011)

DREADD expression is through the well-established "Cre-lox" conditional gene expression approach, where the "Cre" line determines the gene that drives DREADD expression and targets specific sites in a DNA molecule, known as loxP sequences (Fig. 3.3). Cre-*Grik4* or Cre-*Scnn1a* mice were cross-bred with floxed mice for Gq-DREADD (excitatory DREADDs) expression in Cre-expressing cells. A floxed mouse has the gene of interest (in our case gene for DREADD expression) sandwiched between two LoxP sequences. When such floxed mouse is bred with a Cre mouse (cre being on the promoter gene, in our case *Grik4* or *Scnn1a*), the two LoxP sequences are combined with the Cre, releasing the target gene, allowing expression/function.

Henceforth, we will refer to *Grik4*-DREADD and *Scnn1a*-DREADD cells as *Grik4* and *Scnn1a*, respectively.

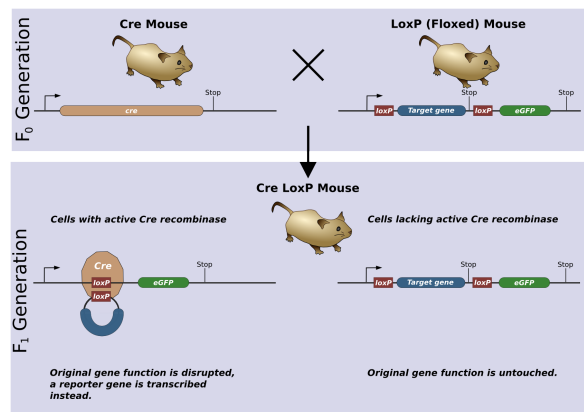


Figure 3.3. A model experiment using the Cre-lox system. The premature stop sequence present in floxed mice is removed only from cells that express Cre recombinase when the mice are bred together. Source: Wikipedia.

Immunohistochemistry

Immunohistochemistry (IHC) is a powerful technique for visualising cellular components, such as proteins or other macromolecules, in tissue samples. This is achieved by using specific antibodies that bind to targeted antigens (proteins) and then visualising the area where this binding has taken place in the microscope (Ozawa, 2019).

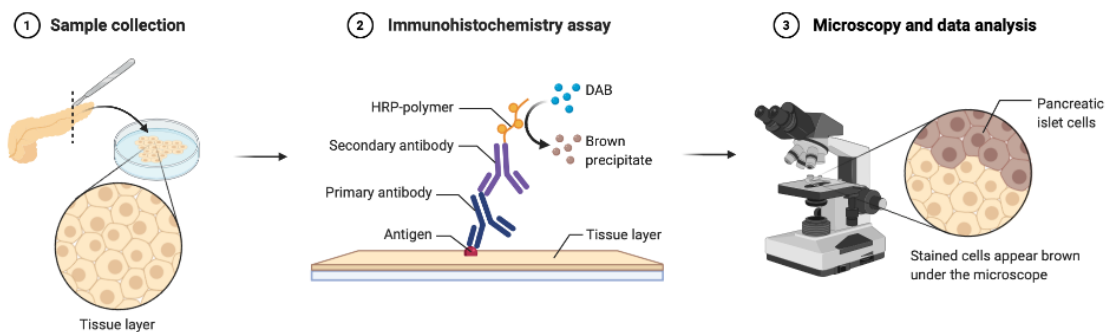


Figure 3.4. Basic principles of Immunohistochemistry. An example of visualising pancreatic islet cells. Source: BioRender

In the context of our project, IHC was employed for the morphological identification and evaluation of retinal neurons. More specifically, it has been used to:

- Provide information on the topographic orientation and the distribution of Grik4 and Scnn1a expressing cells across the retinal layers.
- Characterise the expression patterns of Grik4 and Scnn1a expressing cells by combining multiple markers.

Electrophysiological recordings

Prof. Sernagor’s lab is specialised in techniques for retina stimulation and recordings. The experimental protocol has already been described in detail in Maccione et al., 2014; Portelli et al., 2016; Hilgen et al., 2017a. Briefly, retinal isolation was performed under dim red light following overnight dark adaptation. The isolated mouse retina was placed onto a high-density large-scale multi-electrode array (MEA) featuring 4096 (64x64) electrodes and covering a large proportion of the mouse retina ($2.67 \times 2.67 \text{ mm}^2$). On the MEA, the RGC layer faces directly the extracellular electrodes that measure high amplitude voltage changes (action potentials). Recordings of spontaneous and light-evoked responses were obtained at a sampling rate of $\sim 18 \text{ kHz}$ /electrode from hundreds to thousands RGCs simultaneously, first in control (CTL) conditions and one hour after adding the DREADD agonist, CNO (hereinafter referred to as CNO conditions). Following recordings, raw data was processed for spike detection and single units were clustered using the approach described in Hilgen et al., 2017b.

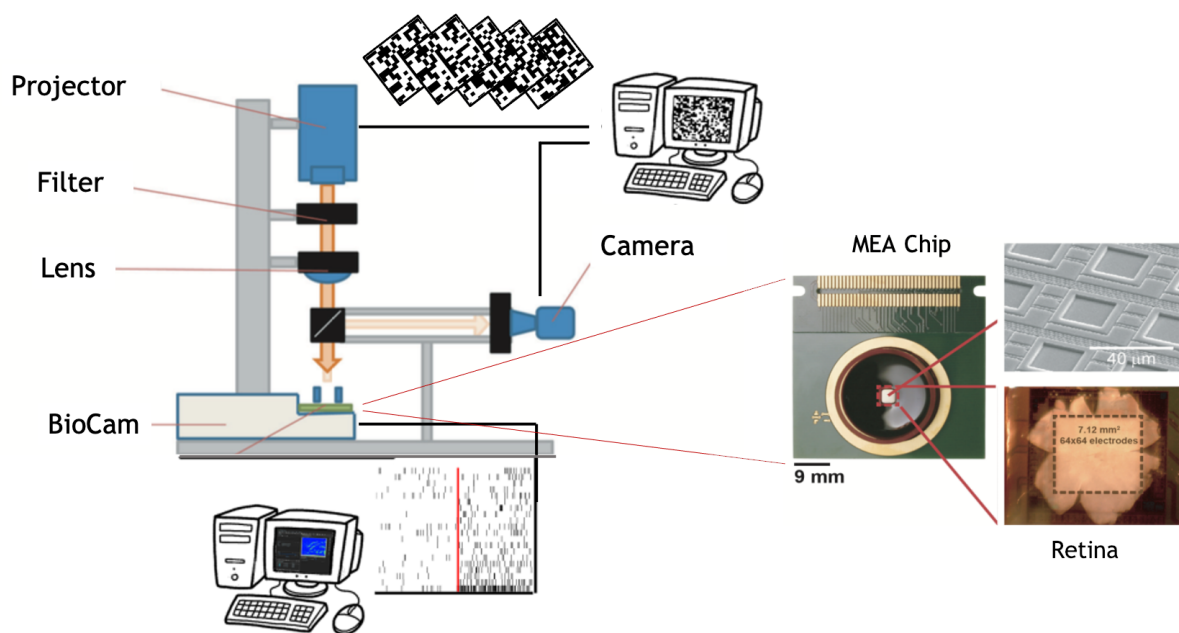


Figure 3.5. Large-scale, high-density multi-electrode array recordings and light stimulation setup. *Left.* Light stimuli are projected onto the retina with a custom built high-resolution photostimulation system. RGCs responses are recorded on the BioCamX platform with high-density MEA Arena chips (3Brain GmbH, Lanquart, Switzerland). *Right.* The MEA chip provides 4096 square microelectrodes in a $2.67 \times 2.67 \text{ mm}^2$ area and aligned in a square grid with $42 \mu\text{m}$ spacing. The isolated retina is placed, RGC layer facing down, onto the MEA chip and flattened. Adapted from (Hilgen et al., 2019; Maccione et al., 2014)

Light stimuli

Light stimuli were projected onto the retina via a custom-built system (Fig. 3.5), as described previously in Portelli et al., 2016. Stimulus design is vital as we want to elicit strong responses from the targeted cells. Depending on which aspect of the response we want to trigger (individual neuron or collective response, static or dynamic, locally or spatially extended), the stimulus should be selected appropriately. For the electrophysiological recordings, a large battery of stimuli was available ranging from simplified synthetic stimuli, such as bars, gratings or full-field, to shifted white noise and natural scenes.

For the data analysis, we handled RGCs responses to the following stimuli:

- **Full-field chirp**: various 1' contrast steps, increasing frequency (1-15Hz) and contrast modulations (1-93 Michelson contrast defined as $(I_{max} - I_{min}) / (I_{max} + I_{min})$ where I_{max} and I_{min} are respectively the maximum and minimum luminance)(Fig. 3.6 (A)). The whole sequence was repeated 5 times.
- **Shifted white noise (SWN)**¹: improved checkerboard stimulus, where checkerboard pixels are shifted randomly in space at fixed time steps (Pamplona et al., 2021). It consists of 27000 images of 664x664 pixels (1px = 4 μ m) of 160 μ m pixel blocks and 40 μ m shift, changing every 33 ms (Fig. 3.6 (B)).
- **Moving bars**: random black and white moving bars (width 100 μ m, 12 directions (30° separation)), 800 μ m/s (Fig. 3.6 (C)). The whole sequence was repeated 5 times.

Functional and anatomical characterisation of cell types

As mentioned earlier, one of the main objectives of the experimental part of the project was to investigate the anatomical and functional features of specific RGC types. By combining the methods described so far, namely, the excitatory DREADD activation (pharmacogenetics), the MEA array recordings (electrophysiology) and the post hoc immunostaining (immunohistochemistry), our collaborators have successfully characterised the anatomy and physiology of Grik4- and Scnn1a-expressing RGCs types.

However, the IHC experiments revealed that Grik4 and Scnn1a cells exist also in the inner nuclear layer, presumably reflecting inhibitory ACs (for more details please refer to the paper Hilgen et al., 2021). To support this hypothesis, our colleagues used specific markers for ACs and identified Grik4 and Scnn1a ACs (though relatively sparse). Considering that ACs make synaptic connections with RGCs, among others, when they are expressing DREADDs and are susceptible to CNO, consequently impacts the level of input onto their post-synaptic partners, hence confounding the interpretation of the results. One might think that the effect is straightforward, meaning that when inhibitory ACs are excited, this will result in stronger

¹SWN has been developed as a former collaboration between Prof. Sernagor's lab and Biovision team.

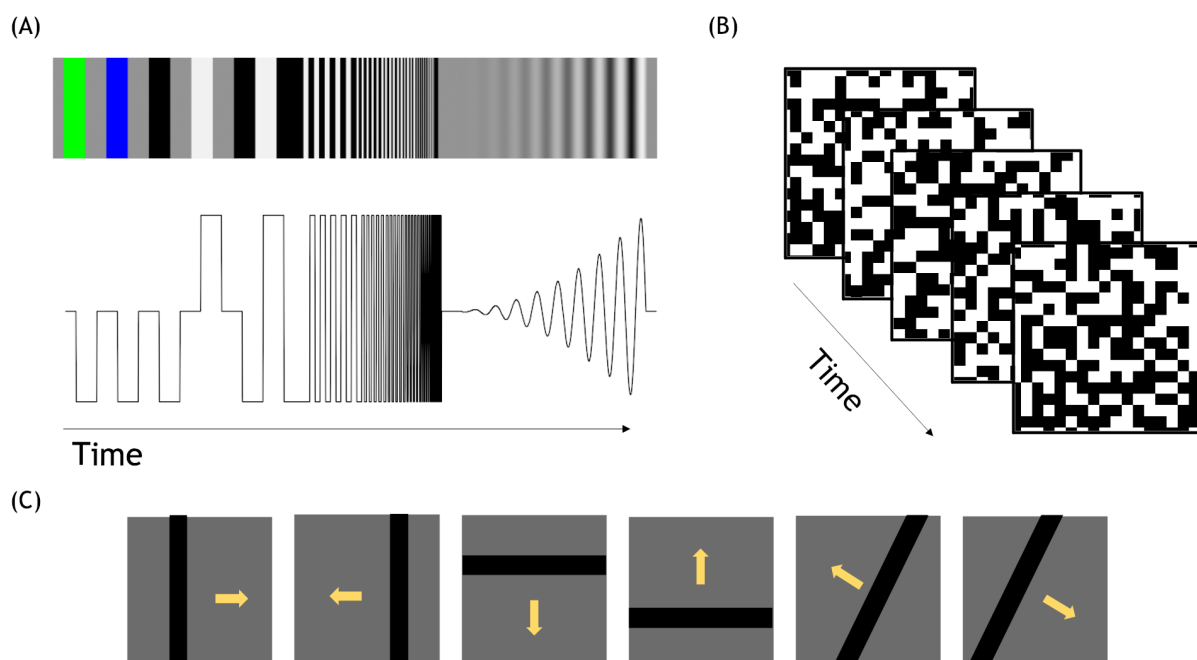


Figure 3.6. Light stimuli. (A). Full-field chirp with various 1' contrast steps, increasing frequency and contrast modulations. (B). Shifted white noise with pixels shifted randomly in space at fixed time steps. (C) Randomly moving black and white bars. Here we show an example of 6 directions for a black moving bar.

inhibition of RGCs these cells synapse with. However, this is only true if these same RGCs do not express DREADDs themselves, when in fact there are many possible scenarios, as illustrated in Figure 3.7. Scenario 1 is simple, if there are no DREADDs, there is no change in the spiking activity of the RGCs (Fig. 3.7 scenario 1). The second scenario is the ideal case, DREADDs are only expressed in RGCs, so increased RGC firing is driven by direct DREADD activation (Fig. 3.7 scenario 2). In the reverse situation, when DREADDs are only expressed in inhibitory ACs, CNO-induced activation leads to an increase of the inhibitory effect of the ACS on RGCs, resulting in decreasing spiking activity of the RGCs (Fig. 3.7 scenario 3). Finally, scenario 4 is difficult to disentangle as there are antagonistic effects on the RGCs response. Here, both RGCs and ACs express DREADDs. CNO-induced activation leads to, on one hand, the depolarisation of ACs and the enhancement of their inhibitory effect on the RGCs and, on the other hand, to increased RGC firing rate. Thus, there are two effects, one direct on RGCs and one indirect via ACs, that compete with each other (Fig. 3.7 scenario 4). So, what is the net effect? Do we notice a decreased or increased RGC spiking activity or is there no net noticeable change?

The first step to isolate Grik4 and Scnn1a RGCs, that is to say, exclude scenarios 1 and 3, was to impose the following criteria: (1) Cells should exhibit 50% increase in spiking activity or bursting activity in the presence of CNO (achieved by analysis of electrophysiological recordings); (2) and these identified cells should also express the Grik4/Scnn1a genes and DREADDs (confirmed by correlating their physical position with micrographs of DREADD

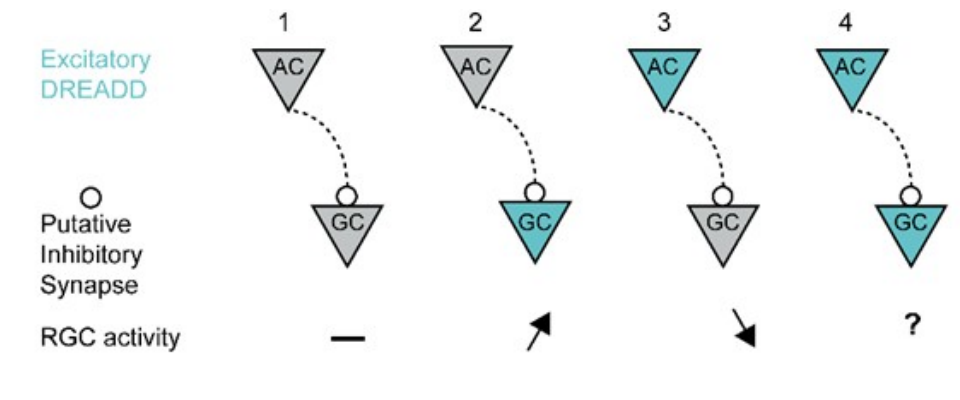


Figure 3.7. Potential scenarios of DREADD activation. 1. ACs and RGCs do not express DREADDs, thus there is no change in the spiking activity of the RGCs. 2. Only RGCs express DREADDs, so DREADD activation is triggering increased RGC firing. 3. Only ACs express DREADDs, so DREADD activation causes an increase of the putative inhibitory effect of ACs on RGCs, resulting in decreased RGC firing. 4. Both ACs and RGCs express DREADDs, therefore DREADD activation triggers an excitatory direct effect on RGCs and an inhibitory indirect effect via ACs on RGCs. The net effect is not clear on experimental grounds. Figure Courtesy Dr. Hilgen.

expressing cells). This processing allowed us to correlate anatomical and functional features of Grik4 and Scnn1a RGCs. However, it was difficult to distinguish on pure experimental grounds the antagonistic effects of CNO on scenario 4. On the contrary, the competition between these two effects under an increasing concentration of CNO could be studied with a computational model. This is one of the main goals of Chapter 4 and 5.

Finally, in order to decipher the functional properties of the isolated Grik4- and Scnn1a-expressing neurons, RGCs were classified into functional groups according to the nature of their responses to light. We employed the automatic classification tool presented in Jouty et al., 2018, which uses a simple stimulus paradigm and a spike train distance measure as a clustering metric. The chirp stimulus was selected in order to elicit responses simultaneously over the entire recording area and the SPIKE distance as a clustering metric (This metric basically compares the distances between the preceding and following spikes of the two spike trains (Kreuz et al., 2011; Kreuz et al., 2013)). RGCs were first grouped in two types, based on their response preference for stationary (e.g. full-field) and non-stationary (e.g. moving bars) stimuli. Next, RGCs in each category were clustered into functional types, using hierarchical agglomerative clustering. To determine the appropriate number of clusters for the clustering algorithm, gap statistics was used (Jouty et al., 2018). Results of this analysis can be reviewed in detail in Hilgen et al., 2021.

Data pool

Overall, 8 experiments were performed consisting of 3 Grik4 and 5 Scnn1a retinas. For the classification analysis, RGCs that did not match the aforementioned criteria were filtered out. Nevertheless, selecting cells with a 50% increase in spiking or bursting activity might disregard interesting effects of CNO, e.g. in scenario 4 the net effect on RGCs might be an increase

or decrease of activity. For this reason, we selected cells only based on the second criterion for further analysis (Grik4/Scnn1a genes and DREADDs expression). Finally, our data pool consisted of 164 Grik4 cells and 378 Scnn1a cells.

3.3 Analytical Methods

As we have seen in the previous section, functional types of RGCs were classified on the basis of their responses to the chirp and moving bar stimuli. Here, we further investigated and characterised the responses of the identified RGCs using white noise stimulation. Our aim was threefold: first, to explore the general behaviour of the entire population of the recorded RGCs and group them into different functional types; second, to characterise the responses within each group and compare them in CTL and CNO conditions; and finally, to extrapolate information that will be later used to constrain our retina model.

In this section, we thus describe the analytical methods. First, we introduce a widely used mathematical model that we employed to fit the experimental data (subsection 3.3.1) and then we describe how we estimated light response parameters from these fits (subsection 3.3.2).

All the scripts for the data analysis have been implemented in Python.

3.3.1 Modelling light responses : The Linear-Nonlinear model

Analysing the response properties of neurons to visual signals requires a quantitative model that can reliably describe the mapping between input stimuli and output firing rate (Rieke et al., 1997). The linear-nonlinear (LN) model has been established as a standard tool for the analysis of electrophysiological data (Chichilnisky, 2001; Paninski, 2003; Simoncelli et al., 2004; Schwartz et al., 2006).

Description The LN model consists of a single linear filter, followed by a nonlinear function (Fig. 3.8). The filter is associated with the neuron's receptive field, i.e. its selectivity to specific stimulus features, while the nonlinear function accounts for cell intrinsic dynamics, such as spike threshold (or current/voltage rectification) and response saturation (Chichilnisky, 2001). First, the linear filter $K(x,t)$ integrates the stimulus $S(x,t)$ over space and time and then, the filtered output $g(t)$ is transformed by the nonlinear function N into the model's output $r(t)$, which typically represents the neuron's membrane potential or its instantaneous firing rate. In fact, $g(t)$ results from the spatio-temporal convolution of the stimulus with the linear filter, represented as $(K * S)(x,y,t)$ and $r(t)$ is the output of $N(g(t))$. This type of model is appealing due to its simplicity and relative ease with which the model parameters can be obtained.

Estimating a linear filter

The LN model advocates a classical view of retinal function, assuming that a neuron's receptive field can be represented by a single linear filter. However, this hypothesis is often questioned

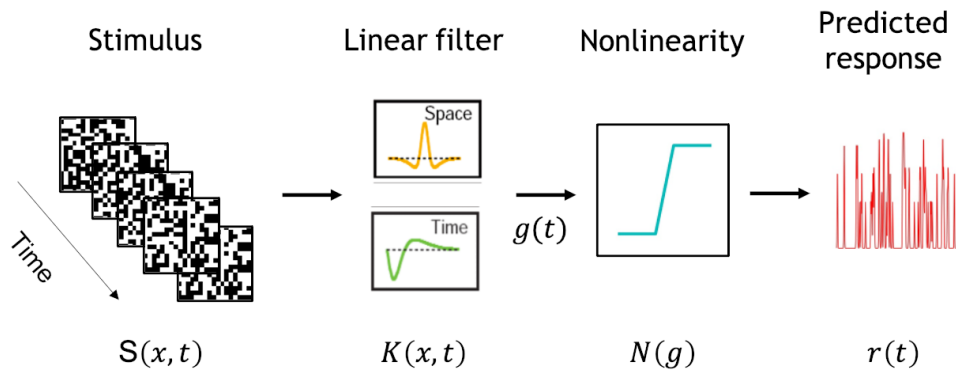


Figure 3.8. Linear-Nonlinear model. The stimulus $S(x,t)$ is convolved with a linear spatio-temporal filter $K(x,t)$, and then the result $g(t)$ is passed through a nonlinearity $N(g)$ to produce the predicted firing rate $r(t)$.

by many studies that probe the retinal function with natural images or artificial grating stimuli and allege the nonlinear spatial integration of excitatory signals, coming from presynaptic BCs (Schwartz et al., 2012; Gollisch, 2013; Karamanlis et al., 2021), or the nonlinear integration of visual signals at the level of BCs (Schreyer et al., 2020).

Depending on the stimulus used to elicit responses, there are different techniques to estimate the linear filter parameters: (1) Spike-triggered analysis methods with white-noise stimulation (Chichilnisky, 2001; Paninski, 2003; Simoncelli et al., 2004; Schwartz et al., 2006), and (2) Maximum likelihood techniques with more complex stimuli, including natural images (Paninski et al., 2004; Pillow et al., 2006).

A widely-used method in the first category is the spike-triggered average (STA) or reverse correlation. By computing the STA of a cell's response to a white noise stimulus, one can obtain an estimation of the spatio-temporal linear filter, where the spatial part describes the neuron's spatial receptive field and the temporal part describes the time-reverse of the neuron's impulse response (Chichilnisky, 2001). In order to have an unbiased estimation, the stimulus should be uncorrelated (e.g Gaussian white noise). From a mathematical point of view, the STA is obtained by averaging the stimulus preceding each spike over a specific time window (Figure 3.9). To better understand this, let us consider neurons as linear time-invariant systems that can be characterised by their impulse response. This can be measured either as the response to a Dirac delta function (brief pulse of unit area) or by reverse correlating the response to a white noise input (Ringach et al., 2004). Thus, knowing the cell's impulse response we can compute the linear response of this cell to any stimulus, basically by convolving the input with the estimated filter. Nonetheless, the STA analysis would fail in identifying ON-OFF cells. As these cells respond both to light increments and decrements, they exhibit ON and OFF RF and thus, a single linear RF would average the ON and OFF filters and mask the diverse presynaptic

inputs that these RGCs receive (Gollisch et al., 2008; Shi et al., 2018).

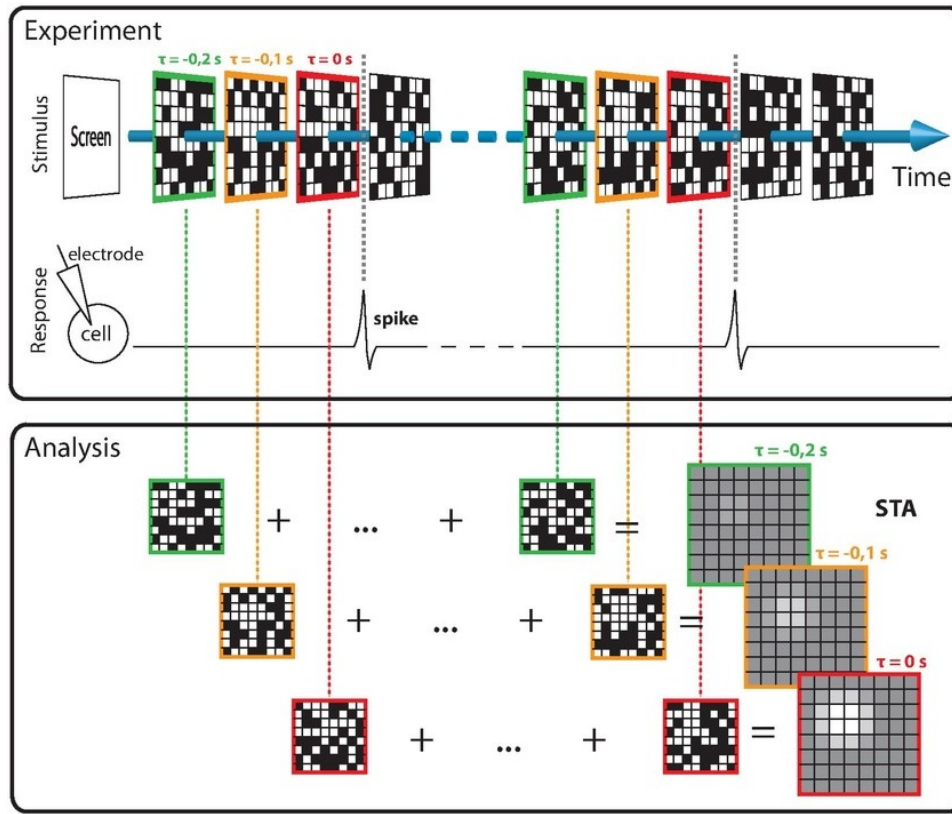


Figure 3.9. Spike-Triggered Average. The stimuli in a specific time window preceding each spike (here 3 time bins) are averaged to obtain the STA. The bright spot of light indicates the neuron's preference for bright stimuli just before the spike. In addition, it informs us about the RF of this neuron, located in the top-left corner of the checkerboard. Source: Wikipedia.

To estimate the spatio-temporal response properties of each RGC, we used a custom-built software that computes the STA using the recorded spike trains to a checkerboard stimulus. This type of stimulus is a standard method for measuring the receptive fields of RGCs. Here, we used an improved version of this stimulus, the so-called shifted white noise (SWN). It has been shown that SWN considerably improves the spatio-temporal resolution of the receptive field (Pamplona et al., 2021). Shifted white noise sequences (typically 600 ms in duration) that preceded each of the detected spikes of an RGC were averaged over the recording to obtain the STA of the RGC. The filter length was chosen empirically so that it exceeds the duration of the impulse response of the cell.

Spatio-temporal profiles from two neurons are shown in figure 3.10 ((A) and (B) for an ON cell, (D) and (E) for an OFF cell). Figures 3.10 (A) and (D) show the average stimulus 58 and 66 ms prior a spike correspondingly. The spatial RF corresponds to the region of the image with deviations from the background, arising from the averaging of pixels that elicit a strong response. The cell on the top (bottom) of Figure 3.10 was excited by brighter (darker) features of the stimulus and was therefore classified as ON (OFF) cell. Figures 3.10 (B) and (E) show

how the STA contrast evolves in time within the receptive field (STA frame with the highest response), preceding a spike.

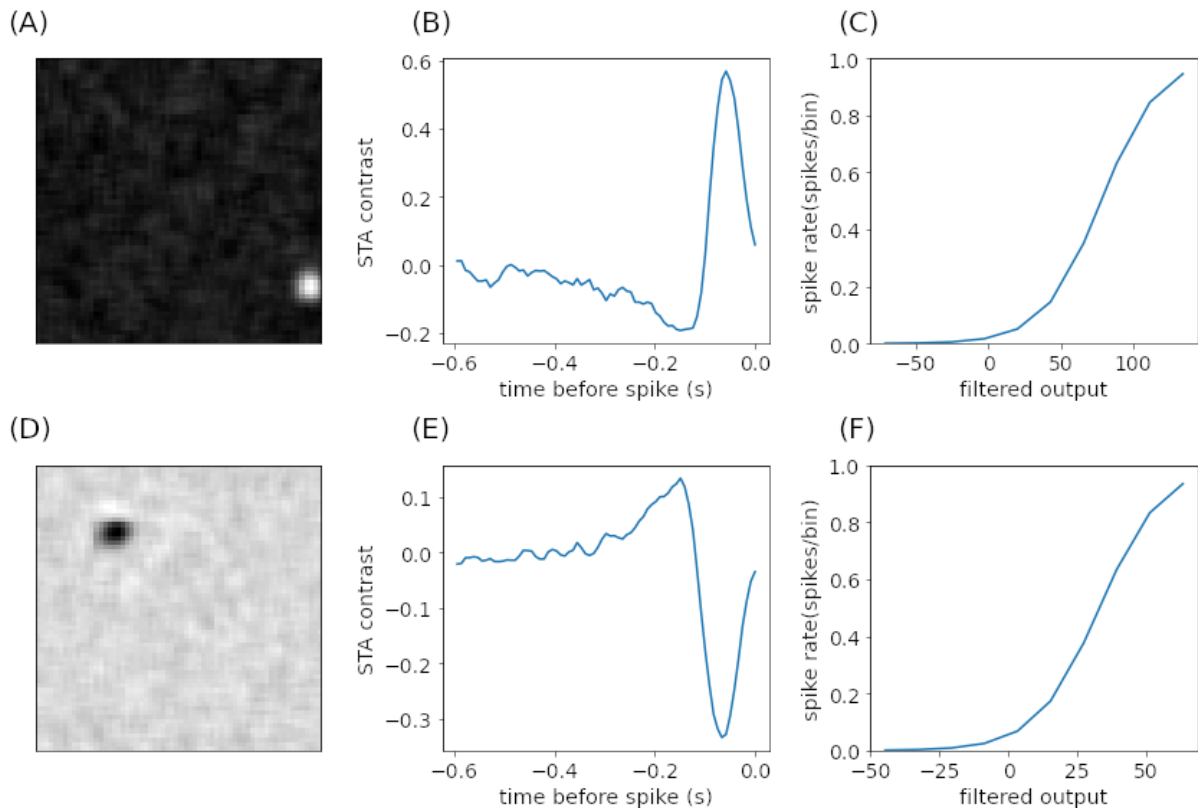


Figure 3.10. Spatio-temporal profile and response nonlinearity for ON and OFF cells. (A) Spatial profile of the STA for an ON-centre ganglion cell 58ms (near time-to-peak) before a spike. (B) Time course of the STA at the centre of the receptive field. The dominant positive peak indicates that this is an ON cell. (C) Static nonlinearity estimated from this cell (D) Same as (A), for an OFF-centre ganglion cell 66ms (near time-to-peak) prior a spike. (E) Same as (B), for the cell in (D). The dominant negative trough indicates that this is an OFF cell. (F) Same as (C), for the cell in (D).

Fitting and parameters estimation To fit the spatial sensitivity profile, we used a 2D Gaussian on the frame with the maximal response (Fig. 3.11 (A)) and we drew an ellipse around the centre with 1 SD of the Gaussian fit (Fig. 3.11 (C)). The temporal sensitivity profile was obtained as the average time course of the contrast at the RF centre along a time window of 600ms preceding a spike (Fig. 3.11 (B)). To fit it, we used the difference of two cascades of low-pass filters, similarly to Chichilnisky et al., 2002.

$$f(t) = a_0 (t/\tau_0)^n \exp(-t/\tau_0) - a_1 (t/\tau_1)^n \exp(-t/\tau_1) \quad (3.1)$$

Parameters were selected to minimise the sum of squared errors using the Levenberg-Marquardt methods (Levenberg, 1944; Marquardt, 1963).

Estimating a nonlinearity

A RGC may encode information in a linear or a nonlinear fashion (Demb et al., 1999; Demb et al., 2015). In the former case, the STA would provide a complete description of their light responses. In reality, however, RGCs' responses are highly nonlinear. To address this and complete the LN model, we need to estimate a nonlinear static function from the data, by mapping the linear response to the real response of the cell (Chichilnisky, 2001). The first step is to compute how the neuron would respond if it was linear, which is achieved by convolving the neuron's estimated linear filter with the stimulus (filtered output - $g(t)$). Here, we used the pyret package. Then, to estimate $N(g)$ we compute the average spike count in time bins with nearly equal values of the filtered output. This gives finally the mean spike rate as a function of the filtered output.

Examples are shown in figures 3.10 (c) and (f), where both cells exhibit a nonlinear response. If responses were linear, we would expect the data to fall on straight lines.

Fitting and parameters estimation The nonlinearity mapping the real to the linear estimated response, can be then fitted using a sigmoid function:

$$r(x) = \beta + a/(1 + \exp(-\gamma(x - \theta))), \quad (3.2)$$

where x is the linear estimated response, $r(x)$ is the firing rate and β, a, γ, θ are free parameters (Fig. 3.13).

Parameters were selected to minimise the sum of squared errors using the Levenberg-Marquardt methods (Levenberg, 1944; Marquardt, 1963).

3.3.2 Characterising neuronal activity at the single-cell level

Characterising RGCs' responses encapsulates the computation of various metrics that can provide useful information, especially when compared statistically among cell types and different experimental conditions. Here, we used white noise stimulation and investigated four main response characteristics: the response polarity, the receptive field, the temporal properties and nonlinearity. In this section, we describe the analysis performed for each characteristic separately.

Response polarity

We examined the response polarity of cells by analysing the temporal profiles of their RF. If a cell is depolarised as light intensity of the stimulus increases, then the filter will exhibit a positive peak right before the spike, that will classify it as an ON cell. Contrarily, a negative peak represents an OFF cell that is depolarised as light intensity of the stimulus decreases. An example of an ON cell is shown in figure 3.10 (b), while an OFF cell can be seen in figure 3.10 (e).

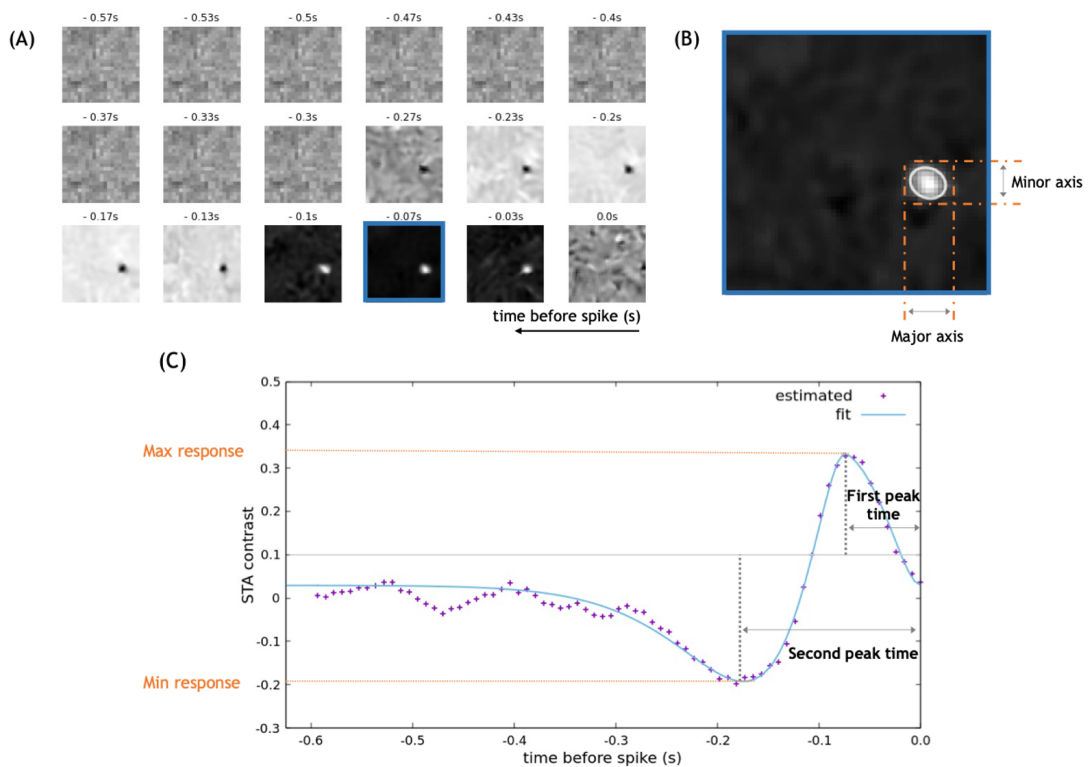


Figure 3.11. Estimating spatio-temporal response properties. (A) STA movie for an ON cell 600ms prior a spike. The frame with the maximal response corresponds to the spatial profile of the RF (blue frame). (B) The spatial RF obtained from (A), was fitted with an ellipse around the centre with 1 SD of the Gaussian fit. (C) Temporal profile of the same cell. Purple dots represent the estimated time course at the centre of the RF, while the blue line is the fitting curve (equation 3.1).

One should, however, keep in mind that the STA is not well suited for identifying ON-OFF cells. Such cells respond equally to the onset and offset of a stimulus, whereas the averaging of the STA suppresses such behaviour (Gollisch et al., 2008; Shi et al., 2018).

Temporal properties

We assessed the temporal properties of cells by analysing the temporal profiles of their RF. Each profile was obtained as the contrast value of the RF centre 600ms preceding a spike and fitted as defined in (3.1). We then computed several temporal characteristics, such as the first peak's and the second peak's (if any) time and amplitude. Figure 3.11 (B) shows these characteristics on the temporal trace of an ON cell. In addition, we computed the biphasic index (BI), i.e. the absolute ratio of the second peak (Fig. 3.12 blue triangle) to the first peak (Fig. 3.12 purple triangle) amplitude. A BI value closer to 0 indicates a monophasic filter (the cell doesn't have a second peak), while a value larger than 0 signifies a biphasic filter (the cell exhibits a second peak). Examples of an OFF monophasic and an OFF biphasic filter are illustrated in figure 3.12. Typically, biphasic features are seen as a measure of the cell's transience.

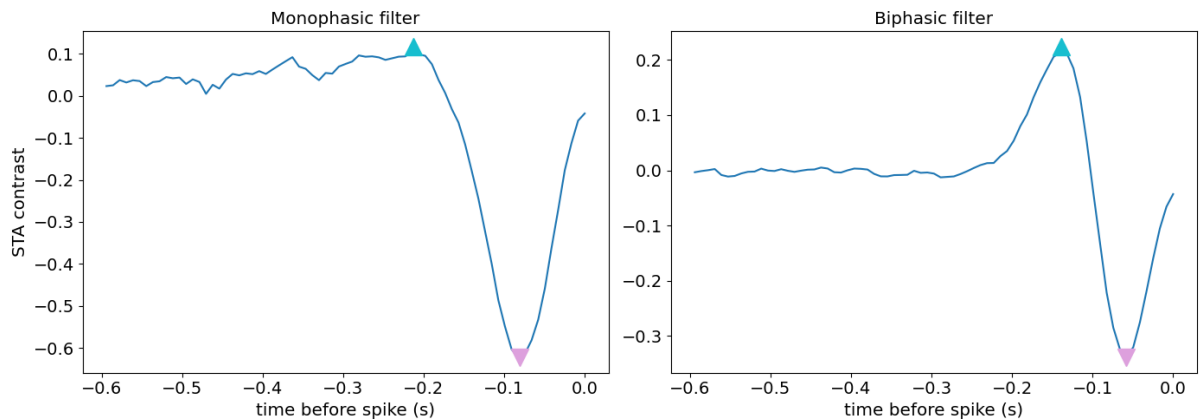


Figure 3.12. Estimating the biphasic index of the temporal profile. Temporal filters for an OFF-monophasic RGC (left) and an OFF-biphasic RGC (right). The BI for the monophasic filter is 0.1, while for the biphasic filter is 0.66.

Spatial properties

We examined the spatial properties of cells by analysing the spatial profiles of their RF. Each profile was obtained by fitting a 2D Gaussian to the temporal frame with the maximal response and then fitting an ellipse around the centre with 1 SD of the Gaussian fit. We then computed spatial properties, such as the RF location (centre of the ellipse), RF diameter (major and minor axis of the ellipse), angle and RF eccentricity. (Fig. 3.11 (C)). The eccentricity is given by $e = \sqrt{1 - \frac{b^2}{a^2}}$, where b is the length of the semi-minor axis of the ellipse and a is the length of the semi-major axis of the ellipse. Eccentricity shows how much the ellipse varies from being circular.

Nonlinearity

We approximated the response nonlinearity N using a sigmoid function (equation 3.2) and we focused on nonlinearity properties, such as baseline (β), the peak (α), the slope (γ) and the threshold (θ , the point where sigmoid reaches half activation) (Fig. 3.13). The peak of the sigmoid corresponds to the maximum firing rate of the neuron, the slope is the sensitivity of the neuron to fluctuations of the voltage (linear estimate) and the threshold determines the spike rate in the absence of net visual stimulation.

The parameters γ and θ mainly quantify the nonlinearity represented in the sigmoid function.

3.4 Results

Let us now turn to the findings which emerged from the data analysis presented in the previous section. We analysed 164 cells collected from 3 Grik4 retinas and 378 cells collected from 5 Scnn1a retinas. We used the LN model, which models the cell's response using a linear filter followed by a static non-linear function. The linear filter was estimated using the STA (see

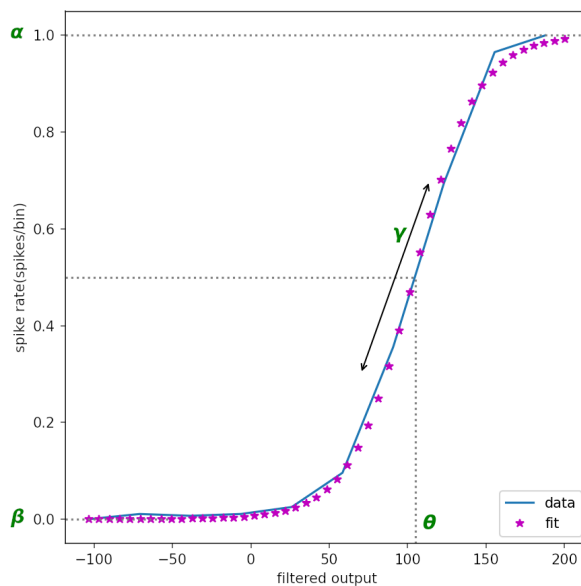


Figure 3.13. Estimating the parameters of the nonlinearity. The response nonlinearity is approximated using a sigmoid function. Blue line corresponds to the estimated nonlinearity and purple dots to the sigmoid fit.

3.3.1) and the non-linear function was approximated by comparing the STA-filtered output to the recorded cells' spike counts (see 3.3.1). Next, we computed multiple response characteristics based on these functions; namely, the response polarity, receptive field, temporal properties and nonlinearity for each cell (see 3.3.2).

We first classified Grik4- and Scnn1a-expressing RGCs (section 3.4.1) and then we characterised and compared their responses to the shifted white noise stimulus (section 3.4.2) in CTL and CNO conditions.

3.4.1 Cell classification

Classification of RGCs relies on several cell features, such as anatomy, physiology, molecular properties, etc. and it still remains a challenging task. Here, we adopted a pragmatic approach inspired by the most basic classification scheme, introduced by Hartline in 1938, that characterises a RGC as ON, OFF, ON-OFF or OFF-ON cell, based on its response to variations of light (Hartline, 1938). Previous studies have identified these functional cell types based on the shapes of the spike-triggered average (Segev et al., 2006), or on specific features through spike-triggered covariance (Ahn et al., 2020).

In this thesis, we employed the former method and we obtained the spatio-temporal profiles for the RGCs in our data pool. We filtered out cells with a noisy STA manually. Basically, we considered cells with valid STAs in both CTL and CNO conditions. After this pre-processing, we ended up with 67 Grik4 cells and 51 Scnn1a cells. Finally, we classified the remaining RGCs according to their response polarity (ON or OFF, see 3.3.2) and the biphasic index of their

temporal profile (see 3.3.2). We remind that the BI is the absolute ratio of the second peak to the first peak amplitude. We set the threshold of BI at 0.4 (arbitrarily chosen), meaning that cells with a BI smaller than this value are considered monophasic, whereas cells with a BI larger than 0.4 are classified as biphasic. According to these criteria, four functional types emerged; namely, ON monophasic, ON biphasic, OFF monophasic, OFF biphasic.

Four Grik4 RGCs were selected as representatives of the different types. Figure 3.14 shows the spatio-temporal profiles and the non-linearities of these cells in CTL conditions, obtained by fitting the LN model on their responses to SWN stimulus.

3.4.2 General response characterisation

We aimed to characterise RGCs based on multiple response properties not only to explore the general behaviour of the identified cells but also to investigate the effect of CNO at the single-cell level. For this purpose, we estimated the response polarity, spatial and temporal properties and nonlinearity for RGCs that showed a valid STA in both CTL and CNO conditions. Then, we undertook systematic statistical comparison of these properties and investigated the effects induced by CNO activation.

Before presenting the results of this analysis, let us briefly remind the underlying mechanism of excitatory DREADD activation and its expected effects on the response of a RGC. CNO activation leads to an increase of intracellular concentration of free calcium which leads to membrane depolarisation. Consequently, the ionic diffusion across the cell membrane through ion channels increases and this in turn affects the permeability and electrical conductance of these channels to the respective ions. A larger conductance would yield a shorter time constant, which would make the cell faster. To sum up, we expect that DREADD activation would have two direct effects on a cell's response: 1) Increase of the baseline activity 2) Decrease of the time constant. This means that the cell would become more active and respond faster to a visual stimulus. However, RGCs are embedded in a network, receiving synaptic inputs from many presynaptic neurons, including ACs. As we have seen in Section 3.2, DREADDs are also expressed in ACs, thus CNO activation has a direct impact on their response and a potential indirect effect on RGCs response. Assuming that a RGC receives input from DREADDs-expressing inhibitory ACs and does not express DREADDs itself, we expect to notice a decrease in the baseline activity of its response and perhaps an increase in the time constant, meaning that the cell will become more sluggish. If, though, this RGC is also susceptible to CNO, the reinforced inhibitory effect of the ACs competes with the direct effect of CNO activation on the RGC's response. In this scenario, the net effect of CNO might vary widely, as further developed in this thesis.

Response polarity

Grik4 RGCs were almost equally ON and OFF cells, while Scnn1a RGCs were mostly ON cells (Fig. 3.15). We investigated whether the response polarity changes under CNO influence for

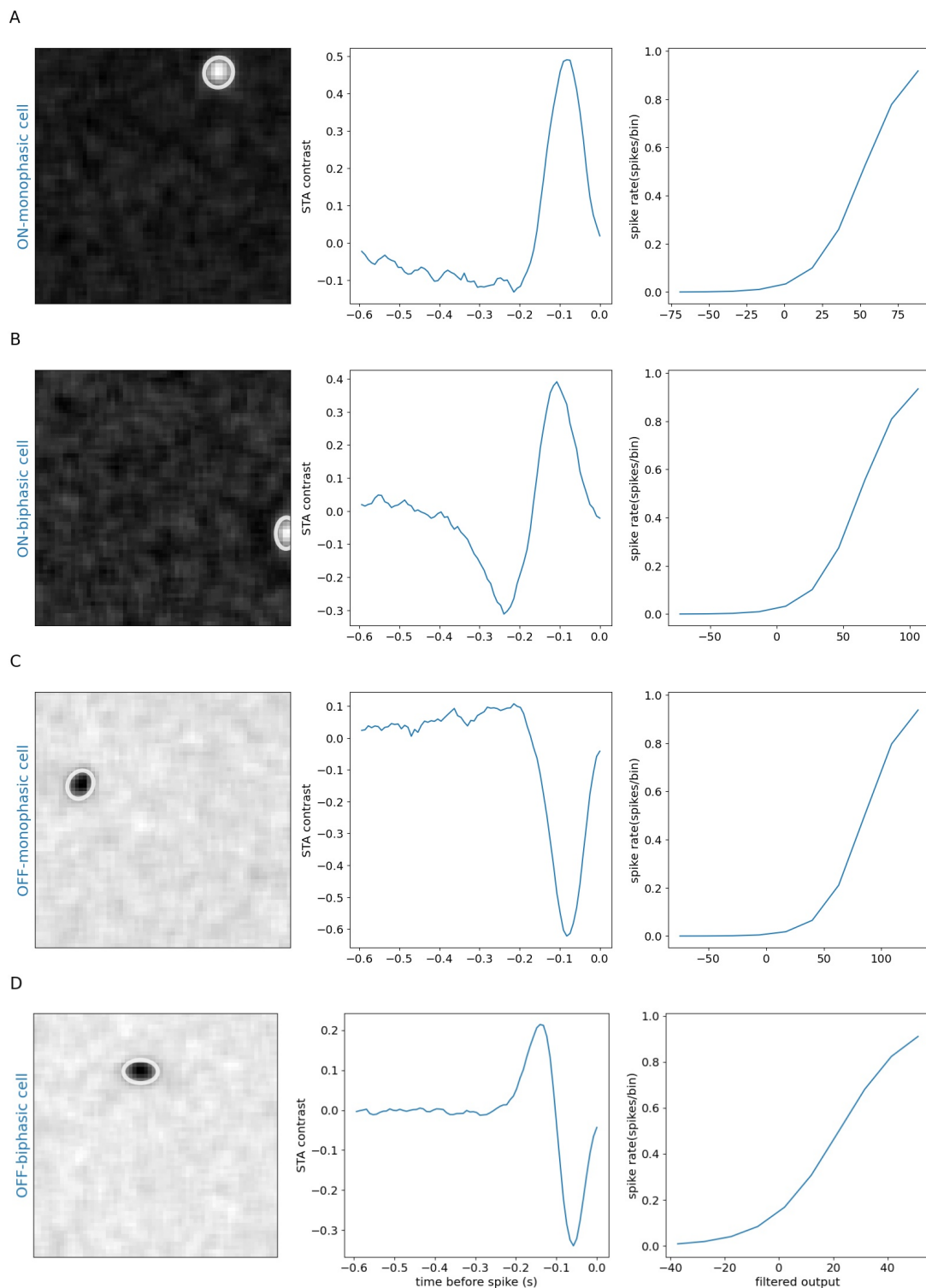


Figure 3.14. Spatio-temporal profiles and non-linearities of the selected ganglion cells. (A & B) ON cells - top monophasic filter, bottom biphasic filter. (C & D) OFF cells - top monophasic filter, bottom biphasic filter. For each cell type three panels show from left to right: the spatial filter, the temporal profile and the nonlinearity.

each group. For the Grik4 cells we did not observe any change, while for the Scnn1a we found 1 cell out of 51 that switched polarity from OFF to ON (Fig. 3.16). A possible explanation

could be that the activity of this cell is modulated by an amacrine cell. Indeed, it has been shown experimentally that a RGC can switch from one response type to another, and specifically from OFF to ON, due to the depolarisation of nearby wide-field amacrine cells (Geffen et al., 2007).

	#Grik4 cells		#Scnn1a cells
On-monophasic	16	On-monophasic	4
On-biphasic	18	On-biphasic	30
Off-monophasic	21	Off-monophasic	11
Off-biphasic	12	Off-biphasic	6

Figure 3.15. Number of RGCs per functional type in Grik4 and Scnn1a retinas.

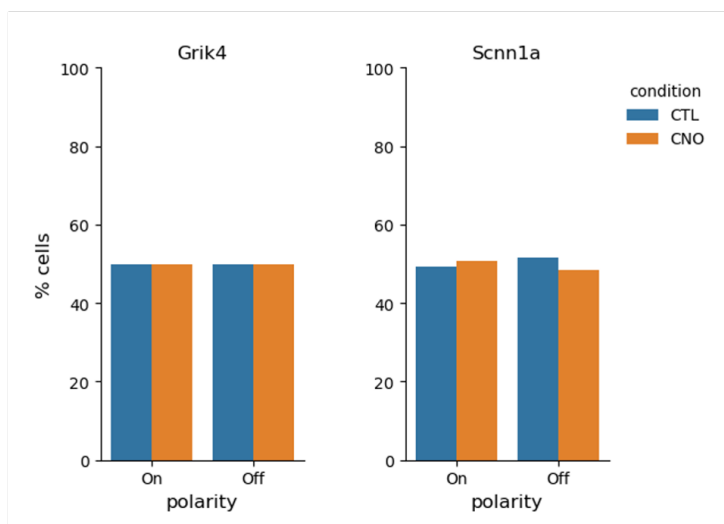


Figure 3.16. Change of RGCs polarity in CTL and CNO conditions. *Left.* Grik4 cells *Right.* Scnn1a cells.

Temporal properties

First, we examined the average temporal responses per cell type and compared them in the different experimental conditions. Figures 3.17 and 3.18 show the average response in CTL condition (top panel, blue line) and in CNO condition (middle panel, orange line) per cell type in Grik4 and Scnn1a cells respectively. In both panels, we also illustrate the standard deviation (peach error bars). Finally, the third panel of each figure compares the two average temporal responses.

For the Grik4 cells (Fig. 3.17), we generally noticed a slight increase in amplitude and a positive shift in time of their responses. Specifically, the ON-biphasic and ON-monophasic cell types exhibit a positive shift in time (increase in time constant, cells become more sluggish), but an insignificant increase in the amplitude of the response. In the latter case, the effect in

amplitude is even negligible. In addition, no significant effect was found in the OFF-biphasic cell type. Interestingly, the OFF-monophasic cell type shows a clear shift in time and an increase in amplitude.

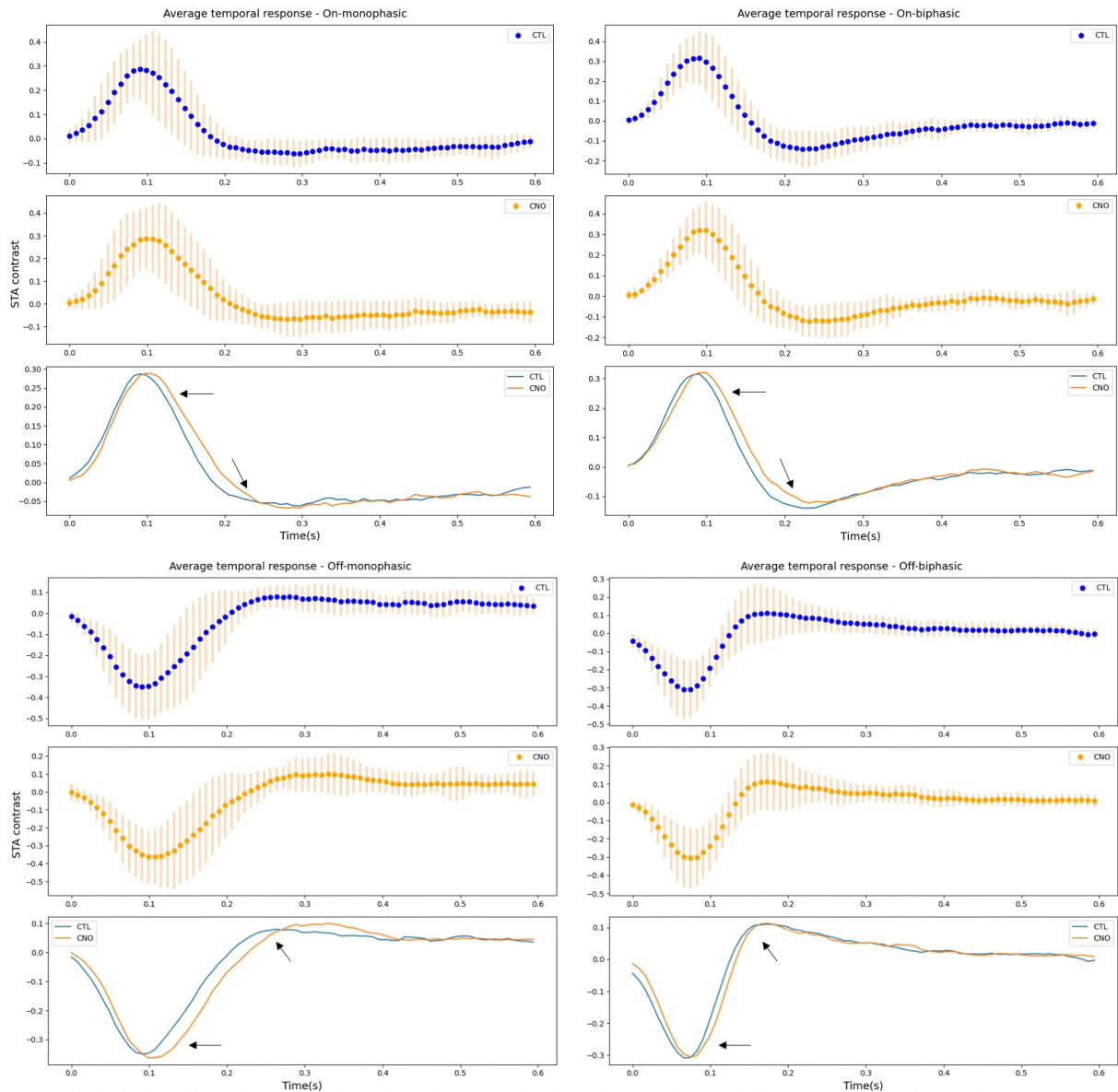


Figure 3.17. Assessing the average temporal responses of Grik4 ON and OFF cell types in CTL and CNO conditions. *Top left.* ON-monophasic cell type. *Top right.* ON-biphasic cell type. *Bottom left.* OFF-monophasic cell type. *Bottom right.* OFF-biphasic cell type. For each cell type three panels show from top to bottom: the average response in CTL condition (blue line) and the standard deviation (peach error bars), the average response in CNO condition (orange line) and the standard deviation (peach error bars), a comparison of the average traces in CTL and CNO conditions. Arrows point out the differences in the first and second peak of the responses.

For the *Scnn1a* cells (Fig. 3.18), we observed diverse patterns of the CNO effect. No significant differences were found between CTL and CNO conditions for both OFF cell types, whereas the ON types are shown to be more affected. In particular, the ON-biphasic cell type

showed a similar effect to ON-biphasic Grik4 cell type, meaning a slight increase in the amplitude and a positive shift in time. The more striking effect of CNO was on the ON-monophasic type, where we noticed a decrease in the amplitude of the response along with a slight positive shift in time.

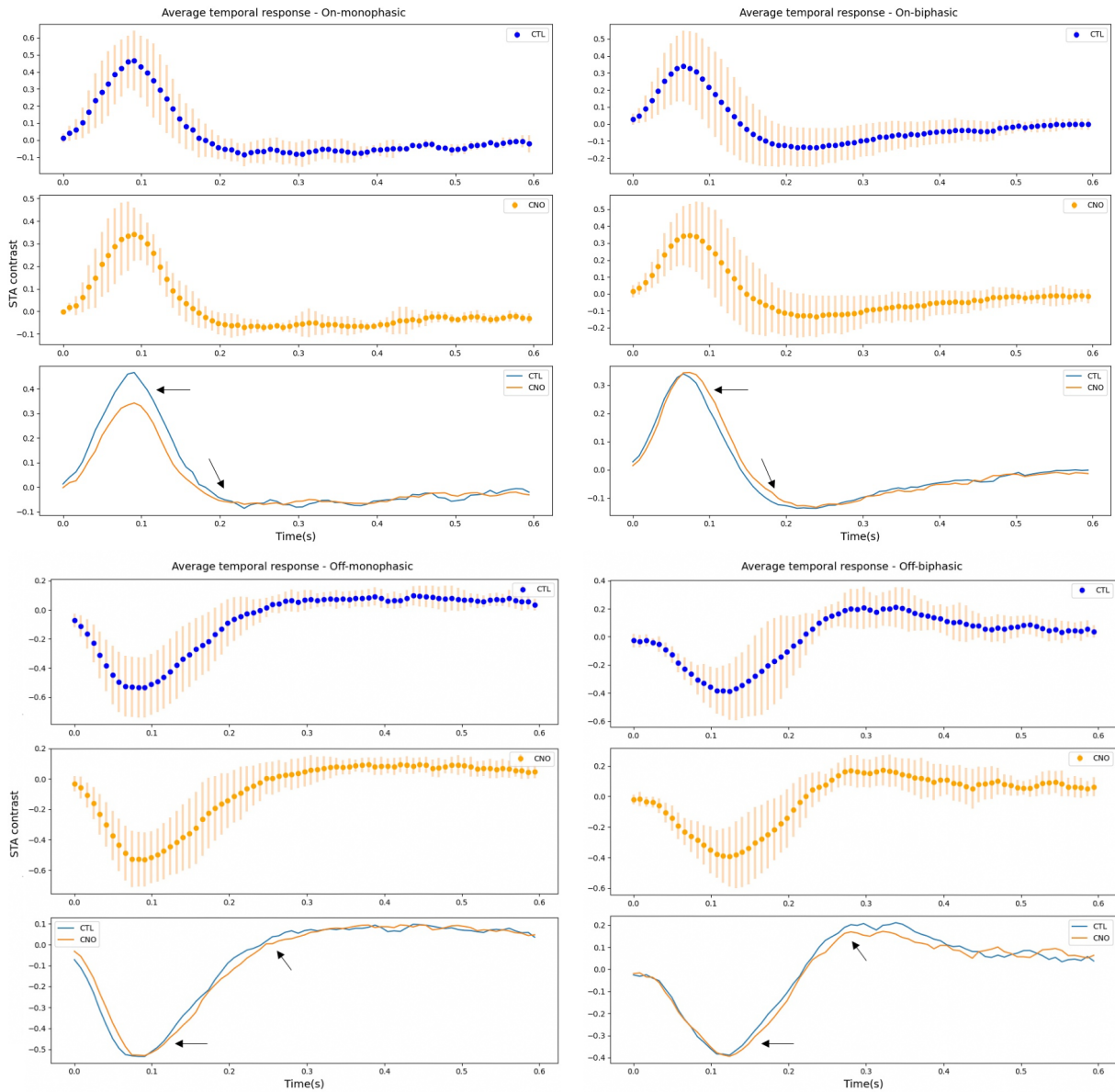


Figure 3.18. Assessing the average temporal responses of Scnn1a ON and OFF cell types in CTL and CNO conditions. Same as Fig. 3.17.

Even though investigating the average temporal responses underlined noteworthy effects, it's possible that this analysis also hid significant features of the individual cell responses in CNO condition. The high standard deviation in some cell types (e.g Fig 3.17 On-monophasic or Off-monophasic) further support this idea. To better determine and quantitatively assess the effects of CNO, we also computed several characteristics on the temporal response of each cell and we compared them in CTL and CNO conditions per functional type (see 3.3.2). A scatterplot

was drawn for each temporal property, where the horizontal axis is its value in CTL condition and the vertical axis is its value in CNO condition. Whenever possible, a linear regression model (y equals x) was also fitted and the resulting regression line was plotted with a 95% confidence interval for that regression. Figures 3.19 and 3.20 present these relations for Grik4 and Scnn1a cells respectively.

Grik4 cells' (Fig. 3.19) temporal characteristics show potentially similar effects to what we observed in the average traces. Yet, in many cases there are many outliers that did not allow the identification of a clear trend. The ON-monophasic cells (first column) exhibit a slight increase in the amplitude and time of the first peak (similar to the average trace in figure 3.17 top left panel), whereas they show diverse patterns with regards to the second peak. In contrary, the ON-biphasic cells' (second column) first peak may vary in terms of amplitude and time, while the second peak shows a significant tendency to increase its amplitude and time (similar to the average trace in Fig. 3.17 top right panel). Next, the OFF-monophasic cells (third column) show mostly a decrease of the first peak's amplitude and an increasing effect on the second peak's amplitude (similar to the average trace in figure 3.17 bottom left panel). However, the times of these peaks appear to be increasing, decreasing or staying the same. Lastly, the OFF-biphasic cells (last column) demonstrate an insignificant change in the amplitude of both peaks, as expected from the average trace (Fig. 3.17 bottom right panel) and a slight positive shift of their response with regards to both peaks, except few outliers.

Then, we explored how the temporal characteristics of Scnn1a cells' responses change between CTL and CNO conditions. The ON-monophasic cells (first column) exhibit a decrease in their amplitude (in accordance with the average traces Fig. 3.18 top left panel), except one cell. The rest of the scatter plots did not allow us to conclude in a clear tendency, partially due to the limited number of cells in this type. The ON-biphasic cells (second column) show a positive shift in time, yet there were cells with negative shift or no shift at all. The amplitude of both peaks appears to change in diverse ways. Next, the OFF-monophasic cell (third column) exhibit diverse patterns in the first peak's amplitude and mostly a slight decrease in the second peak's amplitude. Interestingly, this cell type seems to clearly become slower in CNO condition, as most of the cells increase the time of their first peak. No specific trend could be identified for their second peak time. Finally, the OFF-biphasic cells (last column) do not show a similar tendency as in the average traces (Fig. 3.18 bottom right panel). To conclude, all temporal properties can either remain unchanged, increase or decrease, in contrast to what would be expected in case of a direct effect. We suspect that this is due to a network effect, although there is a lot of noise in the data.

So far, our exploratory analysis has emphasised the variability of the effect of CNO on the RGCs responses within the same type. In some cases, the change of the temporal characteristics agreed with the patterns observed in the average traces. Yet, we noticed that multiple characteristics could increase, decrease or remain unchanged within the same cell type. For this reason, we manually checked the individual responses per type, considering the relatively small number of cells. As expected, the temporal responses varied largely within the same cell type between

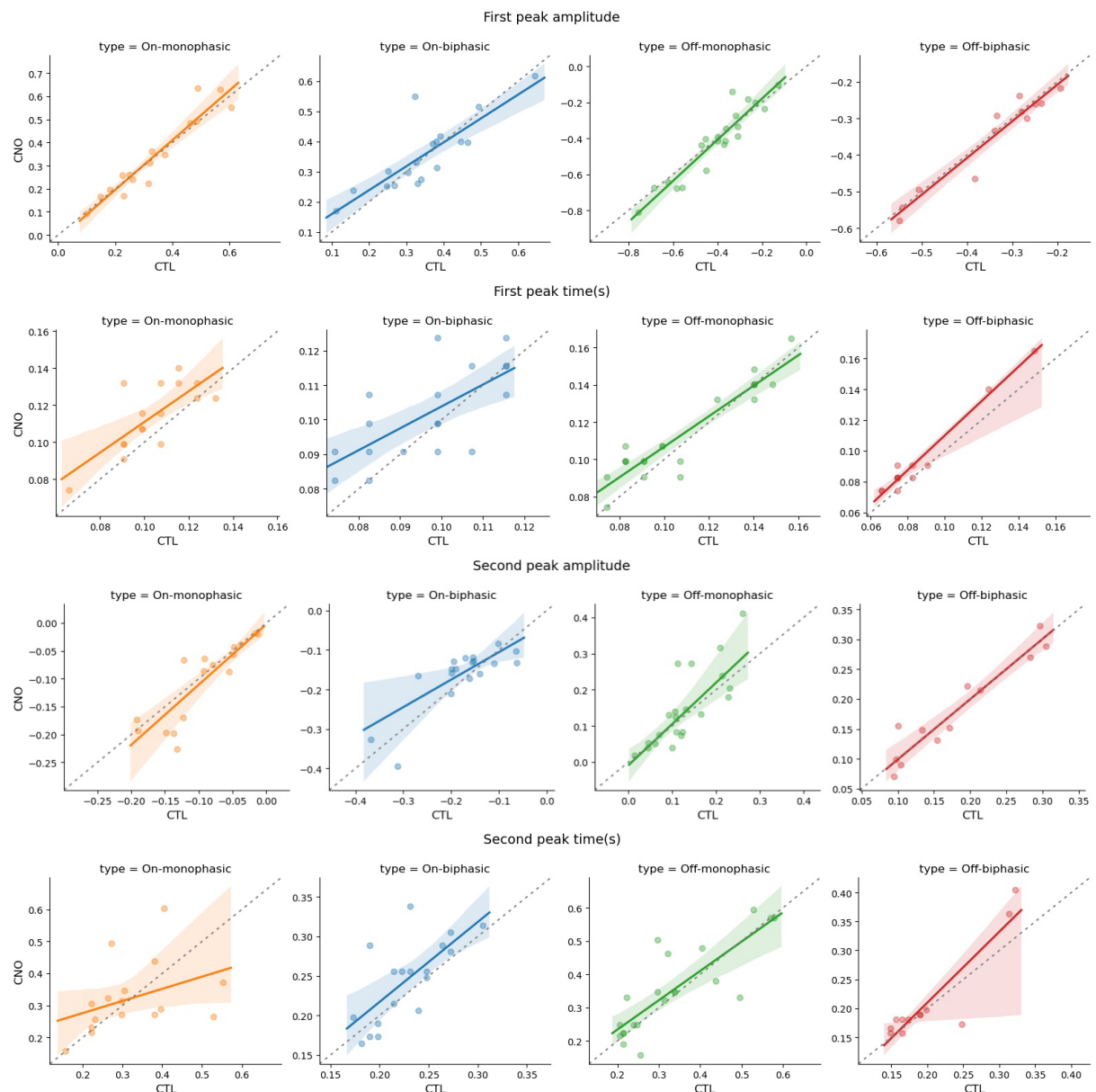


Figure 3.19. Investigating the temporal properties of Grik4 cells in CTL and CNO conditions. *First row.* First peak amplitude. *Second row.* First peak time. *Third row.* Second peak amplitude. *Final row.* Second peak time. For each temporal property a scatter plot is drawn, where the vertical axis is its value in CTL condition and the horizontal axis is its value in CNO condition. Whenever possible, a linear regression model (y equals x) is also fitted and the resulting regression line is plotted with a 95% confidence interval for that regression.

the two experimental conditions.

Figures 3.21 and 3.22 illustrate this diversity for the Grik4 ON cell types. Specifically, cell (A) (Fig. 3.21) exhibits a similar CNO effect as the average trace, probably reflecting the direct effect of CNO activation on the cell's response. Cell (B) (Fig. 3.21) shows a similar effect, an increase on the first peak but a decrease on the second negative peak. Finally, cell (C) (Fig. 3.21) seems to be affected quite differently, decreasing the amplitude of its response under CNO

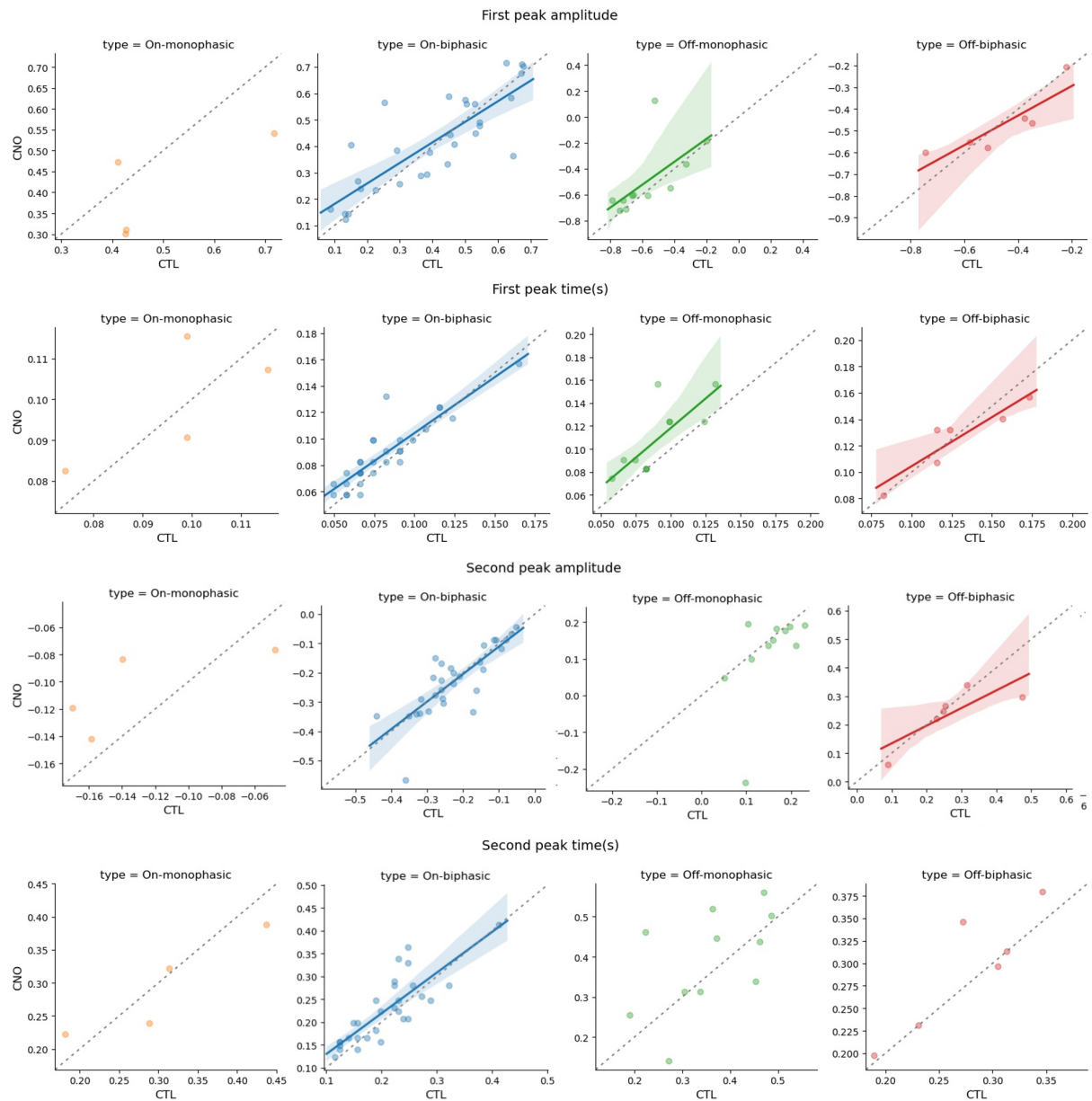


Figure 3.20. Investigating the temporal responses of Scnn1a cells in CTL and CNO conditions. Same as Fig. 3.19.

activation. This could be possibly explained by DREADD ACs making synaptic connections with this particular cell, thereby causing a strong inhibition when activated by CNO. For the ON-biphasic cells (Fig. 3.22), we noticed quite diverse patterns compared to the average trace. Cell (A) tends to be more biphasic, cell (B) becomes more monophasic and cell (C) shows an opposite effect than the average trace.

For the Scnn1a cells, the ON-biphasic type shows quite diverse patterns of the CNO effect (Fig. 3.23). In this figure, cells (A) and (B) increase their activities but with quite different shapes, while cells (C) and (D) decrease their activities with the latter to slightly shift its temporal response (becoming slower).

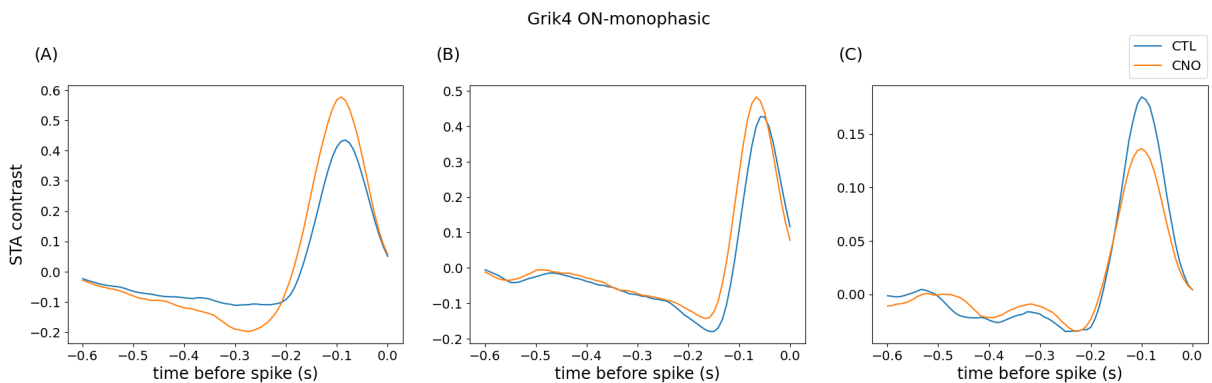


Figure 3.21. Temporal profiles of three Grik4 ON monophasic cells exhibiting diverse effects under CNO activation.

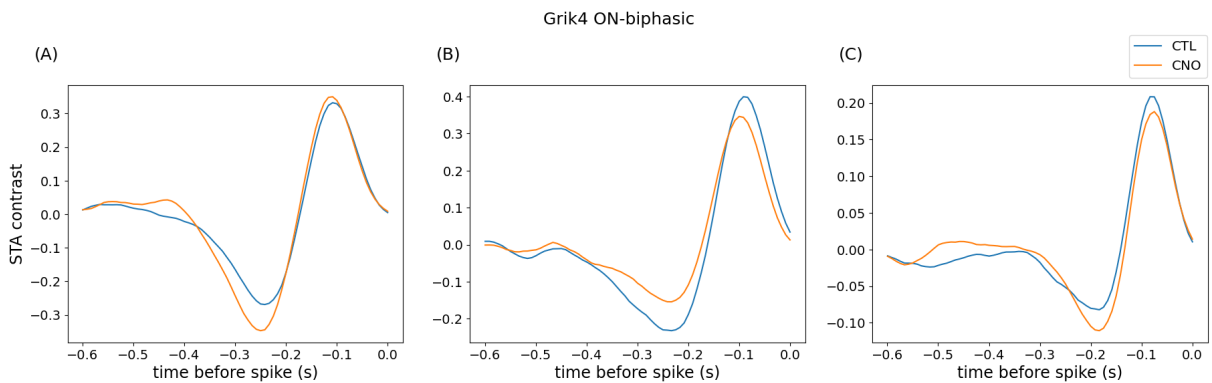


Figure 3.22. Temporal profiles of three Grik4 ON biphasic cells exhibiting diverse effects under CNO activation.

Finally, we identified two OFF-monophasic cells with interesting response patterns in CNO condition (Fig. 3.24). Cell (A) becomes biphasic, while cell (B) exhibits a change in the polarity and modality, becoming ON-biphasic.

Taken together, these findings highlight the breadth of RGC's temporal responses in CNO condition and implicate the role of network contribution as a potential underlying mechanism. We remind that the cells used for this analysis express the DREADD receptors, so it may be assumed that they fall into scenarios 2 or 4 of figure 3.7. Yet, we observed that the effect of CNO-induced activation varies substantially and we cannot clarify it only by analysing the RGCs' responses.

Spatial properties

The next step of our analysis was the characterisation of the cells' spatial properties based on the spatial profile of their RF, which was obtained by fitting a 2D Gaussian to the temporal frame with the maximal response. For each cell, we computed the characteristics of a fitted ellipse around the centre with 1 SD of the Gaussian fit (see 3.3.2). The population distribution of the RF

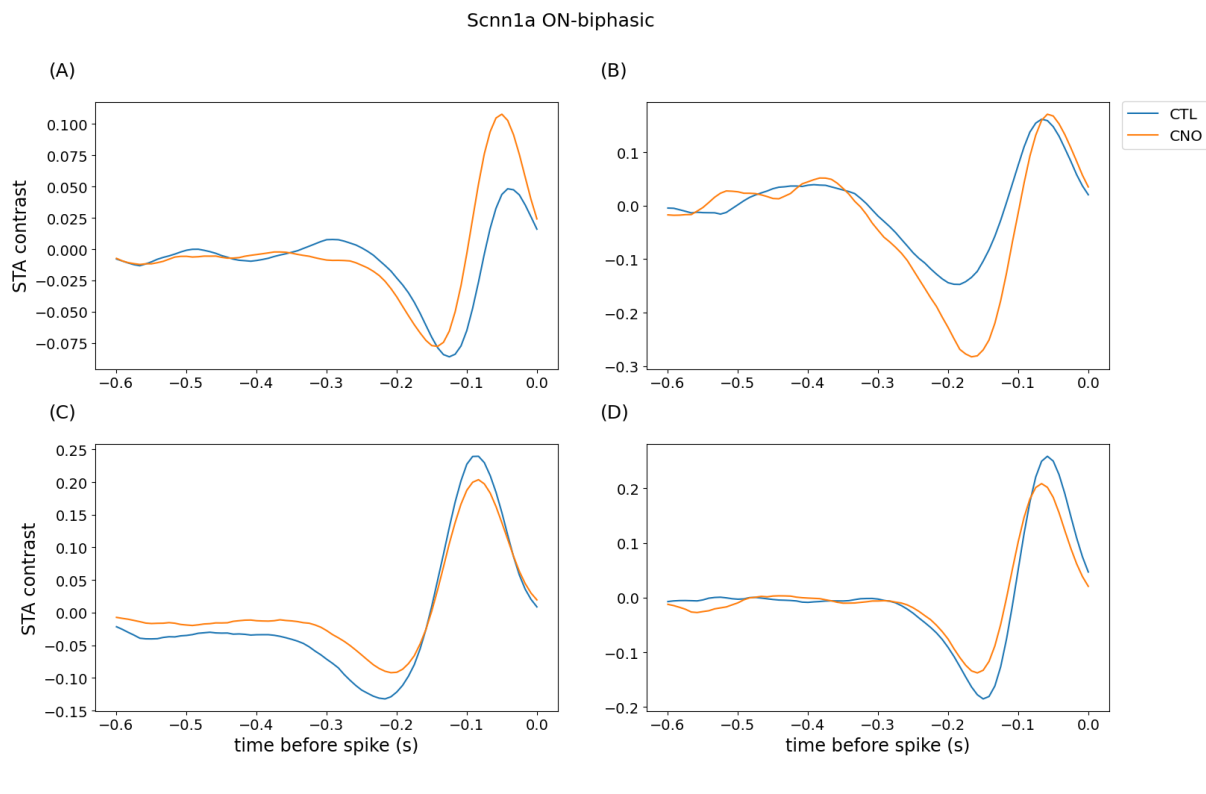


Figure 3.23. Temporal profiles of four *Scnn1a* ON biphasic cells exhibiting diverse effects under CNO activation.

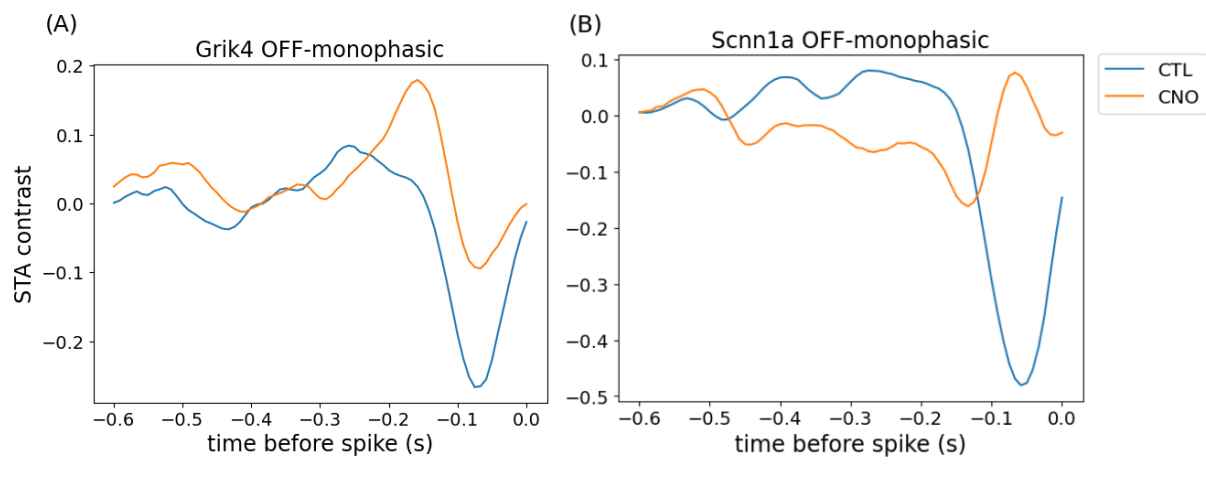


Figure 3.24. Temporal profiles of two ON monophasic cells exhibiting diverse effects under CNO activation. *Left*. *Grik4* OFF-monophasic cell changing modality and becoming biphasic *Right*. *Scnn1a* OFF-monophasic changing polarity and modality and becoming ON-biphasic.

sizes (major and minor axis of the fitted ellipse) per functional type ranged between 50 to 300 μM and is shown in Figure 3.25.

Next, we compared the spatial characteristics between CTL and CNO conditions in a similar fashion as the temporal characteristics. A scatterplot was drawn for each spatial property, where the horizontal axis is its value in CTL condition and the vertical axis is its value in CNO

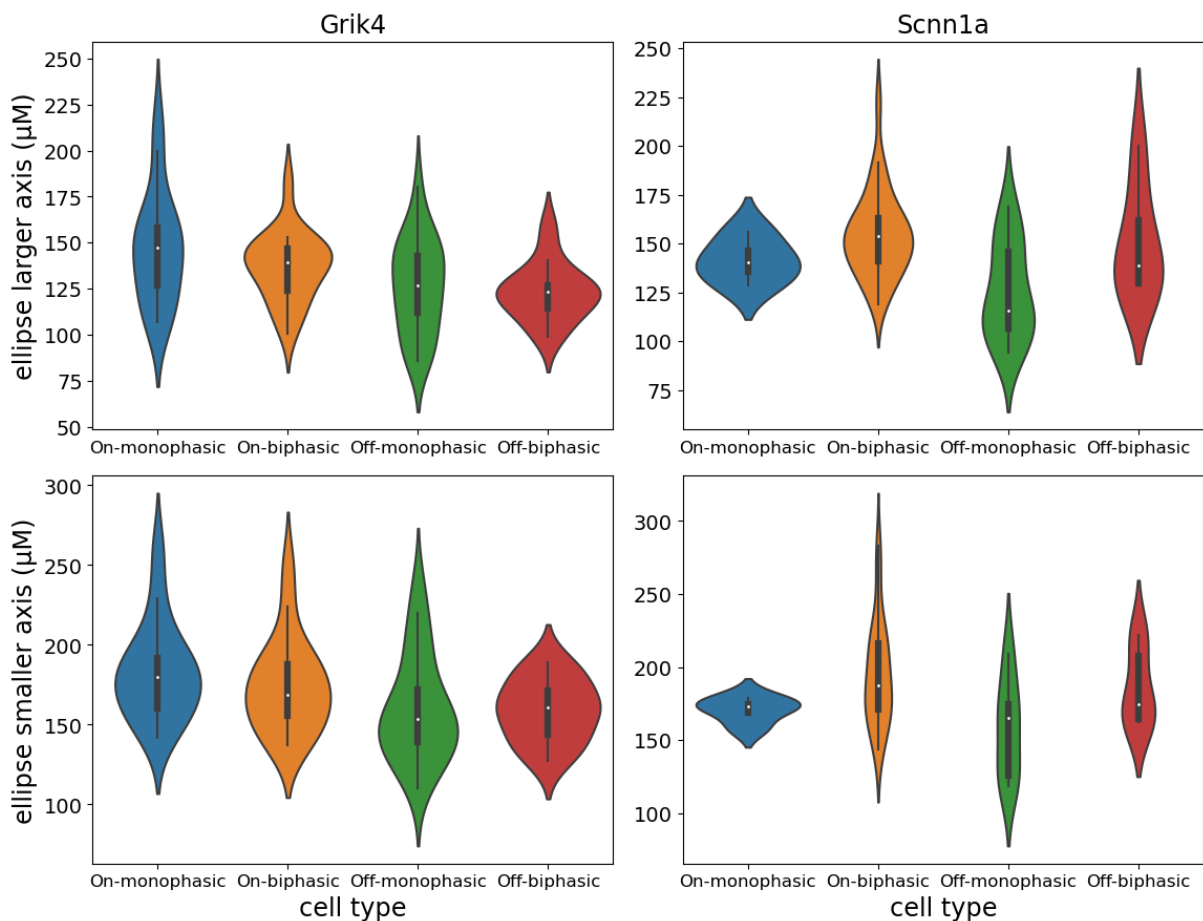


Figure 3.25. Population distribution of the RF sizes per functional type. RF sizes in CTL (top row) and CNO (bottom row) conditions for Grik4 (left column) and Scnn1a (right column) cells

condition. Whenever possible, a linear regression model (y equals x) was also fitted and the resulting regression line was plotted with a 95% confidence interval for that regression. Figures 3.26 and 3.27 present these relations for Grik4 and Scnn1a cells respectively.

Grik4 cells' spatial properties (Fig. 3.26), demonstrate a great variety in the CNO effects. The ON-monophasic cells (first column) appear to increase the minor axis of the fitted ellipse, whereas the major axis may increase, decrease or remain unchanged. It is interesting to note that the eccentricity generally increases under CNO activation, meaning that the cell obtains a more circular RF. The ON-biphasic cells (second column) show diverse patterns in all properties, except the angle of the fitted ellipse which seems to be increasing in CNO condition. Lastly, the OFF types (third and last column) also exhibit variability in the spatial properties, with the monophasic type to show less change in the ellipse's major axis and the biphasic type to change insignificantly in terms of the ellipse's minor axis.

Turning now to the Scnn1a cells' spatial properties (Fig. 3.27), we first note that three out of four cells in the On-monophasic type (first column) seem to be affected in a similar way as far as it concerns the ellipse's smaller axis, angle and eccentricity. We remind that we

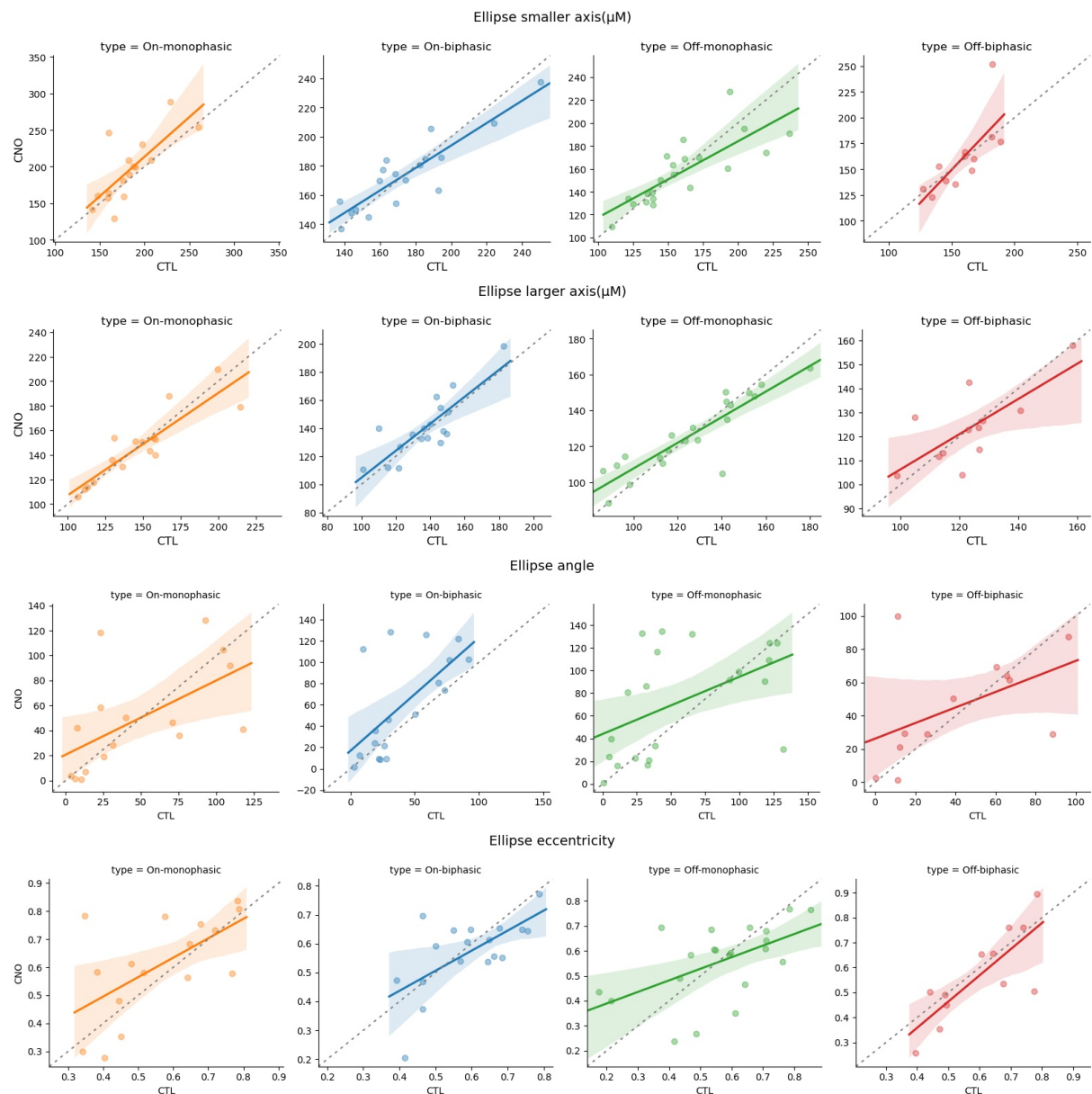


Figure 3.26. Investigating the spatial characteristics of Grik4 cells in CTL and CNO conditions. *First row.* Ellipse smaller axis *Second row.* Ellipse larger axis *Third row.* Ellipse angle *Final row.* Ellipse eccentricity. For each spatial property a scatter plot is drawn, where the vertical axis is its value in CTL condition and the horizontal axis is its value in CNO condition. Whenever possible, a linear regression model ($y = x$) is also fitted and the resulting regression line is plotted with a 95% confidence interval for that regression.

observed a similar effect in the analysis of the temporal properties, where three cells were found to be affected similarly under CNO activation. The ON-biphasic cells (second column) exhibit great diversity, except the smaller axis which seems to be mostly remaining unchanged. Next, the OFF-monophasic type (third column) tends to obtain a more circular RF (increase of the eccentricity) and a greater angle of the fitted ellipse. Finally, the OFF-biphasic type's (last column) RF generally decreases.

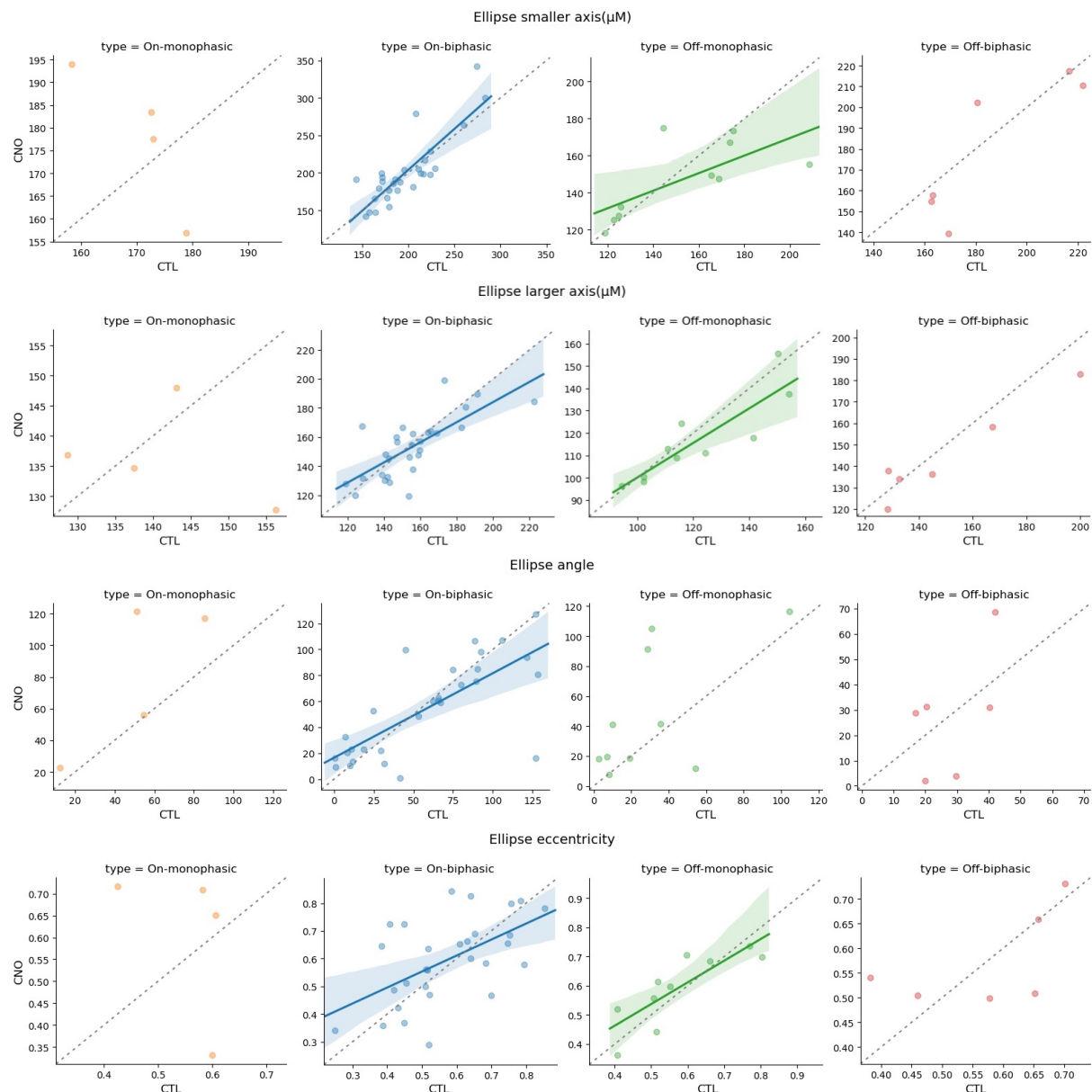


Figure 3.27. Investigating the spatial characteristics of Scnn1a cells in CTL and CNO conditions. *First row.* Ellipse smaller axis *Second row.* Ellipse larger axis *Third row.* Ellipse angle *Final row.* Ellipse eccentricity. For each spatial property a scatter plot is drawn, where the vertical axis is its value in CTL condition and the horizontal axis is its value in CNO condition. Whenever possible, a linear regression model ($y = x$) is also fitted and the resulting regression line is plotted with a 95% confidence interval for that regression.

Taken as a whole, this analysis did not reveal any specific patterns of the CNO effect on the spatial properties, it rather reinforced the existence of various shapes within the same cell type.

Nonlinearity

First, we filtered out cells for which we could not obtain the nonlinear function, we then fitted a sigmoid function to the computed output function (see 3.3.2) and we compared its characteristics

in CTL and CNO conditions for each cell. Figure 3.28 shows the nonlinear properties of Grik4 cells in CTL and CNO conditions. The threshold (eq. 3.2) of the sigmoid changes in different ways for all cell types, except for the OFF-biphasic. In the former case, this basically means that CNO activation may increase or decrease the spontaneous activity of the cells. Moreover, the slope (eq. 3.2) for the ON-monophasic, ON-biphasic and OFF-monophasic types has a tendency to decrease, which means that the cells become more sensitive to large fluctuations of the filtered signal and consequently, they need a higher input voltage in order to fire. The OFF-biphasic cell's slope did not exhibit any significant change. For the Scnn1a we were unable to compare these properties, as we had very few cells after the filtering.

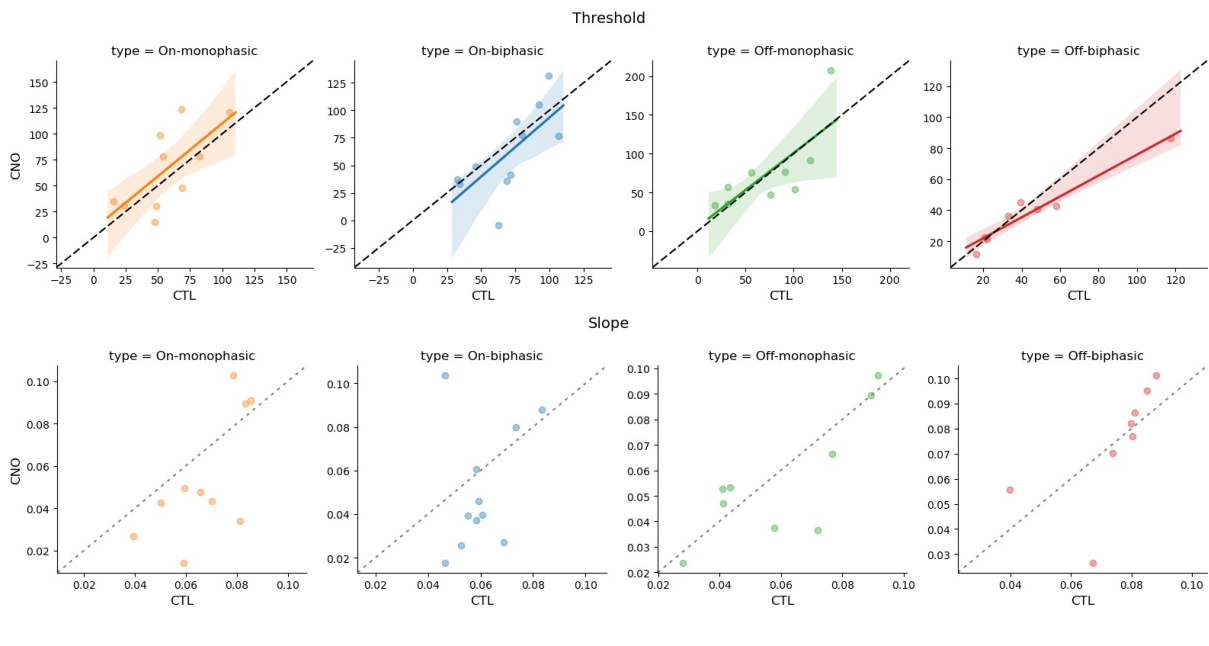


Figure 3.28. Assessing the nonlinear properties of Grik4 cell types in CTL and CNO conditions.

3.5 Summary and Discussion

This chapter presented complementary experimental and theoretical approaches to characterise the functional properties of specific RGCs types. On the experimental side, our colleagues have successfully identified RGCs sharing either Grik4 or Scnn1a gene expression and unequivocally characterised their anatomical and functional features by combining excitatory DREADD activation, MEA recordings and immunohistochemistry. On the theoretical side, we further investigated the responses of these RGCs subgroups in CTL and CNO conditions using white noise stimulation. To do so, we pursued three goals (see section 3.3). Based on LN model analysis, we first explored four main response characteristics: the response polarity, the receptive field, the temporal properties and nonlinearity (first goal) and then, we compared their differences across the given conditions (second goal). Finally, by fitting experimental data with the LN

model we extracted parameters that will constrain our retina model in the later chapters (third goal). Both approaches focused on analysing RGCs response properties at the single-cell level, yet, network contributions arguably already manifest at this scale.

We would like now to discuss some points regarding the methodology and findings presented in this chapter.

What is the effect of CNO activation at the single-cell level?

Throughout our analysis, we observed great variability in the effect of DREADD activation with CNO not only across different RGC types, but also within the same RGC type.

Starting from the response polarity, we found one Scnn1a cell that switched its polarity from OFF to ON. Given the number of cells analysed (67 Grik4 and 51 Scnn1a cells) this might not be statistically significant. However, we believe it's a compelling effect and can be attributed to ACs. In particular, Geffen et al., 2007 have proposed that a RGC can switch polarity from OFF to ON due to the depolarisation of nearby wide-field ACs. In our case, these potential ACs perhaps express DREADDs, thereby depolarising in the presence of CNO, thus leading to the observed effect.

Assessing the temporal and spatial features of the RF of the RGCs, the basic element of retinal information processing, demonstrated the wide range of CNO effect. On the temporal side, averaging the temporal responses per cell type showed that CNO mainly slows down RGCs and may increase or decrease their activity. Further examining the temporal features, emphasised the variability of the CNO effect across cell types and interestingly, revealed that this diversity is reflected even within the same cell type. These findings come in contrast to what was predicted if DREADDs would act only on RGCs and further reinforces our hypothesis that DREADD ACs interact with the RGCs we recorded from. Analysing the spatial properties of the RF did not show any clear trend of CNO activation, but once again, rather emphasised the variability of effects.

To complete our LN model analysis, we assessed the nonlinear properties of Grik4 cell types. The threshold exhibited diverse effects, while the slope for three out of four functional types showed a tendency to decrease. This could mean that cells would need higher input voltage in order to respond. Unfortunately, this analysis was not possible for the Scnn1a cells, as we were not able to compute the nonlinearity for a sufficient number of cells.

Taken as a whole, our data analysis showed that DREADD activation may have a manifold impact on the activity of RGCs, presumably due to the coactivation of DREADD ACs. Examining only the activity changes of RGCs is not sufficient to clarify the situation. It might have been possible if we could record from ACs simultaneously, however, these are very challenging experiments that were not in the scope of this project. Therefore, we will attempt to elucidate the effect of CNO on the RGCs responses using mathematical modelling and simulations. This work will be presented in the next two chapters.

Is the DREADD technology reliable?

DREADD technology has emerged as a popular tool amongst neuroscience researchers, as it allows to manipulate the activity of targeted populations of neurons *in vivo* and dissect neural circuits. Especially for the light-sensitive retina, it appears to be a more appropriate technique compared to optogenetics, because it does not interfere with light stimuli.

In our experiments, DREADDs were not only expressed on the targeted RGCs populations, as initially planned, but they were also found unexpectedly on ACs. This made identifying distinct DREADD RGCs subgroups more challenging, due to increased input inhibition originating from DREADD expressing ACs activated by CNO. For future studies, DREADD expression should be targeted only to RGCs via direct viral transfection rather than using the Cre-lox approach in order to avoid such strong side effects.

Moreover, this tool has drawn criticism for the use of CNO as the DREADD agonist, notably in behavioural studies. Manvich et al., 2018 question the assumption that CNO itself is an inert compound and point out that it is reverse-metabolised in the brain to clozapine, an antipsychotic drug, thereby producing numerous physiological and behavioural effects in rats and mice (although this would have minimal effects on our *in vitro* retinal recordings). Taking into consideration these limitations is thus essential for any study employing this tool.

How accurate does the LN model describe the light responses of neurons?

The LN model is widely used to probe the response properties of RGCs using white noise stimulation e.g. full-field or spatio-temporal white noise. Curiously, its capacity to capture well these characteristics not only depends on the type of stimulus used (Chichilnisky, 2001; Pillow et al., 2008; Schreyer et al., 2020), but also on the cell type (Das et al., 2019). In the context of this thesis, the LN model has been used in two ways: first and foremost, to compute various response characteristics of RGCs (current Chapter 3) and, secondly, to provide a baseline for comparison with our model's performance (Chapter 5).

Although the LN model allowed us to characterise the recorded RGCs in CTL and CNO conditions, it does suffer from a number of flaws. Indeed, despite the fact that the LN model can successfully discriminate between ON and OFF cells, it fails to identify ON-OFF cells. Moreover, it is not able to include nonlinear phenomena e.g. nonlinear integration from presynaptic BCs. These limitations are due to the fact that it compresses the diverse presynaptic inputs to RGCs into a single linear filter (Asari et al., 2012). Possible solutions entail considering multiple linear filters instead of one, or using more elaborated methods such as the spike-triggered covariance (STC). In the latter case, employing a holistic approach by combining STA and STC analysis methods could also allow us to characterise more complex patterns in the RFs. Similarly to Ahn et al., 2020, STC has the potential to reveal different sub-types of mouse RGCs and their physiological implications. In particular, different patterns can be related to either the excitatory

input from BCs or the inhibitory inputs from ACs. Finally, it would be interesting to compare the accuracy of the STA method with full-field and spatio-temporal white-noise.

To evaluate the LN model in terms of generalisation and predictions of responses to novel stimuli and to avoid the risk of overfitting, the model is built with a training set (response to SWN) and the response to a test set (response to full field) is predicted. This will be discussed in Chapter 5.

Perspectives

Towards a comprehensive data analysis So far, we have analysed the functional properties of Grik4 and Scnn1a RGCs using diverse stimuli. Chirp and moving bars were used to classify RGCs, whilst SWN was used to characterise multiple response characteristics. Due to practical constraints, this thesis did not engage with a comprehensive RGC characterisation across the various stimuli used in the experimental setup. Nevertheless, further analysis should be done to investigate whether these RGC types exhibit the same properties using different stimuli. Preliminary results indicate that RGCs response polarity changes according to the stimulus used (Chirp or SWN). This finding has important implications for the stimulus design and choice when targeting specific RGC populations.

Moreover, the current study has only examined RGCs expressing DREADDs, which constitute less than half of the total number of recorded RGCs. In addition, our colleagues identified many RGCs with substantial change in their activity but without DREADD expression. These cells outnumbered the DREADD RGCs by a factor of 10, and are most likely affected by DREADD ACs. A natural progression of this work would be to analyse the response characteristics of these RGCs and assess the effect of CNO when only ACs express DREADDs (Fig. 4.8.3 Scenario 3). A more conclusive interpretation of the CNO effect will be possible once all the possible scenarios have been taken into consideration.

Do ganglion cells act as independent encoders? It is well established that spiking activity across neurons in the visual system is correlated (Meister et al., 2001). This means that spikes at different times move in relation to each other, either at the single-cell level (among several trials of the same cell) or at the population level (across spike trains from multiple neurons). In the retina these correlations are presumably reflected in the spikes generated by RGCs and can be divided in two categories: signal-evoked and intrinsic noise spike correlations (Tchumatchenko et al., 2011). In more detail, these correlations may emerge from : (1) Space and time correlations between the stimulus pixels, (2) Receptive field overlap between adjacent cells, and, (3) Concerted dynamical activity between RGCs interacting via lateral connectivity originating by ACs (triggered by stimuli with long-range spatial correlations e.g. moving bar) or gap junctions. However, the role of correlated activity in the encoding of visual information is a matter of long-standing debate (Nirenberg et al., 2001; Meister et al., 2001).

Here, we hypothesise that CNO-induced activation of DREADD-expressing ACs or RGCs may also have an impact on the spike trains correlations. Assessing and quantifying the degree of correlation between spike trains in different conditions is a way towards deciphering the neural codebook and elucidating the role of network on the retinal response.

Chapter 4. Towards a Large-Scale Retina Model: Definition and Analysis

In this chapter, we present the model we have developed to elucidate the effect of CNO on RGCs' responses to visual stimuli. After introductory remarks and an overview of our model, we detail its structure that potentially allows capturing the essential building blocks of retinal circuitry up to the level of the RGC layer. Based on this model, we first carry out a mathematical analysis of its dynamics and we explore the role of connectivity in the behaviour of the system. Then, we test the validity of the model against recordings from RGCs in diverse experimental conditions. Finally, we propose potential mechanisms that disentangle the effect of CNO on the retinal response, with an emphasis on the role of lateral connectivity originating from amacrine cells.

Contents

4.1	Introduction	52
4.1.1	Neural models of retinal cells	52
4.2	General Structure of the Model	53
4.2.1	Conception of the model	53
4.2.2	Mathematical framework	55
4.2.3	Model assumptions	57
4.2.4	Retinal mosaics	59
4.3	Bipolar cells layer	60
4.3.1	Receptive field and stimulus integration	60
4.3.2	Bipolar cells voltage	62
4.4	Amacrine cells layer	62
4.4.1	Synaptic connections with BCs	63
4.4.2	Amacrine cells voltage	63
4.4.3	CNO effect on ACs	64
4.5	Ganglion cells layer	64
4.5.1	Synaptic inputs to ganglion cells	64
4.5.2	Ganglion cells response	65
4.5.3	CNO effect on RGCs	65
4.6	Model overview/summary	66
4.6.1	Joint dynamics	66
4.6.2	Connectivity patterns	66
4.7	A mathematical analysis of model dynamics	67

4.7.1	Dynamical system	67
4.7.2	Linear approximation	68
4.7.3	Linear analysis	69
4.8	Numerical results	71
4.8.1	Physiological reproductions	71
4.8.2	Role of ACs lateral connectivity	72
4.8.3	CNO effect on the retinal network	73
4.9	Summary and Discussion	77

4.1 Introduction

Experimental and clinical studies have shed important light on the anatomy and physiology of the retina. Yet, there are still many questions that cannot be addressed solely on experimental grounds, as retinal function can only be partially probed by existing electrophysiological and imaging techniques (Roberts et al., 2016). To fill in this gap, mathematical and computational modelling techniques have been widely employed over the past decades, allowing us to study the retina from single cells to network level (Guo et al., 2014; Roberts et al., 2016). Numerous models of the retina have been proposed, with different levels of biological detail and across multiple spatial and temporal scales. Regardless of the modelling technique, they have helped sharpen our understanding of the response dynamics and computations of single neurons and their role in larger neural networks. Nevertheless, experiments and modelling must work in tandem. Similar to the bicycle, maintaining the balance requires both sides to interact, mutually inform and constrain one another.

In the same spirit of research, we evaluated a number of hypotheses raised on the basis of the experimental findings, by means of model definition, mathematical analysis and simulations. We remind that the data analysis has highlighted an important attribute; namely, the variability of cells' responses in CTL and CNO conditions. This could be attributed to lateral inhibition, induced by amacrine cells, and taking place after some delay. This constitutes the theoretical working hypothesis of this thesis.

To explore this hypothesis, we have developed a mathematical model, grounded on biophysics, which:

- (i) accounts for the complexity of retinal circuitry and physiology while making simplifying assumptions (simple, yet useful).
- (ii) mimics the experimental setup and reproduces RGCs' responses to light obtained from the experimental recordings (biologically plausible).
- (iii) allows the mathematical analysis of its dynamics in order to infer the underlying mechanisms that explain what we observe on the data (mathematically tractable).
- (iv) serves as the theoretical framework to predict responses to more complex stimuli and anticipate effects that can be later tested experimentally (predictive).

Before delving into the details of the model structure, let us start by reviewing existing modelling approaches of retinal neurons and introducing the concept of the model. In particular, we strive for justification of the suitability of every chosen method for our model.

4.1.1 Neural models of retinal cells

The retina has an intricate architecture, comprising a myriad of neuronal types and subtypes connected through synapses, thereby forming diverse neural circuits that work in parallel and

together to encode visual information. Modelling such a complex retinal network, consisting of many cell types arranged in different layers, interconnected by feed-forward and lateral connections is therefore a challenging task. It requires a trade-off between biological plausibility (realistic enough to be meaningful) and modelling simplification (simple enough to be useful), so as to reduce the huge number of parameters and equations ruling the behaviour of millions of cells interacting in a sophisticated way.

Currently, there exists a repertoire of modelling techniques, ranging from highly detailed descriptions involving thousands of coupled differential equations to substantially simplified systems. On a micro-scale level, a single neuron can be modelled either as a single-compartment model, a multi-compartment model or a block-structured/cascade model, depending on the objectives and physiological assumptions of the given research problem (Guo et al., 2014). The first class omits the neuron's spatial dimension, whereas the multi-compartment accounts for the neuronal morphological details. Conversely, the cascade models do not take into account the biophysical or morphological details of neurons and focus on capturing the input-output relationship by treating neurons as black boxes. On a macro scale, the level of detail also varies. On one hand, neural networks can be modelled by connecting individual neurons, represented by biophysically or morphologically realistic models, with the mathematical representation of synaptic interactions. These mechanistically detailed models consider the physical architecture and the information flow of the retina, yet they turn out to be cumbersome to analyse and simulate (Guo et al., 2014). Other large-scale models may take a more functional approach, based on a series of linear and nonlinear filters. Unlike the former approach, these models are usually assembled by cascade models of neurons and aim mostly at providing a functionally efficient output rather than strong biological precision. Such models can be very useful in investigating the role of single neurons and their interactions in the encoding of visual scenes.

In a nutshell, each model has advantages and disadvantages and there may be no ideal one. Thus, our selection should be guided by the questions we aim to address, the experimental information available and the physiological assumptions on which the model will be based.

4.2 General Structure of the Model

4.2.1 Conception of the model

In seeking to mathematically describe the retina, we had to consider two major issues. First, we wanted to have a structure quite similar to that of a real retina and a functionality quite close to that of the experimental setup. Second, we needed to make simplifications that reduce the complexity to the essential characteristics in order to make the model mathematically and computationally tractable. Therefore, the model developed in this work falls somewhere in between the previously mentioned models and it is definitely inspired by some of them (Chen et al., 2013; Souihel et al., 2021). It is a multi-stage, phenomenological model, with simplifications regarding the complex retinal structure. Nevertheless, it aims to be relatively precise from a

biological perspective, by mimicking the experimental setup and realistically reproducing RGCs' responses to light from the experimental recordings. Our primary goal is to gain insights about the underlying biophysical processes giving rise to certain experimentally observed phenomena, rather than proposing an exact model of the retina.

Let us first briefly recapitulate how information processing occurs within the different layers of the retina and then explain how we translate it into a computational network model (Fig. 4.1). In the retina, light from a visual scene follows a vertical pathway, from photoreceptors to bipolar cells (BCs) and onwards to ganglion cells (RGCs), modulated by inhibitory interneurons comprising two groups; horizontal and amacrine cells (ACs) (There are also excitatory amacrine cells but we will not consider them here). Retinal neurons communicate mostly via graded potentials and their output signals are integrated into the receptive fields of RGCs. At the final stage, RGCs convey the spatio-temporal information encoded in sequences of spikes to the brain.

Following this biological order, while including only the features which we thought to be significant and relevant to the questions we aimed to address, we built our theoretical model. It consists of three layers of neurons, BCs, ACs and RGCs, represented by single-compartment models that neglect the morphological structure of neurons and assume that the dynamics of an entire multi-compartment neuron can be characterised by a uniform membrane potential that can be recorded in the soma. In addition, the biophysical mechanisms responsible for action potentials (voltage-dependent potassium/sodium channels) are not explicitly included in these models. This modelling approach is justified for three reasons. First, most retinal neurons considered here are not spiking (except RGCs), but rather communicate via graded potentials. Second, modelling such conductances would require access to parameters that are not available from the experiments performed by our collaborators. And lastly, including ion channels would make the mathematical analysis and simulation cumbersome. However, as RGCs are spiking neurons, we have introduced a nonlinear function to associate their voltage with their spiking activity (firing rate). For the sake of simplicity, we did not model in detail the photoreceptor and horizontal cells. Instead, we took a functional approach and considered that the influence of the cascade stimulus-photoreceptors-horizontal cells is represented by the convolution of the stimulus with spatio-temporal kernels, mimicking the information processing happening at the OPL, and inducing voltage variations on BCs (Dayan et al., 2001; Wohrer et al., 2009).

BCs then transmit these signals to RGCs directly or indirectly via ACs. To account for this signal transmission in our model, we coupled the three layers of neurons with synaptic connections. A synapse is a complex structure that serves as a signal transmission device from one neuron to another. Similar to the neuron models, mathematical models for chemical or electrical synapses range from phenomenological to more biophysically realistic ones (Destexhe et al., 1994; Graupner et al., 2005; Sterratt et al., 2011). Note, however, that many of these models deal with spiking neurons whereas, here, most cells do not generate spikes, as in the real retina. Moreover, modelling in detail the complex biophysical mechanisms underlying synaptic function would hinder the mathematical analysis and simulation of the model. Therefore, we used

a phenomenological model, a simple waveform, that captures the essence of the post-synaptic electrical response: multiplexing, temporal filtering and spatial integration and, last but not least, the capacity of the postsynaptic cell to respond to continuous variations of the pre-synaptic voltage (Sterratt et al., 2011). All the above considered, BCs, ACs and RGCs are organised into multiple, local, functional circuits with specific connectivity patterns and these local circuits are also laterally connected, via ACs, thus sharing local information and dynamically interacting (Gollisch et al., 2010; Demb et al., 2015).

As a final note to this section, we would like to emphasise the benefits of using single-compartment models both for single-cells and whole networks. In the former, they can provide insights about the underlying mechanisms of the neuron information processing and can be used to study effects of pharmacological agents related to a specific conductance on the neuron's response (e.g. CNO). In the latter, connecting single neuron models in a network facilitates the study of network dynamics and interactions between neurons (ACs connectivity).

4.2.2 Mathematical framework

We will now introduce the mathematical framework that has served as a reference for our work. The fundamental equation that determines the membrane potential V of a neuron q for a single-compartment model is (Dayan et al., 2001):

$$C_m \frac{dV_q}{dt} = \sum_i I_i(t) - \sum_j g_j (V_q - \mathcal{E}_j), \quad (4.1)$$

where C_m is the membrane capacitance, $\sum_i I_i(t)$ represents the sum of external input currents (e.g. electrode currents) and the term $\sum_j g_j (V - E_j)$ is the sum of the currents due to all the different types of ion channels within the cell membrane, such as voltage-gated, ligand-gated or leak channels (always open), with g_j being the corresponding conductance and \mathcal{E}_j the corresponding reversal potential.

We may rewrite (4.1) in a more detailed form:

$$\begin{aligned} C_m \frac{dV_q}{dt} = & -g_L (V_q - \mathcal{E}_L) + \sum_i I_i(t) - \sum_{X,ion} g_q^{(X)}(\bullet) (V_q - \mathcal{E}_X) \\ & - \sum_{Y,syn} \sum_{p \in Y} g_q^{(Y,p)}(V_p, \bullet) (V_q - \mathcal{E}_Y) \end{aligned} \quad (4.2)$$

where g_L is the leak conductance and \mathcal{E}_L the leak reversal potential. $\sum_{X,ion}$ denotes the sum over all currents of voltage-gated channels tuning the neuron's activity (for example sodium or potassium), $g_q^{(X)}(\bullet)$ is the corresponding conductance (where \bullet stands for all variables on which g_X may depend, and which may have their own dynamical evolution) and \mathcal{E}_X is the corresponding reversal potential. Likewise, $\sum_{Y,syn}$ represents the summing currents due to all the possible types of synaptic inputs, shaping the membrane potential of neuron q (for example glutamate-NMDA,

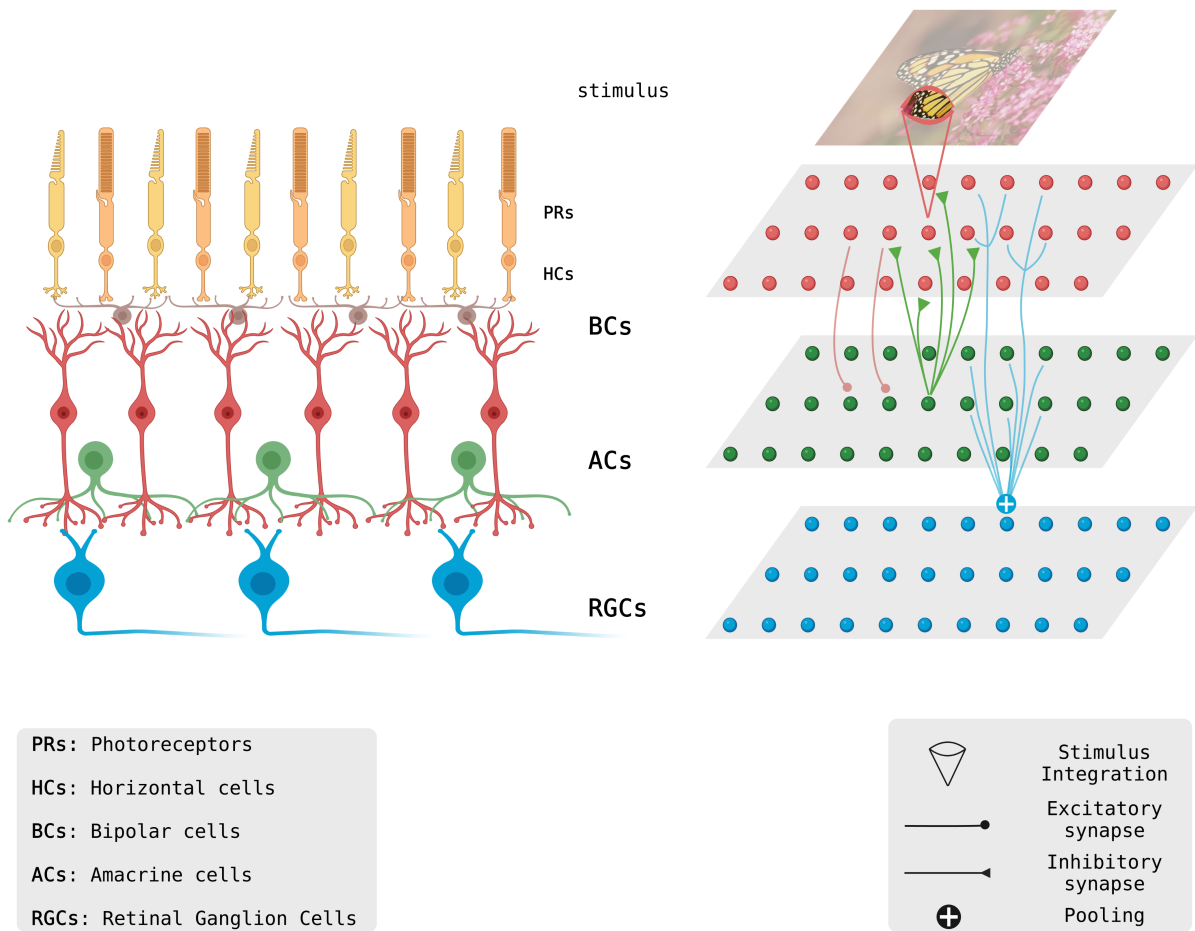


Figure 4.1. Translation of the retinal circuit to a computational network model. *Left.* Schematic of the retina. Light activates the photoreceptor cells (PRs), that transduce the input into a cascade of biochemical and electrical events that can stimulate BCs and onwards RGCs. This vertical excitatory pathway is modulated by inhibitory interneurons comprising two groups; horizontal (HCs) and amacrine cells (ACs). All these neural signals are integrated by RGCs and finally converted into action potentials going to the brain. *Right.* Schematic view of the model. BCs integrate the stimulus, modelled as the convolution of the stimulus with their RFs, represented by spatio-temporal kernels. BCs make one-to-one excitatory synaptic connections with ACs and ACs inhibit many BCs. Finally, RGCs pool over many BCs and ACs in their neighbourhood.

or glutamate-mGluR). The sum $\sum_{p \in Y}$ stands for the contribution of presynaptic neurons p connecting to post-synaptic neuron q via a synapse of type Y . The conductance $g_q^{(Y,p)}(V_p, \bullet)$ depends, in general, on the pre-synaptic voltage V_p and additional variables represented by a \bullet .

From equations (4.1) and (4.2), we can finally write:

$$\frac{dV_q}{dt} = -\frac{V_q}{\tau_q} + J_q + \frac{1}{C_m} \sum_i I_i(t), \quad (4.3)$$

where,

$$\tau_q \equiv \tau(\vec{V}, \bullet) = \frac{C_m}{g_L + \sum_{X,ion} g_q^{(X)}(\bullet) + \sum_{Y,syn} \sum_{p \in Y} g_q^{(Y,p)}(V_p, \bullet)} \quad (4.4)$$

and:

$$J_q \equiv J_q(\vec{V}, \bullet) = \frac{1}{C_m} \sum_{X,ion} g_q^{(X)}(\bullet) \mathcal{E}_X + \frac{1}{C_m} \sum_{Y,syn} \sum_{p \in Y} g_q^{(Y,p)}(V_p, \bullet) \mathcal{E}_Y, \quad (4.5)$$

\vec{V} being the vector of all V_p (all voltages in the network). Note that V_p is the voltage expressed when \mathcal{E}_L is the reference (assuming that all cells have the same leak reversal potential \mathcal{E}_L and the same leak conductance g_L).

4.2.3 Model assumptions

Let us now review the assumptions that this model relies on.

Cells Neurons are passive (e.g. no spike generating ion channels). This is appropriate as retinal neurons considered here are not spiking (except RGCs). In addition, we do not reckon with the total surface area of each neuron, so the membrane capacitance is constant throughout all neurons ($C_m = C$ and is expressed in pF).

Chemical Synapses Cells are connected via chemical synapses¹, structures that allow a neuron to transmit an electrical signal to another neuron using chemical transduction. Models of such structures range from simple phenomenological models of voltage waveforms to more complex and realistic models, including vesicle recycling and release, neurotransmitter release, gating of postsynaptic receptors etc.

In this thesis, as we have emphasised many times, we strive for simplicity, to enable the mathematical analysis of the model dynamics, and biological precision according to the experimental information available. For this reason, we have used a simple phenomenological model for the chemical synapse, that represents the evoked post-synaptic response as a convolution of the pre-synaptic voltage with an exponential α -profile (Destexhe et al., 1994) of the form:

$$\alpha_q^p(t) = \exp\left(-\frac{t}{\tau_q^p}\right)H(t), \quad (4.6)$$

where the upper index, p , is the pre-synaptic cell type and the lower index, q , the post-synaptic cell type. τ_q^p is the characteristic integration time and H is the Heaviside function that ensures causality and defined such that $\alpha_q^p(0) = 0$. Figure 4.2 shows how the α -function evolves in time, first by rapidly increasing and thus capturing the effect of the neurotransmitter binding to the receptors of the postsynaptic neuron, and then, by decaying exponentially with a relatively slow time constant, which account for the delay that is usually observed in chemical synapses. The advantage of this form (4.6) is that it depends only on one parameter; namely, the characteristic

¹The model allows to connect cells via electrical synapses, however, here we only consider chemical synapses.

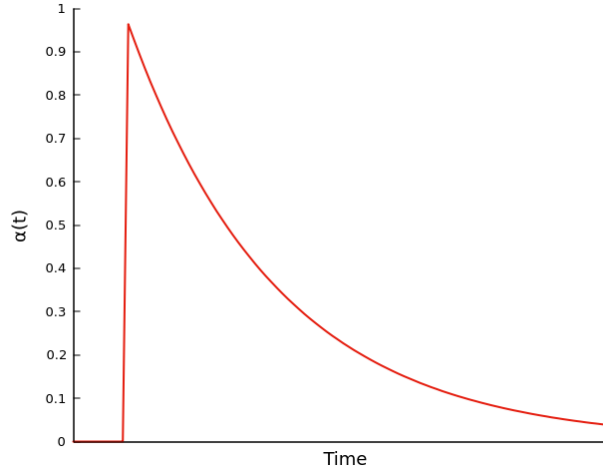


Figure 4.2. α -function to model the postsynaptic activity in a chemical synapse.

time τ_q^p . This is also called first-order kernel because it solves a differential equation of first order (Faugeras et al., 2009). Higher order convolution kernels, represented by higher order linear differential equations could be considered, integrating more details of the biological machinery. But this would require more parameters to tune.

Moreover, cells of type q may receive multiple input by cells of type p . Thus, the total post-synaptic potential at a post-synaptic cell q_i , of type q , connected with chemical synapses to pre-synaptic cells p_j , of type p , is:

$$P_{q_i}^{(c)}(t) = \sum_{j=1}^{N_p} W_{q_i}^{p_j} \int_{-\infty}^t \alpha_q^p(t-s) \mathcal{N}_p(V_{p_j}(s)) ds, \quad (4.7)$$

where the exponent (c) stands for "chemical", and $W_{q_i}^{p_j}$ is the chemical synaptic weight from cell p_j to cell q_i . We use the implicit convention $W_{q_i}^{p_j} = 0$ when there is no chemical synapse from cell p_j to cell q_i . \mathcal{N}_p is a linear voltage rectification of the form:

$$\mathcal{N}_p(V_{p_j}) = \begin{cases} V_{p_j} - \theta_Y, & \text{if } V_{p_j} > \theta_Y; \\ 0, & \text{otherwise} \end{cases} \quad (4.8)$$

The parameter θ_Y is a voltage threshold ensuring that the synapse is not active when pre-synaptic voltage becomes too low. Typically, in the case of inhibitory synapses involving potassium, this ensures that the synapse does not becomes excitatory if the pre-synaptic potential becomes lower than \mathcal{E}_K .

The derivative of (4.7) with respect to time then reads:

$$\frac{dP_{q_i}^{(c)}}{dt} = -\frac{1}{\tau_q^p} P_{q_i}^{(c)} + \sum_{j=1}^{N_p} W_{q_i}^{p_j} \mathcal{N}_p(V_{p_j}(t)), \quad (4.9)$$

thereby corresponding to a formal synaptic current $I_{q_i}^{(c)}(t) = C_m \frac{dP_{q_i}^{(c)}}{dt}$.

CNO sensitivity As we have seen in Chapter 3, experiments are performed on retinas where RGCs and/or ACs express the (excitatory) DREADD receptor. DREADD-expressing cell populations can be activated by CNO, which depending on the receptor type can lead either to an excitatory or inhibitory effect on the cell's response. Essentially, CNO activation induces a current that is attributed to the diffusion of ions inside and outside of the neuron via specific channels.

To account for this effect, we consider that there is only one ion channel active under the CNO influence and we model the current in the form $-g_{CNO} (V_q - \mathcal{E}_{CNO})$, where g_{CNO} is the conductance of the channel affected by CNO and \mathcal{E}_{CNO} the reversal potential. $\mathcal{E}_{CNO} < 0$ for inhibitory DREADDs and $\mathcal{E}_{CNO} > 0$ for excitatory DREADDs. The conductance of this channel is constant and depends only on the cell type. It is zero for bipolar cells, following the experimental setup. In addition, $g_{CNO} = 0$ in the absence of CNO. The reader should bear in mind, though, that this is just a modelling shortcut as a thorough modelling of the exact mechanism would require parameters that we do not have access to and would make the model very complicated to treat mathematically.

Under these assumptions, the characteristic time (4.4) reads:

$$\tau_q = \frac{\tau_L}{1 + \lambda_{CNO_T} \tau_L + \tau_L \sum_{Y, \text{syn}} \sum_{p \in Y} W_q^{(Y,p)} \mathcal{N}^Y(V_p)}, \quad (4.10)$$

and:

$$J_q = \sum_{Y, \text{syn}} \sum_{p \in Y} W_q^{(Y,p)} \mathcal{N}_Y(V_p) + \zeta_T, \quad (4.11)$$

where $\tau_L = \frac{C_m}{g_L}$, $\lambda_{CNO_T} = \frac{g_{CNO_T}}{C_m}$ and $\zeta_T = \frac{g_{CNO_T} \mathcal{E}_T}{C_m}$.

For τ_q , we assume that it is only controlled by the rest part of the voltage V_p and that $V_p > \theta_Y$.

Finally, the equation of cells voltage takes the general form:

$$\frac{dV_q}{dt} = -\frac{1}{\tau_q} V_q + \sum_{Y, \text{syn}} \sum_{p \in Y} W_q^{(Y,p)} \mathcal{N}_Y(V_p) + \zeta_T + \frac{1}{C_m} \sum_i I_i(t), \quad q = 1 \dots N, \quad (4.12)$$

4.2.4 Retinal mosaics

We assimilate the retina to a flat, two dimensional square of edge length L mm. Spatial coordinates are noted x, y . Therefore, we do not integrate the third, vertical, coordinate z in the model merely for mathematical convenience.

A common feature of retinal organisation is the semi-regular distribution of neurons belonging to the same type, with each cell type forming a mosaic pattern (Wässle et al., 1978). Yet cell

distributions are not necessarily uniform across the retina. Moreover, mosaic arrangements are thought to be independent across the retinal layers (Rockhill et al., 2000). Following the same principle, in the model each cell population tiles the retina with a regular square lattice. The density of cells is therefore uniform for convenience but the extension to non uniform density is afforded by the model. Note, for example, that mouse RGCs are often not uniformly distributed (Bleckert et al., 2014). For the population p we note δ_p the lattice spacing in mm, and N_p the total number of cells. Without loss of generality we assume that L , the retina's edge size, is a multiple of δ_p . We note $L_p = \frac{L}{\delta_p}$, the number of cells p per row or column so that $N_p = L_p^2$. Each cell in the population p has thus Cartesian coordinates $(x, y) = (i_x \delta_p, i_y \delta_p)$, $(i_x, i_y) \in \{1, \dots, L_p\}^2$. To avoid multiples indices, we will often associate to each pair (i_x, i_y) a unique index $i = i_x + (i_y - 1)L_p$. The cell of population p , located at coordinates $(i_x \delta_p, i_y \delta_p)$ is then denoted by p_i . We note $d[p_i, p'_j]$ the Euclidean distance between p_i and p'_j .

4.3 Bipolar cells layer

Bipolar cells (BCs) tile the retina with a lattice spacing δ_B . For each cell, there is a unique index $i = 1 \dots N_B$ and spatial coordinates x_i, y_i , corresponding to their receptive field centre.

4.3.1 Receptive field and stimulus integration

Each neuron in the different layers of the retina has a receptive field (RF), a specific region of the visual field where light stimulus will modify the activity of this neuron. The term RF is not limited only to the spatial region but it is often extended to include the temporal structure within this region. The RF usually exhibits a centre-surround organisation and it is assumed that BCs are the first neurons along the visual pathway to follow this principle (Werblin et al., 1969). Each BC receives synaptic inputs from its upstream circuitry, a combination of dendritic excitatory inputs from photoreceptors and axonal inhibitory inputs from horizontal cells (Franke et al., 2017b) and this interaction emerges on their RF.

A popular approach to simplify the complex process involved is to model the RF as a single spatio-temporal linear filter that essentially represents the opposition between the centre of the receptive field, driven by photoreceptors, and the surround signal transmitted by horizontal cells. The membrane potential of the BC's soma can then be linearly approximated by the convolution of the spatio-temporal kernel $\mathcal{K}_{B_i}(x, y, t)$ with the visual stimulus $S(x, y, t)$:

$$V_{i_{drive}}(t) = \left[\mathcal{K}_{B_i} \overset{x,y,t}{*} S \right] (t) \equiv \int_{x=-\infty}^{+\infty} \int_{y=-\infty}^{+\infty} \int_{s=-\infty}^t \mathcal{K}(x - x_i, y - y_i, t - s) S(x, y, s) dx dy ds, \quad (4.13)$$

where $\ast^{x,y,t}$ means space-time convolution. We consider a separable kernel, so $\mathcal{K}_{B_i}(x, y, t)$ can be written as $\mathcal{K}_S(x, y) \mathcal{K}_T(t)$, where \mathcal{K}_S accounts for the spatial part and \mathcal{K}_T for the temporal part, assuming to vanish at time $t = 0$.

The spatial receptive field can be mathematically expressed as a difference of Gaussian kernels, called DOG, with different space constants. (Enroth-Cugell et al., 1966; Rodieck, 1965). Yet, some cells may exhibit a more complex structure that cannot be captured by a simple DOG model. Here, we consider simple receptive fields that can be modelled with circular Gaussian functions as in eq. (4.14).

$$K_S(x, y) = \frac{1}{2\pi\sigma_c^2} \exp\left(-\frac{(x^2 + y^2)}{2\sigma_c^2}\right) - \frac{1}{2\pi\sigma_s^2} \exp\left(-\frac{(x^2 + y^2)}{2\sigma_s^2}\right) \quad (4.14)$$

We model the temporal receptive field with an exponential cascade, as in (4.15).

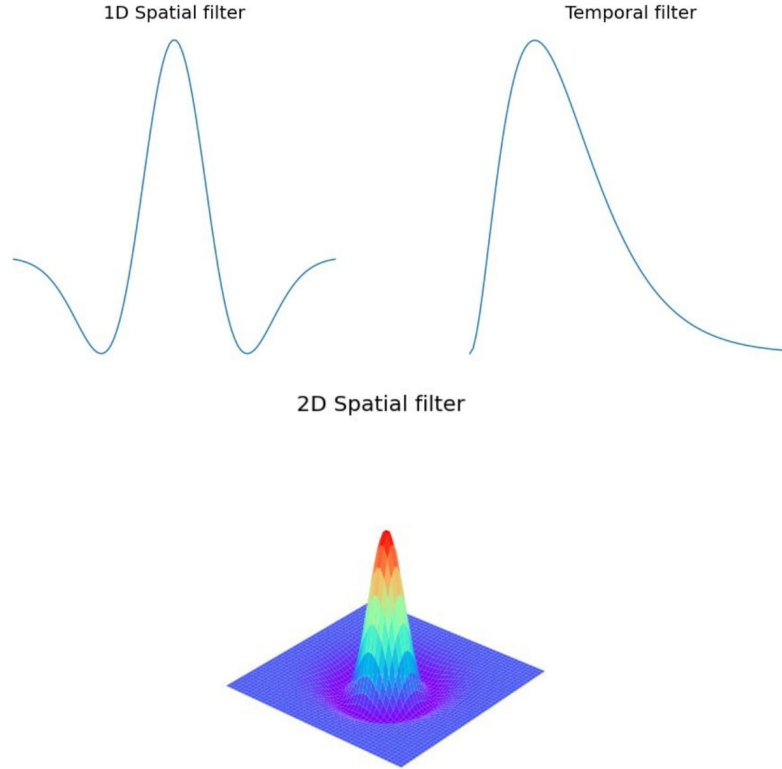


Figure 4.3. Spatio-temporal linear filter that models the receptive field of a neuron. *Top*. Spatial and temporal kernels in one dimension. *Bottom*. Two-dimensional representation of the spatial kernel.

$$K_T(t) = (nt)^n \frac{\exp(-nt/\tau_c)}{(n-1)!\tau_c^{n+1}}, \quad n = 2 \quad (4.15)$$

Bipolar cells are considered to be the first neurons to exhibit substantial diversity, with more than ten morphological types forming distinct circuits to encode different stimulus properties

(Euler et al., 2014). Typically, BCs can be functionally categorised according to the way they respond to light into ON and OFF cells, the former depolarised and the latter hyperpolarised by light. Here, we consider ON monophasic BCs², whose spatio-temporal kernel is illustrated in Fig. 4.3, however both types of BCs are afforded by the model. Finally, we fit the spatio-temporal filters on the basis of the experimental recordings.

4.3.2 Bipolar cells voltage

We consider that a BC's voltage is the sum of the external drive (4.13) and of the post-synaptic potential $P_{B_i}^{(c)}$, induced by the ACs making synaptic connections with BCs:

$$V_{B_i}(t) = V_{i_{drive}}(t) + P_{B_i}^{(c)}(t) \quad (4.16)$$

where $P_{B_i}^{(c)} = \sum_{j=1}^{N_A} W_{B_i}^{A_j} \int_{-\infty}^t \alpha_B^A(t-s) \mathcal{N}_A(V_{A_j}(s)) ds$, according to (4.7). ACs release either GABA or glycine, neurotransmitters that have an inhibitory effect which is represented by the negative synaptic weight $W_{B_i}^{A_j}$. By convention, when there is no ACs connectivity, the post-synaptic potential for all BCs is equal to 0. In addition, BCs are not sensitive to CNO, according to the experimental setup.

Differentiating (4.16) with respect to time, using (4.9):

$$\frac{dV_{B_i}}{dt} = -\frac{1}{\tau_{B_i}} V_{B_i} + \sum_{j=1}^{N_A} W_{B_i}^{A_j} \mathcal{N}_A(V_{A_j}) + F_{B_i}(t), \quad (4.17)$$

where:

$$F_{B_i}(t) = \frac{V_{i_{drive}}}{\tau_B} + \frac{dV_{i_{drive}}}{dt} = \left[\mathcal{K}_{B_i}^{x,y,t} * \left(\frac{S}{\tau_B} + \frac{dS}{dt} \right) \right] (t), \quad (4.18)$$

where we have used, in the second equality, that $\mathcal{K}_T(t)$ vanishes at time $t = 0$. Here, τ_B is the characteristic time scale of BC i response.

This is a differential equation driven by the time dependent term F_{B_i} containing the stimulus and its time derivative. In the case where there is no ACs connectivity, BCs are driven simply by $V_{i_{drive}}(t)$.

4.4 Amacrine cells layer

Amacrine cells (ACs) are involved in the inner plexiform layer, where they integrate and modulate the vertical direct pathway from BCs to RGCs. ACs, along with RGCs, come in many shapes, sizes and functions and this diversity is assumed to be related to the RGCs' variety (Masland, 2012b). Some types have been studied in detail and are thought to carry out a particular function, such as the starburst amacrine cells, involved in direction sensitivity (Euler et al., 2002; Tukker

²Even though we consider only monophasic BCs, the RGCs response can be biphasic, due to AC lateral inhibition, as shown later.

et al., 2004; Enciso et al., 2010) or AII, serving a critical role in signal transmission from rod photoreceptors to RGCs (Demb et al., 2012). Conversely, recent studies have highlighted the potential role of the population of ACs across types in general features of retinal processing, such as parallel processing or motion anticipation (Johnston et al., 2015; Rosa et al., 2016; Franke et al., 2017a; Souihel et al., 2021).

Here, we adopt a similar approach, considering a generic type of ACs to study how the ACs network (connectivity patterns and intensity) affects the population response of the retina to various stimuli under various conditions (CNO induced activation). ACs are simply modelled as linear convolution kernels for two main reasons: (1) from the experimental side, we do not have access to ACs responses, (2) adding a non-linear mechanism would make the mathematical analysis cumbersome, with parameters that we do not know how to tune.

In the model, ACs are arranged on a two dimensional lattice with a lattice spacing δ_A . For each cell, there is a unique index $j = 1 \dots N_A$ and spatial coordinates x_j, y_j .

4.4.1 Synaptic connections with BCs

We consider a simple model of ACs, where an AC's voltage is driven by the synaptic connections with BCs, that induce a post-synaptic potential $P_{A_j}^{(c)}$ of the form (4.7) :

$$P_{A_j}^{(c)} = \sum_{i=1}^{N_B} W_{A_j}^{B_i} \int_{-\infty}^t \alpha_A^B(t-s) \mathcal{N}_B(V_{B_i}(s)) ds \quad (4.19)$$

BCs release glutamate, a neurotransmitter that has an excitatory effect which is represented by the positive synaptic weight $W_{A_j}^{B_i}$. By convention, when there is no bipolar connectivity, the post-synaptic potential for all ACs is equal to 0.

4.4.2 Amacrine cells voltage

ACs differ from BCs in the following: (1) They do not receive input from photoreceptors, so there is no external drive, (2) They can be sensitive to CNO. Thus, the equation that governs ACs' dynamics, according to (4.12), is:

$$\frac{dV_{A_j}}{dt} = -\frac{1}{\tau_{A_j}} V_{A_j} + \sum_{i=1}^{N_B} W_{A_j}^{B_i} \mathcal{N}_B(V_{B_i}) + \zeta_A, \quad (4.20)$$

where:

$$\tau_{A_j} = \frac{\tau_L}{1 + \lambda_{CNO_A} \tau_L + \tau_L \sum_{i=1}^{N_B} W_{A_j}^{B_i} \mathcal{N}_B(V_{B_i})} \quad (4.21)$$

with

$$\lambda_{CNO_A} = \frac{g_{CNO_A}}{C_m}, \quad (4.22)$$

$$\zeta_A = \lambda_{CNO_A} \mathcal{E}_{CNO_A} \quad (4.23)$$

4.4.3 CNO effect on ACs

CNO activation acts on an AC's response on two levels:

- The baseline activity of the cell, via the activation/inhibition term ζ_A (4.23). The sign of this term depends on the reversal potential \mathcal{E}_{CNO_A} , itself related to the type of genes and ionic channels involved in CNO sensitivity. Essentially, in the case of excitatory DREADDs, CNO increases λ_{CNO_A} , and consequently the AC's voltage.
- The characteristic integration time of the cell τ_{A_j} (4.21) in two ways: (i) An increase of the conductance g_{CNO_A} leads to a decrease of τ_{A_j} , (ii) The change in the rest voltage of the cell induces, by network effect (lateral cross interaction between BCs and ACs), a change in the synaptic conductance, thereby leading to an increase or decrease of τ_{A_j} .

Note that both effects vanish when $g_{CNO_A} = 0$.

4.5 Ganglion cells layer

RGCs exhibit astounding anatomical, functional and genetic diversity and each type interprets a different feature of the visual scene (Masland, 2001; Wässle, 2004). There are ~1 million RGCs in humans and ~45,000 in mice (Curcio et al., 1990; Jeon et al., 1998), integrating signals typically across many different BCs and ACs. In addition, RGCs of the same type are organised in mosaic patterns (DeVries et al., 1997).

Here, we focus on specific types that were identified on the basis of the experiments performed, as described in Chapter 3. In the model, RGCs of the same type tile the retina with a lattice spacing δ_G . We index them with $k = 1 \dots N_G$.

4.5.1 Synaptic inputs to ganglion cells

RGCs receive and integrate synaptic inputs from their upstream circuitry, usually involving many BCs and ACs. To do so, they pool excitatory inputs from many presynaptic BCs. At the same time, this excitation is modulated in two ways by ACs, either directly by feed-forward inhibition from amacrine cell synapses onto retinal ganglion cell dendrites or by feedback inhibition, in which amacrine cells contact axon terminals of bipolar cells.

In the model, RGCs are connected to BCs with excitatory glutamatergic synapses and to ACs with inhibitory glycinergic or GABA-ergic synapses (Fig. 4.1).

BCs pooling A ganglion cell G_k pools over the output of bipolar cells in its neighbourhood with a Gaussian function and this is represented by the total post-synaptic potential:

$$P_{G_i}^{B_i}(t) = \sum_{i=1}^{N_B} W_{G_k}^{B_i} \int_{-\infty}^t \alpha_G^B(t-s) \mathcal{N}_B(V_{B_i}(s)) ds, \quad (4.24)$$

where $W_{G_k}^{B_i} > 0$ corresponds to the excitatory effect of bipolar on ganglion cells.

ACs connectivity A ganglion cells G_k pools over many amacrine cells, inducing a post-synaptic potential $P_{G_k}^{(c)}$:

$$P_{G_k}^{A_j} = \sum_{i=1}^{N_A} W_{G_k}^{A_j} \int_{-\infty}^t \alpha_G^A(t-s) \mathcal{N}_A(V_{A_j}(s)) ds \quad (4.25)$$

where $W_{G_k}^{A_j} < 0$ corresponds to the inhibitory effect of amacrine on ganglion cells.

4.5.2 Ganglion cells response

We consider that a RGC membrane voltage is the sum of the post-synaptic potential induced by the pooling of BCs (4.24) and ACs (4.25). In addition, RGCs are sensitive to CNO. As a consequence and according to (4.12):

$$\frac{dV_{G_k}}{dt} = -\frac{1}{\tau_{G_k}} V_{G_k} + \sum_{i=1}^{N_B} W_{G_k}^{B_i} \mathcal{N}_B(V_{B_i}) + \sum_{j=1}^{N_A} W_{G_k}^{A_j} \mathcal{N}_A(V_{A_j}) + \zeta_G \quad (4.26)$$

where:

$$\tau_{G_k} = \frac{\tau_L}{1 + \lambda_{CNO_G} \tau_L + \tau_L \sum_{i=1}^{N_B} W_{G_k}^{B_i} \mathcal{N}_B(V_{B_i}) + \tau_L \sum_{j=1}^{N_A} W_{G_k}^{A_j} \mathcal{N}_A(V_{A_j})}, \quad (4.27)$$

with

$$\lambda_{CNO_G} = \frac{g_{CNO_G}}{C_m}, \quad (4.28)$$

$$\zeta_G = \lambda_{CNO_G} \mathcal{E}_{CNO_G} \quad (4.29)$$

Finally, as RGCs are spiking cells, we introduce a non-linear function to impose an upper limit over the firing rate. Here, we model the spiking activity (firing rate) with a piecewise linear function (Chen et al., 2013):

$$\mathcal{N}_G(V_G) = \begin{cases} 0, & \text{if } V_G \leq \theta_G; \\ \alpha_G(V_G - \theta_G), & \text{if } \theta_G \leq V_G \leq N_G^{max}/\alpha_G + \theta_G; \\ N_G^{max}, & \text{else.} \end{cases} \quad (4.30)$$

4.5.3 CNO effect on RGCs

CNO activation can affect a RGC's response both in a direct and in an indirect way.

Direct effect The effect is straightforward here, as CNO acts only on RGCs without feedback to other cell types. In the case of excitatory DREADDs, increasing g_{CNO_G} leads to a depolarisation of the cell, via the term ζ_G (4.29) and a decrease of its characteristic time τ_{G_k} (4.27). Note that

in general $g_{CNO_G} \neq g_{CNO_A}$. These are two independent control parameters, even if they are both constrained by the CNO concentration.

Indirect effect On the other hand, the indirect effect concerns the cascading effect of direct CNO impact on ACs, onto the whole network. When there is lateral connectivity via ACs, the effect is quite more intricate as it propagates from ACs to BCs and then to RGCs due to the connectivity (4.27), with a potential feedback on ACs. Thus, all cell types can be affected even if the direct effect is on ACs only.

4.6 Model overview/summary

4.6.1 Joint dynamics

To summarise, the joint dynamics of BCs, ACs and RGCs can be described by the following dynamical system:

$$\begin{cases} \frac{dV_{B_i}}{dt} = -\frac{1}{\tau_{B_i}} V_{B_i} + \sum_{j=1}^{N_A} W_{B_i}^{A_j} \mathcal{N}_A(V_{A_j}) + F_{B_i}(t), \\ \frac{dV_{A_j}}{dt} = -\frac{1}{\tau_{A_j}} V_{A_j} + \sum_{i=1}^{N_B} W_{A_j}^{B_i} \mathcal{N}_B(V_{B_i}) + \zeta_A, \\ \frac{dV_{G_k}}{dt} = -\frac{1}{\tau_{G_k}} V_{G_k} + \sum_{i=1}^{N_B} W_{G_k}^{B_i} \mathcal{N}_B(V_{B_i}) + \sum_{j=1}^{N_A} W_{G_k}^{A_j} \mathcal{N}_A(V_{A_j}) + \zeta_G. \end{cases} \quad (4.31)$$

The system of eq. (4.31) depicts the information flow in the model: BCs receive the visual input via the term $F_{B_i}(t)$, which depends on the stimulus and on the cell's receptive field. They are inhibited by ACs via the synaptic weights $W_{B_i}^{A_j} < 0$. At the same time, ACs are excited by BCs via the synaptic weights $W_{A_j}^{B_i} > 0$. BCs and ACs are connected to RGCs via the synaptic weights $W_{G_k}^{B_i} > 0$ and $W_{G_k}^{A_j} < 0$, correspondingly. The characteristic membrane integration time and the activity of ACs and RGCs is controlled by CNO via the terms $\tau_{A_i}, \zeta_{A_i}, \tau_{G_k}, \zeta_{G_k}$.

Remark. As we don't have access experimentally to the terms ζ_{A_i}, ζ_{G_k} , that express how CNO will change the baseline activity, we assume that the rest state of all cells is equal to 0.

4.6.2 Connectivity patterns

BCs, ACs and RGCs are organised into multiple, local, functional circuits with specific connectivity patterns and response dynamics. Each circuit is related to a specific task, such as light intensity or contrast adaptation, motion detection, orientation, motion direction and so on (Masland, 2001; Wässle, 2004; Azeredo da Silveira et al., 2011). Here, we consider a simplified form of connectivity, inspired by the real connectivity in the retina, as shown in Fig. 4.1. For simplicity, we consider that there are as many BCs as ACs ($N_A = N_B = N$). Connectivity is defined through square connectivity matrices Γ_q^p , where $\Gamma_{q_i}^{p_j} = 1$ if cell p_j connects to q_i .

Chemical synaptic connections from a cell type p to another type q take the general form:

$$W_q^p = w_q^p \Gamma_q^p, \quad (4.32)$$

where w_q^p is a real parameter controlling *globally* the synaptic weight amplitude. This is done to reduce the number of parameters of the model and avoid having too many parameters to control.

Consequently, the connectivity matrix W_G^B , representing the connections from BCs to RGCs, is $W_G^B = w_G^B \Gamma_G^B$ with $w_G^B > 0$, and the connectivity matrix W_G^A , representing the connections from ACs to RGCs, is $W_G^A = w_G^A \Gamma_G^A$ with $w_G^A < 0$. Γ_G^B and Γ_G^A are pooling matrices, where a cell i connects to cell j with a Gaussian probability depending on the distance d_{ij} . Likewise, the connectivity matrix W_B^A , representing the connections from ACs to BCs, is $W_B^A = w_B^A \Gamma_B^A$, with $w_B^A < 0$. Γ_B^A is a nearest neighbour connectivity matrix. Finally, the connectivity matrix W_A^B , representing the connections from BCs to ACs, has a special form, merely assumed for mathematical convenience, although with a biological grounding. It is diagonal, with a synaptic weight $w_A^B > 0$ and takes the form $W_A^B = w_A^B \mathcal{I}_N$, where \mathcal{I}_N is the $N \times N$ identity matrix. Actually, mathematical results extend to the case where W_B^A and W_A^B commute.

4.7 A mathematical analysis of model dynamics

In this section, we carry out a mathematical analysis of the model dynamics under different conditions (similarly to Souihel et al., 2021 and Cessac, 2021), to uncover clues about the underlying processes. We investigate the role of lateral connectivity and the effect of CNO activation on retinal response and then, how they interplay in mathematically predicted ways³.

4.7.1 Dynamical system

We first study mathematically the system of nonlinear differential equations (4.31) that we write in a more convenient form. We use Greek indices $\alpha, \beta, \gamma = 1 \dots 3N$ and define the state vector \mathcal{X} as:

$$\vec{\mathcal{X}}_\alpha = \begin{cases} V_{B_i}, & \alpha = i, & i = 1 \dots N; \\ V_{A_j}, & \alpha = N + j, & j = 1 \dots N; \\ V_{G_k}, & \alpha = 2N + k, & k = 1 \dots N. \end{cases}$$

We introduce $\vec{\mathcal{F}}$ with entries:

$$\vec{\mathcal{F}}_\alpha = \begin{cases} F_{B_i}, & \alpha = i, & i = 1 \dots N; \\ \zeta_{A_j}, & \alpha = N + j, & j = 1 \dots N; \\ \zeta_{G_k}, & \alpha = 2N + k, & k = 1 \dots N; \end{cases}$$

³These results are currently integrated in a paper in preparation.

and $\vec{\mathcal{R}}(\vec{\mathcal{X}})$ with entries:

$$\mathcal{R}_\alpha(\vec{\mathcal{X}}) = \begin{cases} \mathcal{N}_B(V_{B_i}), & \alpha = i, & i = 1 \dots N; \\ \mathcal{N}_A(V_{A_j}), & \alpha = N + j, & j = 1 \dots N; \\ 0, & \alpha = 2N + k, & k = 1 \dots N; \end{cases}$$

We define as well the $3N \times 3N$ matrix \mathcal{U} , characterising the inverse integration times (and depending on CNO) :

$$\mathcal{U} = \begin{pmatrix} -\frac{\mathcal{I}_N}{\tau_B} & 0_{NN} & 0_{NN} \\ 0_{NN} & -\frac{\mathcal{I}_N}{\tau_A} & 0_{NN} \\ 0_{NN} & 0_{NN} & -\frac{\mathcal{I}_N}{\tau_G} \end{pmatrix}, \quad (4.33)$$

and the $3N \times 3N$ matrix \mathcal{L} , summarising chemical synapses interactions:

$$\mathcal{L}^{(c)} = \begin{pmatrix} 0_{NN} & w_B^A \Gamma_B^A & 0_{NN} \\ w_A^B \mathcal{I}_N & 0_{NN} & 0_{NN} \\ w_G^B \Gamma_G^B & w_G^A \Gamma_G^A & 0_{NN} \end{pmatrix}, \quad (4.34)$$

0_{NN} is the $N \times N$ zero matrix and I_{NN} the $N \times N$ identity matrix. Finally, the dynamical system (4.31) can be written in vector form:

$$\frac{d\vec{\mathcal{X}}}{dt} = \mathcal{U} \cdot \vec{\mathcal{X}} + \mathcal{L}^{(c)} \cdot \vec{\mathcal{R}}(\vec{\mathcal{X}}) + \vec{\mathcal{F}}(t). \quad (4.35)$$

We remark that (4.35) has a specific product structure: the dynamics of RGCs is driven by BCs and ACs with no feedback. This means that one can study first the coupled dynamics of BCs and ACs and then the effect on RGCs.

4.7.2 Linear approximation

The dynamical system (4.35) has almost the form of a non-autonomous linear system driven by the term $\vec{\mathcal{F}}(t)$. There is, however, a weak non-linearity, due to the piecewise linear rectification (4.8), appearing in the term $\vec{\mathcal{R}}(\vec{\mathcal{X}})$. Let us remind that this term has been introduced to ensure that the chemical synapse becomes silent when the pre-synaptic neuron's voltage is lower than a threshold θ . This corresponds to a biophysical fact: a synapse cannot change its sign. Therefore, when all cells' voltages are higher than these thresholds, the system can be considered linear. Mathematically, there is a domain of \mathbb{R}^{3N} such that:

$$\Omega = \{ V_{B_i} \geq \theta_B, V_{A_j} \geq \theta_A, i, j = 1 \dots N \}, \quad (4.36)$$

where $R(\vec{\mathcal{X}}) = \vec{\mathcal{X}}$ so that (4.35) is linear. We write $\mathcal{L} = \mathcal{U} + \mathcal{L}^{(c)}$ so that finally:

$$\mathcal{L} = \begin{pmatrix} -\frac{\mathcal{I}_N}{\tau_B} & w_B^A \Gamma_B^A & 0_{NN} \\ w_A^B \Gamma_A^B & -\frac{\mathcal{I}_N}{\tau_A} & 0_{NN} \\ w_G^B \Gamma_G^B & w_G^A \Gamma_G^A & -\frac{\mathcal{I}_N}{\tau_G} \end{pmatrix} \quad (4.37)$$

and (4.35) can be written in the form:

$$\frac{d\vec{\mathcal{X}}}{dt} = \mathcal{L} \cdot \vec{\mathcal{X}} + \vec{\mathcal{F}}(t) \quad (4.38)$$

4.7.3 Linear analysis

We consider the evolution of the state vector $\vec{\mathcal{X}}(t)$ from an initial time t_0 . Typically, t_0 is a reference time where the network is at rest, before the stimulus is applied. So, the initial condition $\vec{\mathcal{X}}(t_0)$ will be set to 0 without loss of generality. The general solution of (4.38) is:

$$\vec{\mathcal{X}}(t) = \int_{t_0}^t e^{\mathcal{L}(t-s)} \vec{\mathcal{F}}(s) ds, \quad (4.39)$$

The behaviour of the solution (4.39) depends on the eigenvalues $\lambda_\beta, \beta = 1 \dots 3N$ of the network transport operator \mathcal{L} and its eigenvectors, \mathcal{P}_β (the columns of the matrix \mathcal{P} transforming \mathcal{L} in diagonal form).

One can show that:

$$\mathcal{X}_\alpha(t) = V_{\alpha_{drive}}(t) + \mathcal{E}_{drive_\alpha}(t) + \zeta_A \mathcal{E}_{CNO_{A\alpha}}(t) + \zeta_G \mathcal{E}_{CNO_{G\alpha}}(t), \quad \alpha = 1 \dots 3N, \quad (4.40)$$

where $V_{\alpha_{drive}}(t)$ corresponds to the drive term (4.13) when $\alpha \leq N$, $\mathcal{E}_{drive_\alpha}(t)$ represents the indirect effect of lateral connectivity, and the terms $\mathcal{E}_{CNO_{A\alpha}}(t)$, $\mathcal{E}_{CNO_{G\alpha}}(t)$ are related to the CNO effect on ACs and RGCs (Souihel et al., 2021).

Effect of lateral connectivity

$\mathcal{E}_{drive_\alpha}(t)$ corresponds to the indirect effect, via the network connectivity, of the drive on cells voltages. It takes the following form:

$$\mathcal{E}_{drive_\alpha}(t) = \sum_{\beta=1}^{3N} \sum_{\gamma=1}^N \mathcal{P}_{\alpha\beta} \mathcal{P}_{\beta\gamma}^{-1} \left(\frac{1}{\tau_B^A} + \lambda_\beta \right) \int_{t_0}^t e^{\lambda_\beta(t-s)} V_{\gamma_{drive}}(s) ds, \quad (4.41)$$

For $\alpha = 1 \dots N$, this is the indirect effect of the drive on BCs, for $\alpha = N + 1 \dots 2N$, on ACs, and for $\alpha = 2N + 1 \dots 3N$ on RGCs.

This equation provides an analytic form of the RF of a RGC, depending on network connectivity (Cessac, 2021). This form is used later on, in order to fit the model's parameters to experimental data.

Effect of CNO

The terms:

$$\mathcal{E}_{CNO_{A\alpha}}(t) = - \sum_{\beta=1}^{3N} \sum_{\gamma=N+1}^{2N} \mathcal{P}_{\alpha\beta} \mathcal{P}_{\beta\gamma}^{-1} \frac{[1 - e^{\lambda_{\beta}(t-t_0)}]}{\lambda_{\beta}}, \quad (4.42)$$

and

$$\mathcal{E}_{CNO_{G\alpha}}(t) = \chi_{\alpha \geq 2N+1} \tau_G \left[1 - e^{-\frac{t-t_0}{\tau_G}} \right] \quad (4.43)$$

correspond, respectively, to the effect of CNO applied to AC and RGC on the network activity. The last term with the indicatrix function ($\chi_{\alpha \geq 2N+1}$) indicates that applying CNO on RGCs has no feedback on the other cells.

The structure of these terms is interpreted as follows. The drive (index $\gamma = 1 \dots N$) excites the eigenmodes $\beta = 1 \dots 3N$, with a weight proportional to $\mathcal{P}_{\beta\gamma}^{-1}$. The mode β , in turn excites the variable $\alpha = 1 \dots 3N$ with a weight proportional to $\mathcal{P}_{\alpha\beta}$. The time dependence and the effect of the drive are controlled by the integral $\int_{t_0}^t e^{\lambda_{\beta}(t-s)} V_{\gamma_{drive}}(s) ds$. The cumulative CNO effects are controlled by $\mathcal{E}_{CNO_{A\alpha}}(t)$, $\mathcal{E}_{CNO_{G\alpha}}(t)$.

Spectrum of \mathcal{L}

The core of our analysis relies in the determination of the eigenvalues and eigenvectors of the linear operator \mathcal{L} (eq. (4.37)). The spectrum of \mathcal{L} is related to the spectrum of the connectivity matrices W_B^A (ACs to BCs) and W_A^B (BCs to ACs). Assuming that these matrices commute, one can show that there is a dimensionless parameter μ that controls the stability of the linear system (eq. 4.38) and summarises the effect of network connectivity on the RGCs response (Souihel et al., 2021).

$$\mu = -w_B^A w_A^B \tau^2 \geq 0. \quad (4.44)$$

where:

$$\frac{1}{\tau} = \frac{1}{\tau_A} - \frac{1}{\tau_B}. \quad (4.45)$$

Basically, μ reduces the network contribution on the activity of RGCs to four parameters; namely, the synaptic weights $-w_B^A w_A^B$ corresponding to the reciprocal influence of BCS to ACs and the characteristic time constants of their responses (τ_A and τ_B). In the following section, we will demonstrate with numerical simulations of the model how this parameter controls the variability of RGCs responses.

4.8 Numerical results

Having formulated our model, we now confront it to empirical data using numerical simulations. Our aim was not to compare quantitatively the experimental observations to the simulated responses, but rather to illustrate how our model can capture the broad qualitative features of the data. Specifically, we demonstrate how the model can induce linear kernels close to those measured physiologically, and can also account for the variety of cell responses in any of the two experimental conditions, proposing potential underlying mechanisms that explain this diversity.

4.8.1 Physiological reproductions

The first test of our model was the reproduction of the physiological difference between monophasic and biphasic cell types in control condition. RGCs receive and integrate signals typically across many different BCs and ACs, which also interact with each other. We believe that such network connectivity gives rise to various response patterns at the level of RGCs and we show that our model can reproduce this variability qualitatively.

For the following simulations, we consider a network with 40 cells per layer. BCs, ACs and RGCs are placed on a one dimensional horizontal grid, respectively, and are connected as described in section 4.6.2. Two dimensional cases will be studied in Chapter 5.

Parameters tuning In Chapter 3, we have fitted RGCs' responses using the LN model and we have obtained the spatio-temporal profiles and non-linearities for each of them. We remind that the spatio-temporal function obtained using reverse-correlation to white-noise stimulation represents the impulse response of a cell (see 3.3.1). Another way to get the impulse response of a cell is to present a brief pulse (of unit area), mathematically corresponding to a Dirac distribution, and measure its response. Based on this principle, we first performed several simulations of our model with a spatially uniform flashed stimulus and then we tuned our model using a gradient descent algorithm to minimise the L^2 - distance between the experimental RF and the simulated RGC response.

Consequently, we could infer a possible behaviour of the ACs and BCs involved in the RGCs' network leading to a specific response, even if we didn't have access to their responses experimentally. Note, however, that the model does not tell us what the biological ground truth of the entangled BCs, ACs, RGCs dynamics is, rather it suggests what it might be.

Responses variability Now that our model is calibrated to best fit the experimental responses of a monophasic and a biphasic cell, we show the simulated responses in Figures 4.4 and 4.5. Each figure illustrates: the simulated responses of the OPL, BC and AC (top panel) and the simulated response of the RGC located at the centre of the network vs the experimental temporal STA of this cell (middle panel) in CTL and CNO conditions. Finally, the bottom panel shows a different

representation of the middle panel, by comparing the experimental traces (left) to the simulated ones (right) in CTL and CNO conditions.

Here, we focus on understanding the underlying mechanisms that can produce different response patterns at the level of RGCs in CTL condition (left column, top and middle panel). More details on the CNO condition will be given in a later section. We start by comparing the top panels of Figures 4.4 (monophasic cell) and 4.5 (biphasic cell), that present the synaptic inputs that RGCs receive.

BCs' (blue dotted line) response to the stimulus follows first the OPL response (black line). The depolarisation of BCs consequently excites the connected ACs (red dash-dotted line) and RGCs (green line in middle panel). However, the excitation of ACs gradually hyperpolarises BCs and RGCs, through their inhibitory synaptic drive. Thus, RGCs in both cases receive a combination of excitatory and inhibitory inputs from their afferent circuit, yet they exhibit quite different response patterns. This can be potentially explained by the characteristic time scale of ACs and the synaptic weights. Specifically, in the case of the biphasic cell (Fig. 4.5) ACs respond faster than in the case of the monophasic cell (Fig. 4.4), leading to a strong hyperpolarisation and biphasic response pattern in RGCs.

4.8.2 Role of ACs lateral connectivity

Under the assumption about the role of ACs' time constant on the RGCs' response, we run several simulations where we vary the value of parameter τ_A , the characteristic time constants of ACs, while keeping all the other parameters fixed. Figures 4.6 and 4.7 present these simulations for the previously shown monophasic and biphasic cells, respectively. Each figure illustrates: the simulated responses of the OPL, BC and AC (panel A) and the simulated response of the RGC located at the centre of the network, for different values of the parameter τ_A vs the experimental temporal STA of this cell (panel B).

These simulations are revealing in several ways. Changing the characteristic time of ACs, not only affects how slow or fast ACs will respond but also the amplitude of their response as well. These two effects, when combined, may lead to a switch from monophasic to biphasic response, and vice versa, of the BCs and consequently of the RGCs.

This finding is in line with the mathematical analysis of the model dynamics, that emphasised the role of the reduced parameter μ (4.44). This parameter tunes the spectrum of the transport operator \mathcal{L} , which controls the dynamical network effects. In particular, variations of μ can lead to a situation where eigenvalues of \mathcal{L} are real to a situation where some eigenvalues become complex conjugates. The switch from monophasic to biphasic corresponds to the existence of complex eigenvalues.

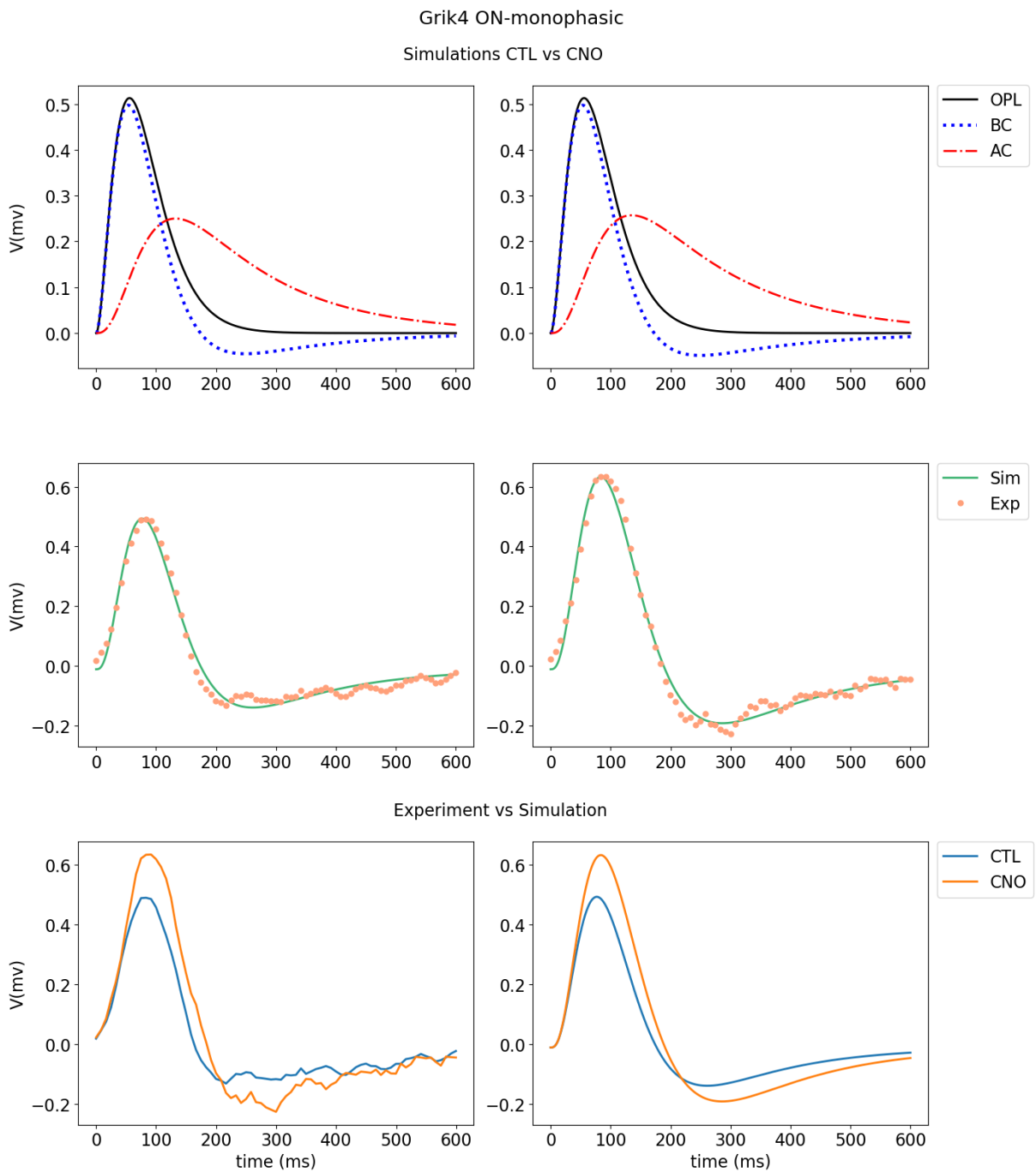


Figure 4.4. Model simulation of a Grik4 ON-monophasic RGC's response to a spatially uniform flashed stimulus. *Top*. Temporal response of the OPL, BC and AC in CTL (left) and CNO (right) condition. *Middle*. Simulated RGC response (green) and experimental temporal STA (orange dotted) in CTL (left) and CNO (right) condition. *Bottom*. Experimental RGC response (left) vs simulated RGC response (right) in both conditions.

4.8.3 CNO effect on the retinal network

The final section addresses the impact of CNO on the retinal network. As described earlier, DREADD activation with CNO acts on a RGC's response in two ways: (1) Directly, by increasing

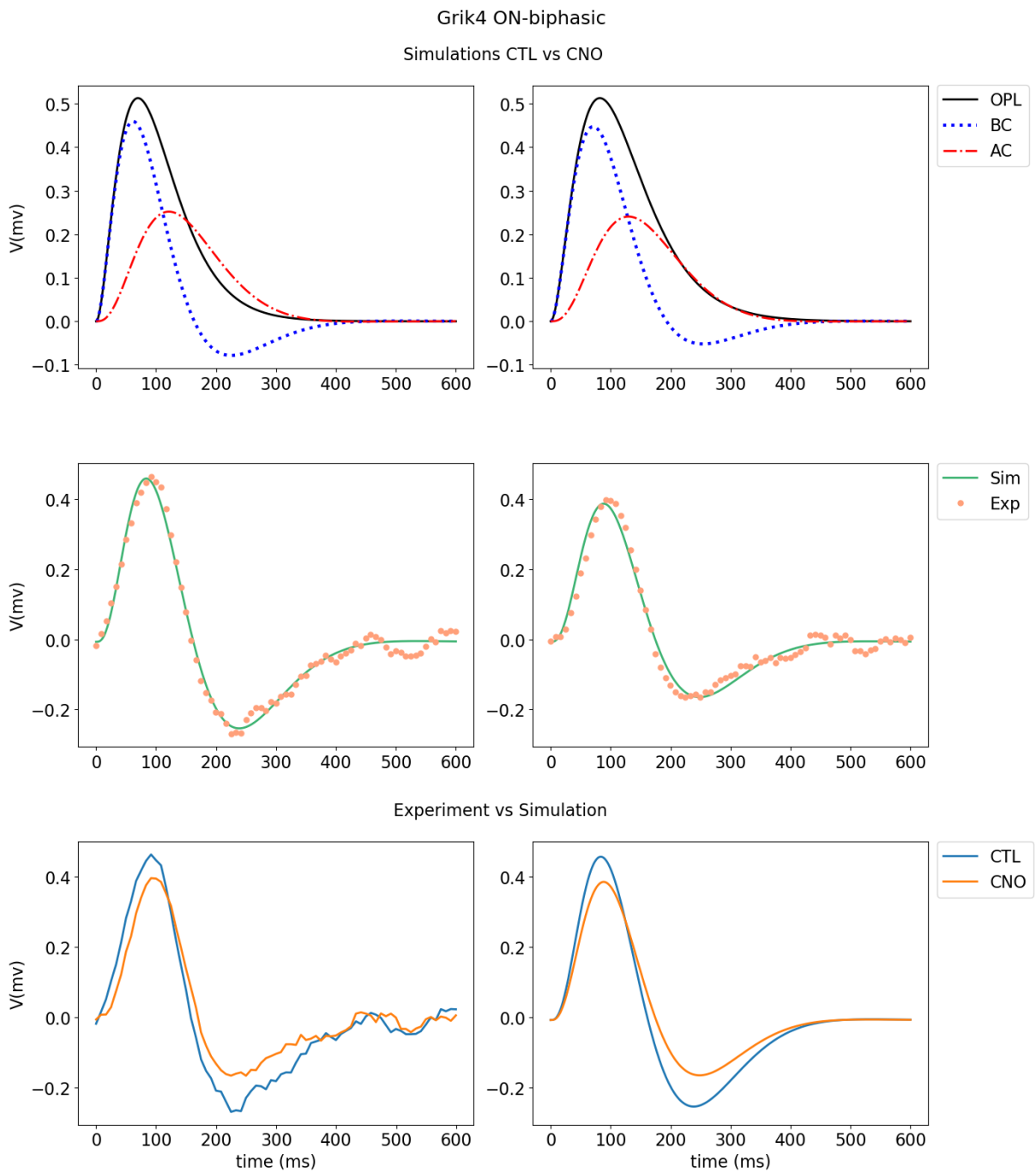


Figure 4.5. Model simulation of a Grik4 ON-biphasic RGC's response to a spatially uniform flashed stimulus. *Top*. Temporal response of the OPL, BC and AC in CTL (left) and CNO (right) condition. *Middle*. Simulated RGC response (green) and experimental temporal STA (orange dotted) in CTL (left) and CNO (right) condition. *Bottom*. Experimental RGC response (left) vs simulated RGC response (right) in both conditions.

its baseline activity and membrane conductance, with the latter causing a decrease on the cell's time constant, (2) Indirectly, by the propagation of the enhanced inhibitory effect of ACs to the whole network. Untangling these combined effects is difficult on purely experimental grounds, as we do not have access to BCs and ACs. This is further supported by the experimental results

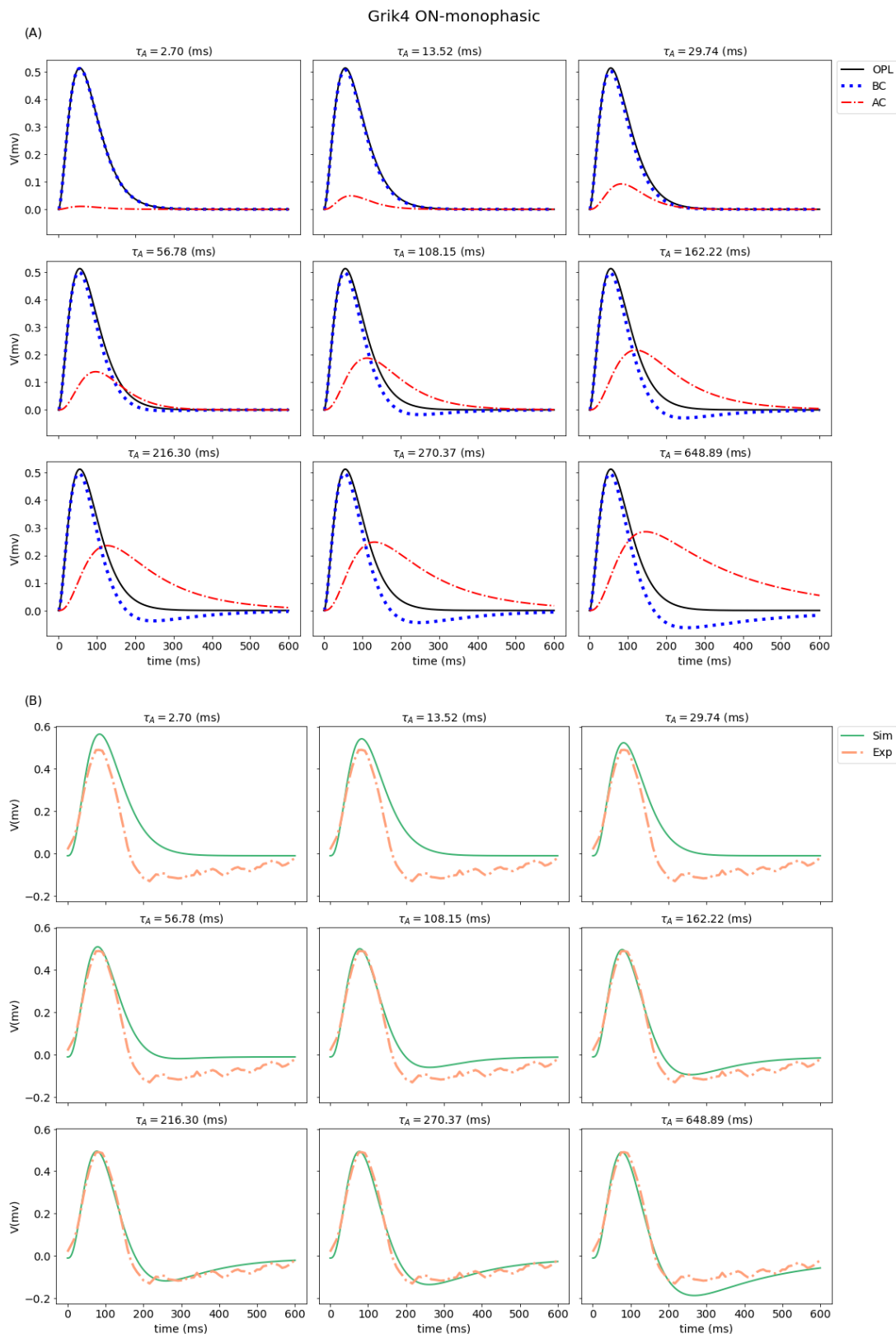


Figure 4.6. Simulating the variation of the characteristic time constant of ACs for a Grik4 ON-monophasic cell. *Top.* Temporal response of the OPL, BC and AC. *Bottom.* Simulated RGC's response (green) and experimental temporal STA (orange dotted).

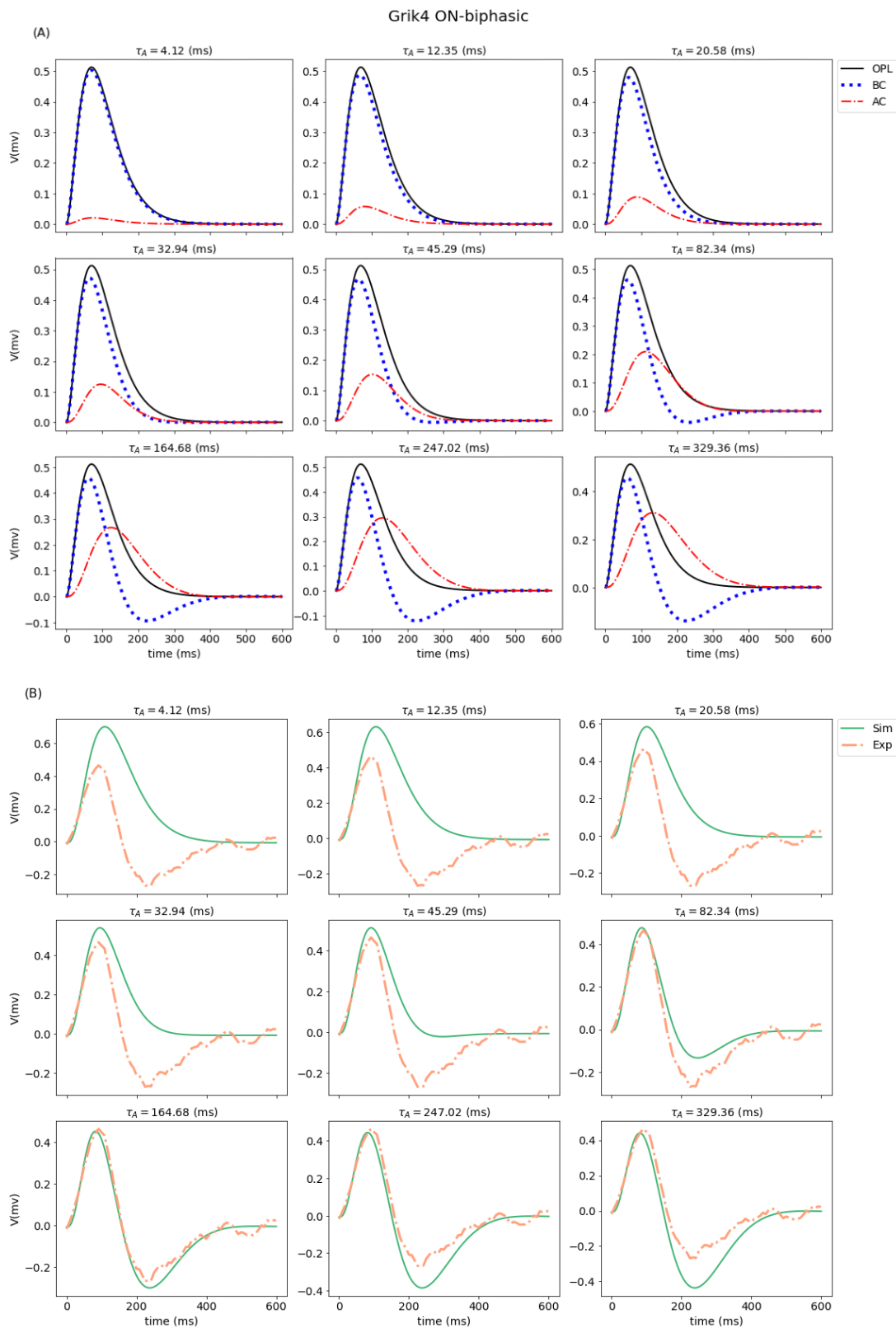


Figure 4.7. Simulating the variation of the characteristic time constant of ACs for a Grik4 ON-biphasic cell. *Top*. Temporal response of the OPL, BC and AC. *Bottom*. Simulated RGC's response (green) and experimental temporal STA (orange dotted).

(Chapter 3), which underlined the existence of various response patterns in CNO condition, even within the same cell type.

Here, we attempt to clarify this diversity using numerical simulations. First, we demonstrate how the model can reproduce the cells' responses in CNO condition and then, we suggest possible interpretations of this variability.

We run simulations of the model in CTL and CNO conditions of four cells that exhibit different response patterns in CNO condition. Figures 4.4, 4.5, 4.8, and 4.9 show these simulations. Each figure illustrates the simulated responses of the OPL, BC and AC (top panel) and the simulated response of the RGC located at the centre of the network vs the experimental temporal STA of this cell (middle panel) in CTL and CNO conditions. Finally, the bottom panel shows a different representation of the middle panel, by comparing the experimental traces (left) to the simulated ones (right) in CTL and CNO conditions.

Regarding the monophasic type (Fig. 4.4 & 4.8), we observe that the former cell tends to become more biphasic, while the latter shows a slightly different effect with an amplitude increase of the peak and an amplitude decrease of the trough. Interestingly, the biphasic cells (Fig. 4.5 & 4.9) show an opposite response pattern in CNO condition. The first cell becomes less biphasic in contrast to the second one that becomes more biphasic. The main difference between the simulations in CTL and CNO conditions, lies in the time scales of the responses of BCs, ACs and RGCs. In particular, the response diversity in CNO condition can be justified as the conjunction of the following:

1. Direct effect on the activity of ACs and RGCs, with ensuing membrane depolarisation.
2. Direct effect on ACs and RGCs membrane conductance which increases as ion channels open.
3. Indirect effect due to network connectivity. As ACs depolarise, their inhibitory effect on BCs and RGCs is enhanced. Consequently, inhibition of BCs leads to less excitation of ACs and RGCs. There is therefore a feedback inhibitory network effect from ACs to ACs that competes with the direct effect of CNO.

Effect (1) impacts directly the RGCs' voltage, whereas (2) and (3) affect the characteristic times of the responses of RGCs. As a result, RGCs' activity may increase or decrease, depending on a fine balance between direct excitation (1), network excitation (BCs) and network inhibition (ACs).

4.9 Summary and Discussion

This chapter introduced a model for disentangling the impact of pharmacological manipulation of neural activity in different cell types on the retinal response to visual stimuli. Based on the mathematical analysis of its dynamics, we made speculations about the implication of

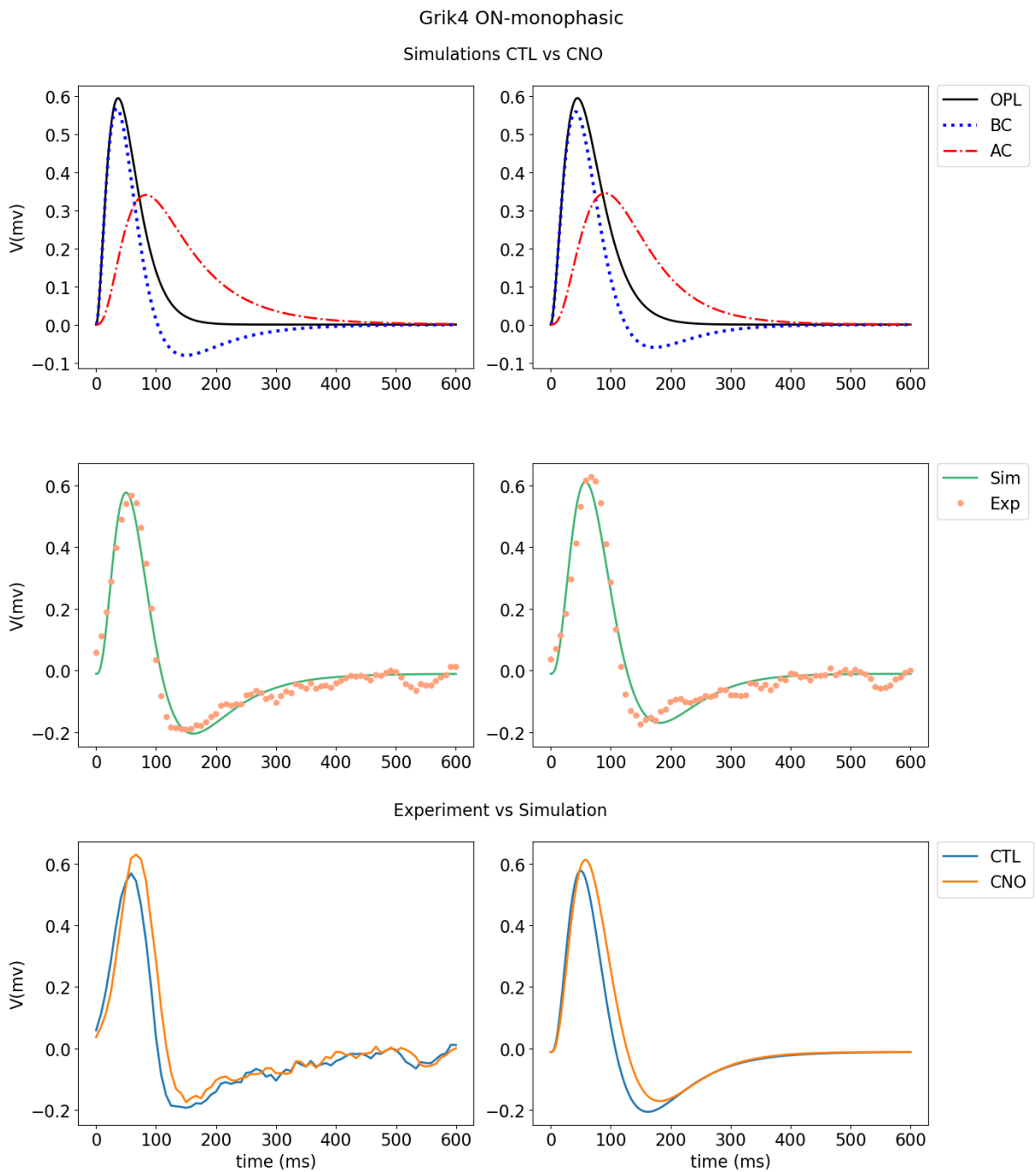


Figure 4.8. Model simulation of a Grik4 ON-monophasic RGC's response to a spatially uniform flashed stimulus. *protectTop*. Temporal response of the OPL, BC and AC in CTL (left) and CNO (right) condition. *Middle*. Simulated RGC's response (green) and experimental temporal STA (orange dotted) in CTL (left) and CNO (right) condition. *Bottom*. Experimental response vs simulated response in CTL and CNO conditions.

lateral connectivity via ACs and we proposed potential underlying mechanisms that explain the experimental observations of Chapter 3. Then, numerical simulations not only showed the ability of the model to capture the response diversity in different experimental conditions, but also illustrated the assumptions underlying such diversity. Our approach, consequently, provides

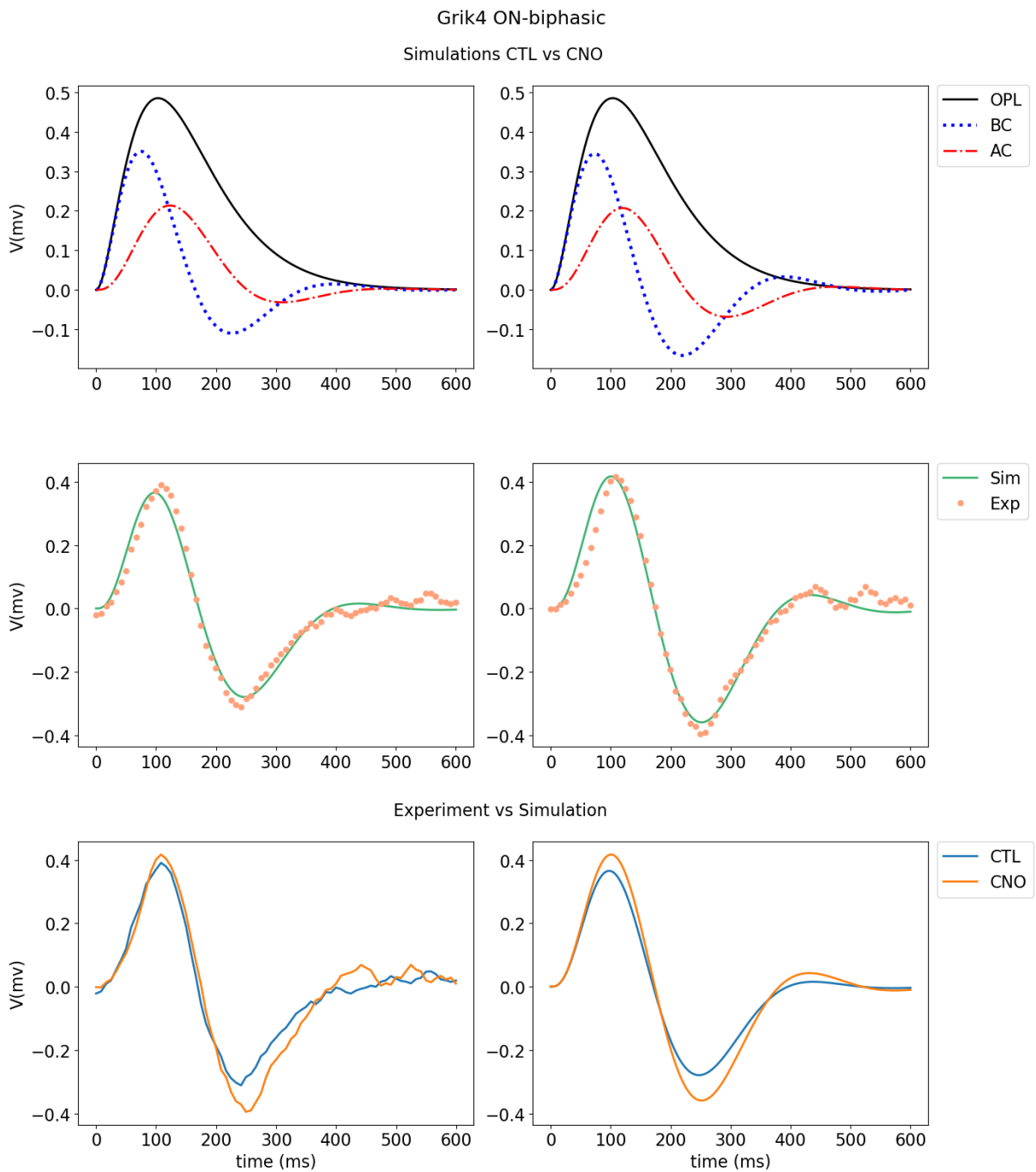


Figure 4.9. Model simulation of a Grik4 ON-biphasic RGC's response to a spatially uniform flashed stimulus. *Top*. Temporal response of the OPL, BC and AC in CTL (left) and CNO (right) condition. *Middle*. Simulated RGC's response (green) and experimental temporal STA (orange dotted) in CTL (left) and CNO (right) condition. *Bottom*. Experimental response vs simulated response in CTL and CNO conditions.

a theoretical framework to anticipate results not yet observed experimentally.

Our finding that the net CNO effect depends on a fine blend of the presynaptic inputs and inner retina connectivity, questions the suitability of DREADDs as a tool for cell identification. Selecting cells only based on their change of activity or if they express DREADDs, might not be

enough and multiple criteria have to be taken into consideration.

So far, our approach is based on modelling the different retinal cell layers, addressing questions directly linked to pharmacological manipulation of their activity in 1D. Nevertheless, this might be too naive as the retina is performing more sophisticated tasks. We could argue that we first explored basic stimuli in order to understand and explain the effect at the baseline, and then we will investigate complex stimuli in 2D with Macular in Chapter 5.

Chapter 5. Probing Retinal Function with a Multi-layered Simulator

In this chapter, we introduce the simulation platform *Macular*, designed to model and simulate the response of the early visual system to visual stimuli or electrical stimulation produced by retinal prostheses, across a range of scenarios, spanning the healthy, developmental and diseased states. To aid with the research presented in this thesis, *Macular* is used to implement on a large-scale the model presented in Chapter 4 and to study the effect of CNO on the retinal response to various stimuli.

This chapter is organised as follows. We start by briefly reviewing the existing simulators, we justify the development of *Macular* by finding its niche and by shortly presenting the software's characteristics and we finally review my personal contributions (Section 5.1). Afterwards, we explain *Macular*'s core architecture and main modules (Section 5.2) and demonstrate its usage with a scenario related to this thesis, the simulation of the model presented in Chapter 4 (Section 5.3). Finally, using numerical simulations, we study the CNO effect on the retinal response to complex stimuli both at the local and global level (Section 5.4).

Contents

5.1	Introduction	82
5.1.1	Yet another simulator?	83
5.1.2	Developing <i>Macular</i>	83
5.1.3	How do we use <i>Macular</i> in the context of this thesis?	85
5.1.4	Software development	85
5.1.5	Contributions	87
5.2	Software Architecture	87
5.2.1	Core concepts	88
5.2.2	Workspaces	93
5.3	Usage Scenario	96
5.4	Simulation Results	98
5.4.1	Physiological reproductions	98
5.4.2	Complex stimuli	101
5.5	Summary and Discussion	108

5.1 Introduction

During the last 50 years, our understanding of the molecular, cellular, anatomical and functional aspects of the nervous system, both in healthy and pathological conditions, has significantly improved (Altimus et al., 2020). This was largely driven by major advances in molecular biology, electrophysiology, genetics and computational neuroscience. In particular, the premise that retinal degeneration is one of the leading causes of visual impairment (World Health Organization, 2019) has drawn significant attention to retinal research, which has substantially benefited from this tremendous progress and has provided unprecedented insight into the retina's anatomy and physiology under normal and pathological conditions, leading to the development of new diagnostic and therapeutic strategies to detect and treat retinal diseases. The ability to record the activity of thousands of neurons simultaneously (e.g. MEA recordings), turning on or off specific neurons in order to elucidate their role in neural circuits (e.g. pharmacogenetics, optogenetics), the rapid evolution of innovative diagnostic modalities (e.g. non-invasive visualisation of retinal structures techniques) together with therapeutic improvements (stem cell and gene therapies as well as retinal prostheses), are among the few breakthroughs that have furthered the development of the field.

However, there still exist formidable challenges that need to be addressed, both at experimental and technological levels (Markram, 2013). On the one hand, the increasing wealth of anatomical and electrophysiological data calls for the rapid development of efficient tools for data collection, sharing, analysis and interpretation. On the other hand, experiments suffer from substantial drawbacks, ranging from time, resource and accessibility constraints, to growing ethical concerns over the use of animals in laboratory, to the variability and lack of reproducibility. At the translational stage, improving diagnostic and therapeutic technologies not only requires powerful software and hardware innovations, but also deepening our understanding of the main mechanisms underlying the behaviour of the retina in health and disease.

Numerical simulation is one key to overcome these challenges. It allows to perform *in silico* experiments so as to reduce the experimental costs, explore and validate intractable hypotheses at the experimental level, design models and test algorithms. Its advantages are manifest in many potential scenarios: affording simulations with a large number of retinal cells (up to millions) in agreement with the real retinal scales, monitoring and recording experimentally inaccessible neurons, as long as their physiological properties are represented as model parameters, mimicking specific deficiencies or pharmacologically induced impairments; emulating electrical stimulation by prostheses, and the list goes on. In a nutshell, simulation has the potential to overcome the ethical, financial and technical barriers of *in vivo* or *in vitro* experiments. Nevertheless, numerical simulations and experiments are widely complementary. Experiments are necessary to constrain the numerical model, check its validity and especially, its predictions, while simulations may unleash their potential. The ultimate goal of this alliance is to unravel the workings of the retina across a range of scenarios, spanning the healthy, developmental and diseased states (Roberts

et al., 2016).

5.1.1 Yet another simulator?

Currently, there exist a plethora of freely-available, open-source and well-documented tools for numerical simulations of neuron models (spiking, non-spiking or firing rate-based) and neural networks, with different levels of biological details and across multiple spatial and temporal scales. Moreover, users have a wide choice of models, ranging from very detailed morphological or biophysical representations of individual neurons, to simpler models, such as the integrate-and-fire (IF) model, particularly handy for large-scale network simulations, or to models that follow a more functional approach.

Popular neural simulators, such as Neuron (Hines et al., 1997) or Genesis (Bower et al., 2003) focus on biologically realistic and detailed models of individual neurons (multi-compartment) and small neuronal networks, while simulation software like NEST (Gewaltig et al., 2007) or Brian (Goodman et al., 2009) favour large network models (single-compartment neuron models), with the latter laying an emphasis on simple user syntax and incorporating user-defined functions easily. Such tools make use of common properties of neurons in order to offer a general framework for neural modelling with tools for analysis and visualisation via either a graphical user interface or an external front-end (such as Python or Matlab). Among simulation software dedicated to the retina and the early visual system, there is a limited number of tools that usually attempt to generalise and capture different mechanisms of retinal processing, thus proposing a functional model of the whole retina (Virtual Retina - Wohrer et al., 2009, Corem - Martínez-Cañada et al., 2016, Pranas - Cessac et al., 2017). However, there exist many other software packages, either as toolboxes in Matlab (Dynasim) or Python (Convis for early visual system processing or pulse2percept for visual prostheses simulations), or web-based platforms (Geppetto).

So, which simulator is "right"? Choosing the "one" simulator is far from trivial, and nearly impossible, as it not only depends on the given modelling problem and the questions one aims to answer, but also on many system quality attributes. Ultimately, each tool works well in the niche it was created for by finding a compromise between computational performance, flexibility, scalability, ease of use and amount of programming knowledge required (Brette et al., 2007).

5.1.2 Developing Macular

During the last years, the Biovision team has developed simulation tools in order to better understand the function of the early visual system in healthy conditions. Virtual Retina (Wohrer et al., 2009) allows large-scale simulations of biologically-plausible retinas, with customizable parameters and different biological features. B. Cessac et al. have developed Enas (Cessac et al., 2016), a platform that integrates tools for the statistical analysis of spike trains and simulation. Lastly, both tools have been merged into Pranas (Cessac et al., 2017), targeting neuroscientists

and modellers by providing a unique set of retina-related tools; namely a retina simulator and a toolbox for the analysis of spike train statistics.

Concerned with the dramatic increase in the number of people affected by visual impairments worldwide, due to population growth, ageing, behavioural and lifestyle changes, and urbanisation (World Health Organization, 2019), our research group aims to study the retina in pathological conditions and better understand the mechanisms linking visual impairment with retinal function. For this purpose, we have developed Macular, a novel platform for large-scale numerical simulations of the early visual system, reproducing the neural response to visual stimuli in the healthy retina (immature or mature), or emulating electrical stimulation produced by retinal prostheses in diseased states. What started as an effort to extend Pranas and overcome its technological limitations, has evolved into a mature and flexible tool that can be used for various studies of the early visual system. To name but a few, the platform can simulate neonatal retinal waves, retinal and cortical responses to prosthetic stimulation, specific inherent or pharmacologically induced impairments, retinal anticipation etc.

Macular has been designed in a modular fashion and can be extended on multiple levels, in a way that is accessible for users from various backgrounds and levels of expertise. The objective is threefold: firstly, to provide a tool that can be used by neuroscientists in order to reproduce experimental results, and in particular, to guide their experiments through hypotheses that can be tested in the simulator; secondly, to provide a flexible and customizable tool which could evolve in synergy with experimental data analysis and according to the user needs/requirements; finally, to facilitate the collaboration between experimentalists and modellers and promote reproducible research.

Macular is similar in spirit and scope to the Brian or Neuron simulators and their ability to simulate models (pre-existing or user-defined) based on equations. However, it is more devoted to visual aspects, providing a large set of features that simplify building and visualising in 3D complex neural models, exploring their dynamics interactively by manually tuning model parameters, running large-scale simulations, recording and plotting the responses of many neurons simultaneously (quantitatively) and monitoring the perceived visual scene (qualitatively). Moreover, it provides an interactive graphical user interface (GUI) with a simple and intuitive ergonomic design for users without a background in programming and mathematics. Macular also offers a software 'front-end', the Macular Template Engine (MTE), which enables users to design their own models in a unified format, describing neurons, synapses and connections with a given set of equations, variables and parameters, without having to write any code. This is achieved by employing code generation techniques that transform high level description of models into efficient low level code, a popular approach that raises flexibility and performance limits in computational neuroscience (Blundell et al., 2018).

Hence, Macular incorporates the best features of existing tools, while providing new ones that are lacking in other simulators. To the best of our knowledge, there does not exist yet such a platform in the community.

5.1.3 How do we use Macular in the context of this thesis?

Here, we use Macular to implement the model presented in Chapter 4 and study the effect of CNO on the retinal response to various stimuli, by controlling the CNO level with tunable parameters and visualising retinal processing at each level. Macular allows us to perform large-scale simulations of our model, to mimic the experimental setup and reproduce experimental responses to specific stimuli, and ultimately to explore retinal behaviour to more complex stimuli.

5.1.4 Software development

Macular has been developed in the context of an AMDT (Action Mutuelle de Développement Technologique - Mutual Technological Development Action) driven by Inria Sophia Antipolis-Méditerranée Research Centre's service SED (supporting experiments & development). AMDT's goal is to develop highly innovative software for Inria's research teams while increasing the level of software engineering skills of the research team through pair programming, using good practices and standard development tools (git, continuous integration, test driven development, etc). The development involves a team of SED engineers and members of the research team, who are incorporated in the development team in order to define which functionalities are needed, to validate the ongoing tasks and to tackle the likely difficulties or bugs.

The SCRUM framework, an agile software development methodology, was used for the development of Macular. SCRUM's fundamental unit is the SCRUM team, consisting of a Product Owner, Scrum Master and the developers. A product owner understands the customer's requirements, prioritises the work and tells the developers what is important to deliver. A Scrum Master plays the role of the facilitator, ensuring the scrum framework is followed. Finally, the developers carry out all the tasks in order to deliver the product.

The idea is to divide the project into milestones (product backlog) that can be completed within time-boxed iterations called sprints. Each sprint starts with a planning that sets the sprint goal and ends with a review and a retrospective, that reviews and presents the work that was completed and identifies future improvements.

In more detail, the SCRUM workflow consists of the following phases:

- Create the **product backlog**, a prioritised list of software requirements that define new features, changes to existing features, bug fixes and infrastructure changes. These are described in an informal, natural language from the perspective of an end user or user of a system, called *user stories*. Lastly, the user stories are broken up in tasks.
- **Sprint Planning**. Select product backlog items to be completed and discuss the sprint scope and goal.
- **Sprint**. The SCRUM team works on the development/testing of the software, as agreed during the sprint planning. Progress and issues are discussed in the *daily standup meetings*,

usually lasting 15'. Each team member answers three questions: (1) What did I achieve yesterday? (2) What am I going to do today (3) Are there any impediments for the realisation of the sprint goal?

- **Sprint Review.** At the end of each sprint, the team reviews the work that was and was not achieved and presents the completed work in the form of a demo of the new features.
- **Sprint Retrospective.** Finally, the team reflects on the past sprint and creates a plan for improvements for the next sprint.

The SCRUM framework was adapted to the nature of this project, the available resources and skills. Macular has been mainly developed in 6 sprints, each lasting for two weeks and scheduled every four months approximately, over the course of 2-3 years. Sprint interims enabled the research team to assimilate the results of each sprint and further test and develop features related to the research conducted in individual projects. Throughout the whole period, 11 SED engineers and 6 members of the Biovision research team collaborated in the realisation of the Macular project. At each sprint, the SCRUM team consisted of approximately 6 people. On the one hand, SED engineers' expertise served the software development in terms of architecture design, GUI, documenting, testing and bug fixing. On the other hand, the members of the Biovision team highly contributed in the aforementioned tasks and were particularly responsible for conceiving, modelling, modifying, unit testing and validating aspects of the project.

Technical details Macular is written in C++ and uses various libraries including, dtk/VTK for visualisation, Qt for developing the GUI, xtensor for numerical analysis with multi-dimensional array and GSL for ODE solvers.

Version Control The latest development version of Macular is hosted on Inria GitLab, where we use the version control system git. This facilitates scientific collaborations on software development projects among people working at Inria.

Software Package Conda constructor is used to create custom installers of Macular for the 3 main operating systems: Linux, Mac, Windows. There are shell installers, MacOS .pkg installers, and Windows .exe installers. Each of these will create an environment on the end user's system that contains the provided specifications, along with any necessary dependencies. These installers are similar to the Anaconda and Miniconda installers.

Installation Macular can be installed with or without Conda, an open source package management system and environment management system. In the first case, Conda handles seamlessly the installation of Macular and its dependencies, while in the latter one will first need to manually install the dependencies and then clone and compile the source code.

5.1.5 Contributions

I have had the opportunity to work on the development of Macular in its infancy (I participated in all sprints) with my contributions spanning various tasks, ranging from laying the cornerstones of the software in terms of architecture, GUI and modelling, to software debugging, to addressing specific questions related to my PhD thesis. I could say that I had to play an intermediary role in the SCRUM team and I could describe myself as an interpreter and the glue that held everything together. Why? On the one hand, I worked closely with the product owner (B. Cessac, a theoretical physicist with limited experience in software development), contributing to the creation of the product backlog and defining new features and changes in the form of user stories. On the other hand, I was part of the developer team, working on developing and debugging Macular, on validating its results and generally on aspects not directly related to my thesis. Thanks to my interdisciplinary training, I was able to assist both sides and bridge the gap between the different perspectives.

A non exhaustive list of my main contributions are listed below:

- Restructure the Virtual Retina module and validate its results. Specifically, I introduced parameters to handle the conversion between reduced units in VR to physical ones in Macular, I investigated the implementation of retina processing at each stage, I searched a large space of parameters and validated the simulation results.
- Design of new cell types, synapses and connectivity patterns.
- Design of the Visual Flow Worker, an object implementing models of retinal response.
- Implement the model presented in chapter 4 and calibrate it on the basis of experimental recordings.
- Perform in silico experiments of the effects of pharmacological drugs acting on the retinal response.
- Software debugging.
- Together with S.Souihel we applied code cleanup techniques, in order to make the code easier to understand, maintain, and modify.
- Together with B.Cessac we co-supervised a master student who extensively tested Macular.

5.2 Software Architecture

In this section, we describe Macular's software architecture. First, we present the basic building blocks of the software, laying at the core of the architectural model, then we explain how these elements come together to form the main components/modules of Macular: the Workspaces.

Figure 5.1 shows a general diagram of Macular structure.

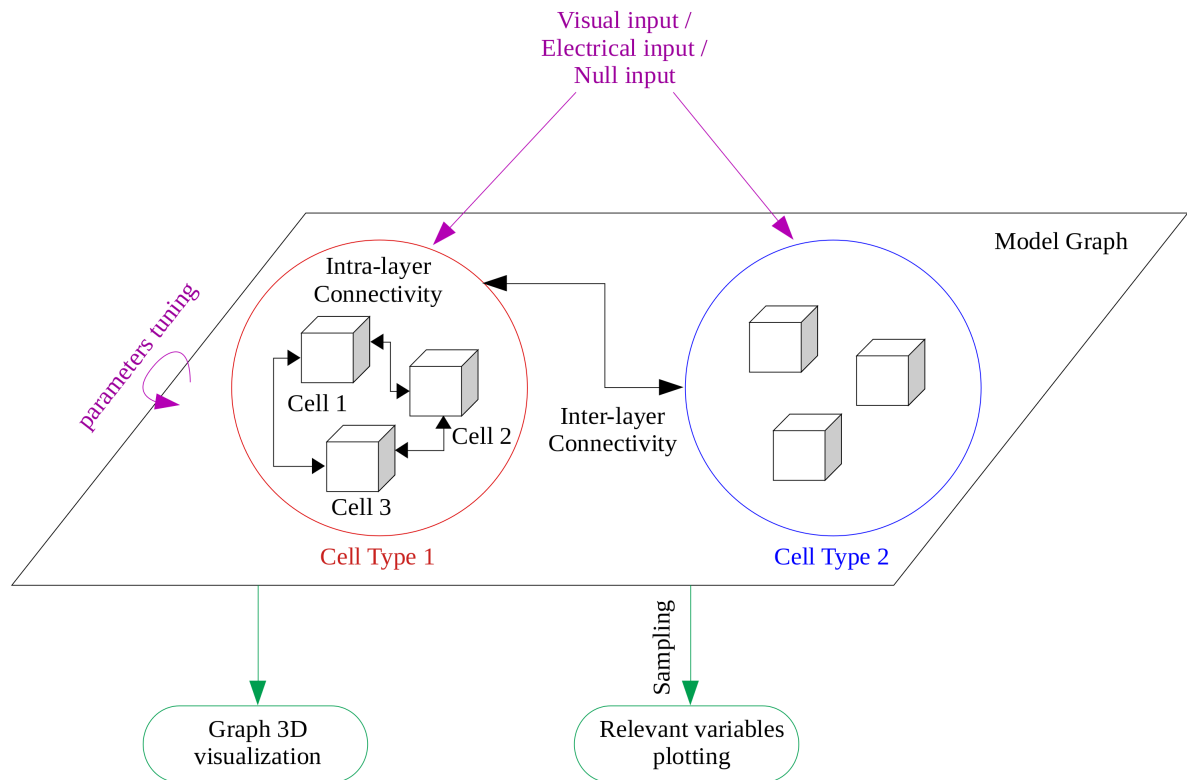


Figure 5.1. General Diagram of Macular architecture. In Macular, a model consists of graph of cell layers, with intra-layer and inter-layer synaptic connectivity, with optional external input. The graph and simulation parameters can be tuned by the User. Finally, the User can visualise cellular activity in a graphic 3D view, or by plotting the relevant variables.

5.2.1 Core concepts

Cells

The core of Macular is an object called "Cell". Basically, it mimics biological cells in the retina or cortex but it is more general than this. It can be, a cell, a group of cells of the same type (e.g. a cortical column), or an electrode in a retinal prosthesis. A cell is noted T_i where T is called the "cell type" and i is the index labelling cells of type T . A cell type can refer either to the cell's biological terminology (e.g. retinal cell layers), to sub-types within these general cell layers, or to its functionality (e.g. excitatory cells).

More precisely, the cell T_i is identified by:

- **An input** $\vec{\mathcal{I}}^{(T_i)}(t)$. The cell receives an entry which can be:
 1. An external input $\vec{\mathcal{I}}_{ext}^{(T_i)}$. For example, an entry corresponding to the input from the Outer Plexiform Layer $\vec{\mathcal{I}}_{OPL}^{(T_i)}$ (defined later on), or the electric current provided by an electrode $\vec{\mathcal{I}}_{stim}^{(T_i)}$. More generally, $\vec{\mathcal{I}}_{ext}^{(T_i)}(t)$ is a vector function depending on time, with several entries.

2. A synaptic input $\mathcal{J}_{syn}^{(T_i)}(t)$ corresponding to synaptic connections with other cells. In general, this contribution sums up the connection with several pre-synaptic cells.

The vector $\vec{\mathcal{J}}^{(T_i)}(t)$ is in general the sum of several contributions (e.g. OPL current and synaptic input).

- **A state.** This is a vector $\vec{\mathcal{X}}^{(T_i)} = (X_0^{(T_i)}, X_1^{(T_i)}, \dots, X_M^{(T_i)})$ of variables evolving in time and characterising the cell's dynamical evolution. Typically, a state variable can be the membrane potential (V), the activity - probability that an ionic channel of a given type is open ($n_k^{(T_i)}$), the concentration of neurotransmitters of a given type released by the cell, etc. By convention, if the set of state variables includes the cell's membrane potential then this is the variable $X_0^{(T_i)}$.
- **A set of parameters.** These are quantities that do not evolve in time, yet they are necessary to constrain the cell evolution. These can be conductances, reversal potentials, membrane capacitance, etc. They can be modified by the user, with sliders or by typing the value in a field on the fly. We note $\vec{\mu}^{(T_i)}$ the vector of these parameters.

Remark. Macular does not check that equations are dimensionally consistent.

- **A function $\vec{\mathcal{F}}^{(T_i)}$.** This controls the time evolution of the cells. In the simplest case, $\vec{\mathcal{F}}^{(T_i)}$ is the vector field of the differential equation:

$$\frac{d\vec{\mathcal{X}}^{(T_i)}}{dt} = \vec{\mathcal{F}}^{(T_i)}(\vec{\mathcal{X}}^{(T_i)}, \vec{\mu}^{(T_i)}, \vec{I}^{(i)}(t)), \quad (5.1)$$

$\vec{\mathcal{F}}^{(T_i)}$ has the same dimension as $\vec{\mathcal{X}}^{(T_i)}$, the state vector.

Cell layers

A Cell layer is the set of cells of type T such that the inputs, state vector, parameters vector and vector field have the same mathematical expression. However, the state values they take can differ. There are preloaded cell types in Macular, but the user can also define his own type.

In Macular, cells are considered as points i.e. soma, axons, synapses belonging to a given neuron are located at the same point. Cells within a given layer are organised in a two dimensional grid, and different Cell layers are located on a 3 dimensional grid, where distances are expressed in *mm*.

Each layer corresponds to a given type and all cells of type T have the same z coordinate. Thus, the cell T_i has coordinates (x_i, y_i, z_T) where the vertical coordinate z_T configures the cell's type and the coordinates (x_i, y_i) the position of cell i in the layer T .

Synapses

Cells can be connected either by chemical synapses or gap junctions. In Macular, the Synapse lies on a spectrum ranging from biophysical to more phenomenological connection models. Macular affords to consider different types of synapses. Some synapse models are preloaded, but the user can also define his own synapse similarly to cell types. A Synapse is noted S_i where S is called the "synapse type" and i is the index labelling synapses of type S . It connects a pre-synaptic cell T_i to the post-synaptic cell T'_j .

A Synapse S_i is identified by:

- **A set of parameters.** These are quantities that do not evolve in time but constrain the connectivity function of the Synapse. These can be conductances, connectivity weights, reversal potentials, etc. They can be modified by the user, with sliders or by typing the value in a field on the fly.
- **A function.** The mathematical representation of the synaptic connection. It could compute either a synaptic current ($I_{syn}^{(T_i \rightarrow T'_j)}$), a voltage ($V_{syn}^{(T_i \rightarrow T'_j)}$) or a firing rate ($FR_{syn}^{(T_i \rightarrow T'_j)}$). These quantities depend in general on the state vector of pre- and post-synaptic cells.

Remark. A post-synaptic cell receives in general many inputs from different cells of different cells types. So, the general form of the synaptic current $\mathcal{I}_{syn}^{(T_i)}(t)$ introduced earlier is:

$$\mathcal{I}_{syn}^{(T_i)}(t) = \sum_{T'} \sum_{j \in T'} I_{syn}^{(T_i \rightarrow T'_j)}(t), \quad (5.2)$$

where the first summation holds on cells layers (types) and the second summation on the cells of type T' pre-synaptic to cell i . The same formulation holds in the case of a voltage or a firing rate input.

Graph

Synapses define a natural notion of intra- and inter-layer connectivity. If the cell T_i is pre-synaptic to cell T'_j , with a synapse of type S , we note $T_i \xrightarrow{S} T'_j$ the oriented edge featuring this connection. The set of edges of type S defines a directed graph $\mathcal{G}^{(T \xrightarrow{S} T')}$. This graph features the set of synaptic connections of type S , from layer T to layer T' . If $T = T'$ we speak of "intra-layer connectivity" of type S , and "inter-layer" if $T \neq T'$. Between two layers there may exist several types of synaptic connections and a cell can be a source or a target to different types of synapses (e.g. an amacrine cell can connect to a bipolar cell through a glycinergic synapse and a gap junction)

In Macular, there are 3 types of connectivity patterns that a graph can implement:

- **Nearest neighbours**, where a cell is connected to the cells that are in a defined neighbourhood.
- **Gaussian**, where the probability to connect to a cell depends on the distance between the cells via a Gaussian distribution.
- **One-to-one**, that holds only for inter-layer connectivity.

Outer Plexiform Layer

The real retina is organised into layers. In particular, the synaptic interactions of photoreceptors with horizontal cells take place at the Outer Plexiform Layer (OPL). In Macular, the OPL is essentially represented by the cell's receptive field (RF). The RF of a cell is a region of the visual field (the physical space) in which stimulation alters the voltage of this cell. It is common, as we do here, to model the RF of cell T_i (if it has one) by a spatio-temporal kernel $\mathcal{K}_{T_i}(x, y, t)$. The linear response of the RF to a visual stimulus is then given by:

$$\left[\mathcal{K}_{T_i}^{x,y,t} * \mathcal{S} \right] (t) \equiv \int_{x=-\infty}^{+\infty} \int_{y=-\infty}^{+\infty} \int_{s=-\infty}^t \mathcal{K}_{T_i}(x, y, t-s) \mathcal{S}(x, y, s) dx dy ds. \quad (5.3)$$

Here $\overset{x,y,t}{*}$ means space-time convolution. In Macular, convolutions are computed using a fast method called Deriche filters (Deriche, 1987; Wohrer et al., 2009). Stimuli are monochrome in Macular, consisting of various levels of gray.

A RF is separable if it can be written in the form $\mathcal{K}_{T_i}(x, y, t) = \mathcal{K}_{T_i,S}(x, y) \mathcal{K}_{T_i,T}(t)$ where $\mathcal{K}_{T_i,S}$ is called the spatial part and $\mathcal{K}_{T_i,T}$ the temporal part. In Macular separable kernels have the following form

- **Difference of circular Gaussians** for the spatial part:

$$\mathcal{K}_{T_i,S}(x, y) = \frac{A_c}{2\pi\sigma_c} e^{-\frac{1}{2\sigma_c^2}((x-x_i)^2+(y-y_i)^2)} - \frac{A_s}{2\pi\sigma_s} e^{-\frac{1}{2\sigma_s^2}((x-x_i)^2+(y-y_i)^2)}, \quad (5.4)$$

where x_i and y_i are the coordinates of the receptive field center which coincide with the coordinates of the cell.

- **Generalised exponential kernels** for the temporal part:

$$\mathcal{K}_{T_i,T}(t) = \begin{cases} e^{-\frac{t}{\tau}} H(t) \equiv E_{\tau}(t), & \text{exponential;} \\ \frac{(nt)^n}{(n-1)!\tau^{n+1}} e^{-\frac{nt}{\tau}} H(t) \equiv E_{n,\tau}(t), & \text{gamma, } n \geq 1; \end{cases}, \quad (5.5)$$

where H is the Heaviside function that mimics causality. These functions mimic the cascade of synaptic and cellular integrations, from photoreceptors to bipolar cells, in a cascade (convolution) of low-pass filters.

Note in particular that $E_{n,n\tau}(t) = \underbrace{E_{\tau}(t) * \dots * E_{\tau}(t)}_n$.

Space and Time Representation

In Macular, there are 3 spaces of representation :

1. **Real space.** This is the space where the visual scene takes place. In Macular, visual scenes are movies made of pixels with light intensity ranging from 0 to 255. So, the real space scale unit is the pixel.
2. **Input space.** This is the space of representation of the projection of the input on the retina. We consider two cases of such projections in Macular:
 - **Receptive field response to a visual stimulus.** Here, space scales (e.g. the size σ_c, σ_s of the center-surround of the receptive field) are expressed in degrees of visual field. The variable "pixels-per-degree" allows the conversion from the real space to the input space.
 - **Prosthetic response to a visual stimulus.** Here, space scales (e.g. spacing between electrodes, or localisation of the prosthesis with respect to the optic disk) are expressed in *mm*.
3. **Retinal space.** In the retinal layers, the space scales are expressed in *mm*. The conversion from the input space (when using degrees) to the retinal space is done multiplying degree scales (in the input space) by the implicit variable "mm-per-degree". This variable depends on the animal species (this is $0.2857 \text{ mm deg}^{-1}$ in humans and 0.03 mm deg^{-1} in mice (Remtulla et al., 1985)).

In addition, when simulating the response of a cell to a visual scene there are several space and time scales involved.

Space Scales

- Cells spacing for cells of type T (mean distance in the case of random location): a_T (*mm*).
- Receptive fields for cells of type T : $\sigma_{T,c}$ (center), $\sigma_{T,s}$ (surround) (*mm*).
- Retina size (square): L (*mm*).

In order to have a realistic simulation these space scales must satisfy:

$$a_T \leq \sigma_{T,c} < \sigma_{T,s} \ll L$$

Time Scales There are many time scales involved in Macular: times scales involved in neurons intrinsic dynamics (e.g. speed of activation/inactivation of ionic channels), times scales involved in synaptic responses, time scale of variation of the stimulus, etc. We summarise them into 3 main time scales:

- Dynamical time scale for a cell of type T : τ_T (s). This is intended to encompass intrinsic neurons dynamics and synaptic dynamics. We define it as the characteristic time for the cell to respond to a flashed light with maximal intensity.
- Characteristic time of variations in the stimulus: τ_S (s). Typically, this can be the time lag between two frames in the movie presented to Macular.
- Time scale of numerical integration: dt (s). Typically, this is the time step in the ODE integrator.

In order to have a realistic simulation these time scales must satisfy:

$$dt \ll \tau_{T,d} < \tau_S$$

5.2.2 Workspaces

Workspaces are the main components of Macular, implementing different functionalities and visualising the results, each using a dedicated graphical user interface. Basically, the user interacts with the GUI to carry out high-level operations with specific data structures and algorithms. There are three workspaces in Macular, the Graph Generator, the Simulator and the Template Engine ¹. In the following, we describe only the first two, as they fall within the scope of this thesis, in terms of functionality, inputs and features.

Graph Generator

Functionality

The Graph Generator allows the user to create a new retinal and/or cortical graph using the existing Cell/Synapse types. In Macular, a Graph can be represented as:

- **A mathematical structure:** made up of vertices, here cell layers, which are connected by edges, here synapses, in an intra- and inter-layer fashion (see 5.2.1).
- **A C++ object:** that stores the Cells, Cell types and coordinates, Synapses and Synapse types.
- **A .mac file:** that is a description of the generated graph, in terms of Cell types and coordinates, Synapse types and connectivity. This file can be then used in the simulator workspace.

¹The Template Engine allows the user to create new Cells and Synapses types on the fly.

Inputs

- **Cell Layers:** a layer is a grid, consisting of Cells of the same type, designed as an $m \times n$ matrix (rows and columns giving the total number of Cells). The layer has a length and width, specifying the spacing between the Cells. The Cells can also be potentially connected with intra-layer Synapses, defined by a type and a connectivity pattern.
- **Synapses:** the inter-layer connectivity of the already created Cell layers. It requires two separate Cell layers, defining the pre-synaptic and the post-synaptic terminals, the Synapse type and the connectivity pattern.
- **States:** the initial range of values of the cells' vector field variables.

Features

- **Generate a new Graph:** The user can create one or multiple Cell layers, specifying the parameters, and the potential intra-layer connectivity. The user can also add inter-layer synapses, to connect the different layers of cells. The graph is then generated and can be visualised in three dimensions (Fig. 5.2).
- **Save the Graph:** The user can save the description of the generated graph in a *.mac* file.
- **Open a Graph:** The user can load a previously saved graph from a *.mac* file and edit it.

Simulator

Functionality

The Simulator allows the user to perform numerical simulations of cell dynamics or cell responses to visual or electrical stimuli.

Inputs

- **Stimulus:** a video input (sequence of images).
- **Graph:** a *.mac* file with the description of a generated graph model.
- **Worker:** a C++ object that implements the model as defined in the Graph. It basically handles the flow of information in the different cell layers, by updating the graph inputs and the graph states. There are currently three implementations of the Worker in Macular, depending on the different input that the model receives, as listed below:
 - **Visual Flow:** Implements models of retinal and/or cortical response, where the input is the OPL response to visual stimuli. Here, the OPL emulation is done with the *Virtual Retina*, a module that has been introduced in Macular after restructuring the homonymous software *Virtual Retina*, developed by Wohrer et al., 2009 and the Biovision team. In the context of this thesis, the Visual Flow Worker is used.

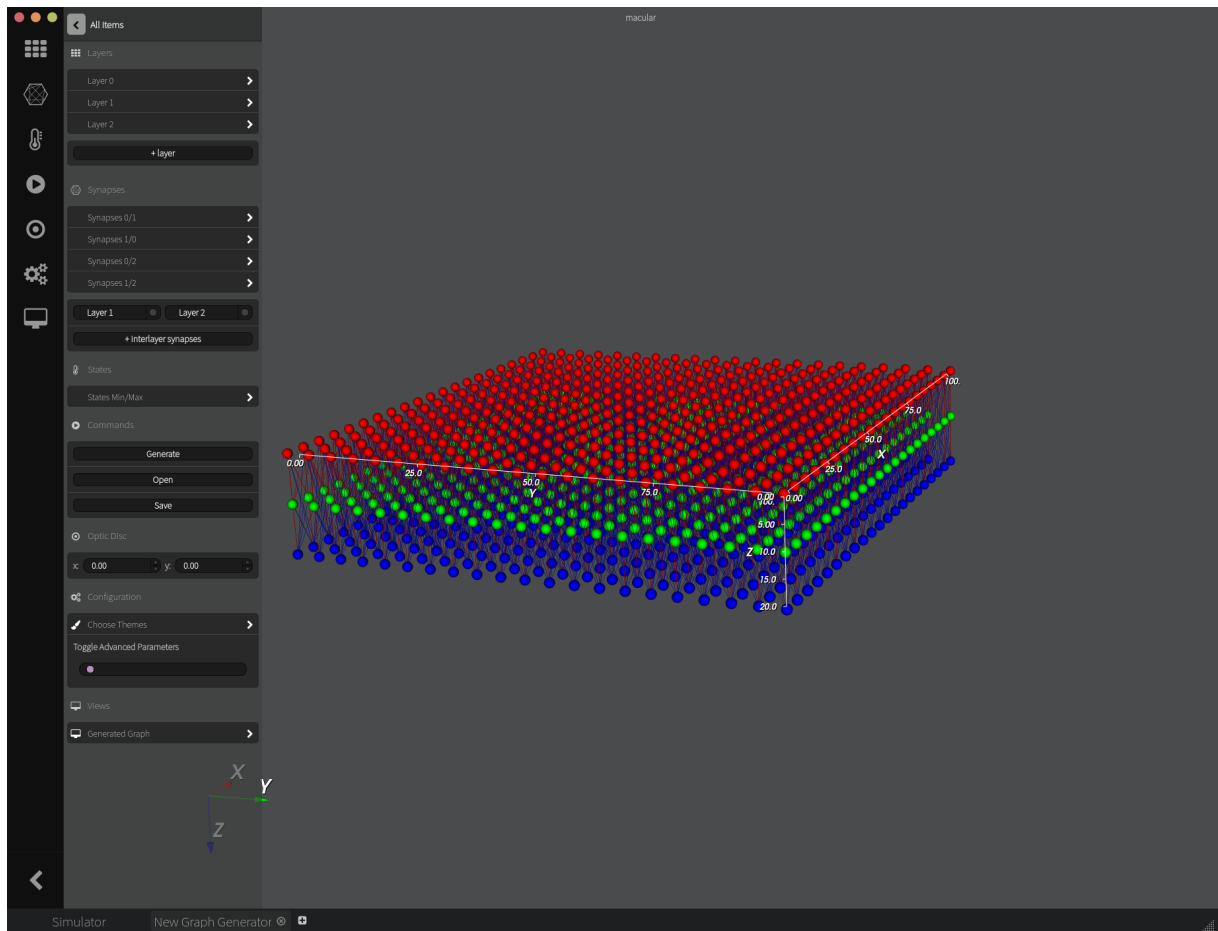


Figure 5.2. Graph generator workspace. A retinal model with three Cell layers: bipolar, amacrine and retinal ganglion cells (from top to bottom), connected with various synaptic patterns. Each layer consists of 21 by 21 cells. On the left panel, the user can add/edit/remove Cell layers and Synapses, set the initial range of the cells states and export the graph in a *.mac* format.

- **Prosthesis:** Implements a model that intends to emulate the retinal prosthesis, where the input is the electric current provided by electrodes.
- **None:** Implements a model with no input stimulus, e.g. in the case of retinal waves.

Features

- **Inputs settings:** The user can load a *.mac* graph file and a stimulus file, as well as select a Worker.
- **Parameters tuning:** The user can tune the parameters related to the Worker, the model (e.g. Cell and/or Synapse parameters), the simulation (e.g. integration time step, frame rate of the stimulus etc.), the storing of the output and the visualisation.
- **Visualisation output:** The graph model can be represented in 2D and 3D views (Fig. 5.3).
- **Plotting:** The user can record and monitor the time evolution of specific cells variables.

- **OPL Output:** The different stages of retinal processing in the OPL as computed by the Virtual Retina module can be seen in a dedicated panel (Fig. 5.4).
- **Saving output:** Cell responses can be saved in a .csv file, where each column corresponds to a selected state.

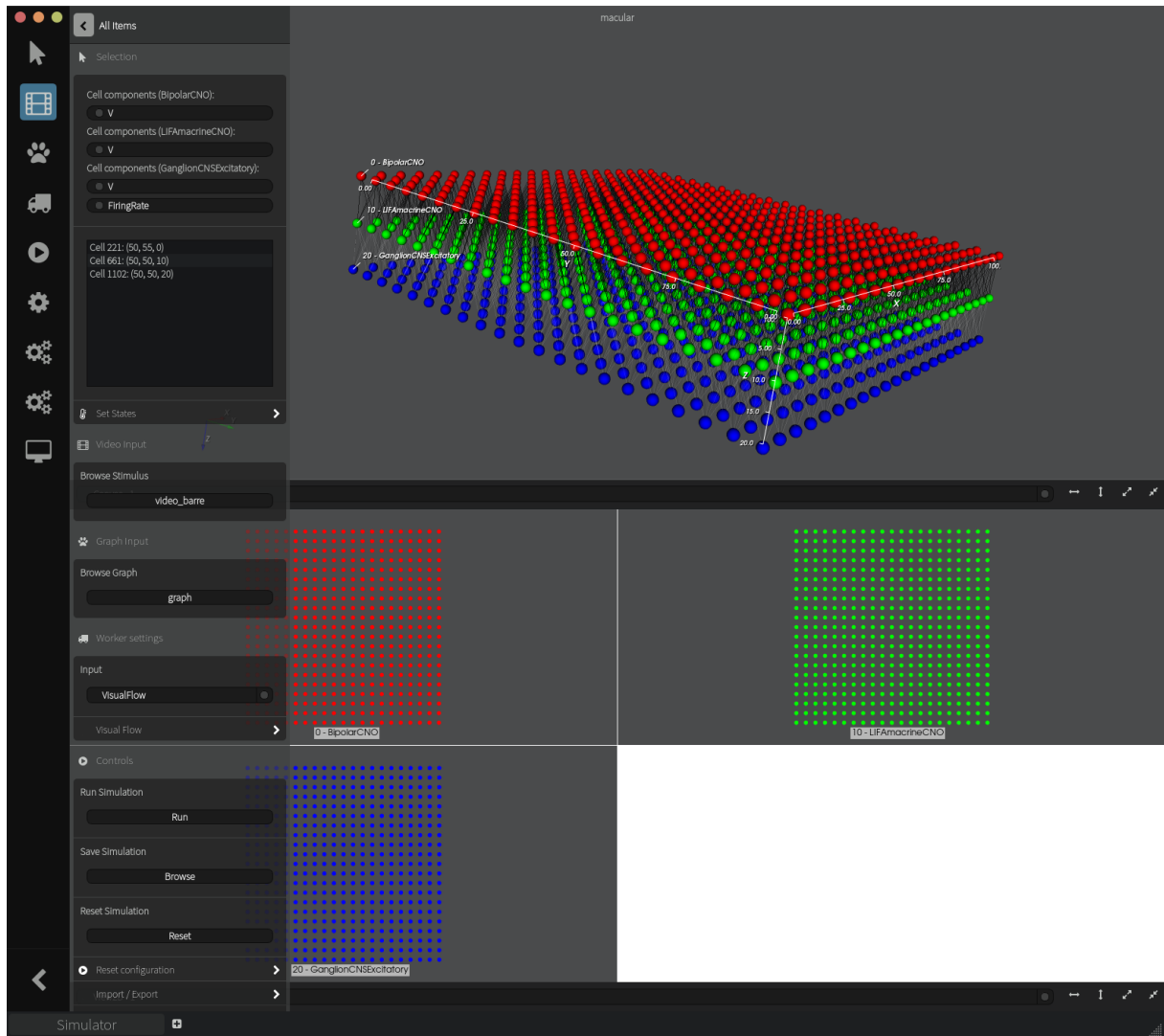


Figure 5.3. Simulator workspace visualisation. There are two visualisation options for the graph: 3D (*top*) and 2D view of each layer separately (*bottom*). On the bottom view, the user can select specific cells in each layer. Then, on the left panel he can select which variables of these cells will be saved in an output file. In addition, the user can load a stimulus file, select a Worker and edit its settings and tune various parameters. Same model as in Fig. 5.2

5.3 Usage Scenario

We now demonstrate how Macular is used in the context of this thesis. We explain step by step how to build the model presented in Chapter 4 and perform numerical simulations. The goal

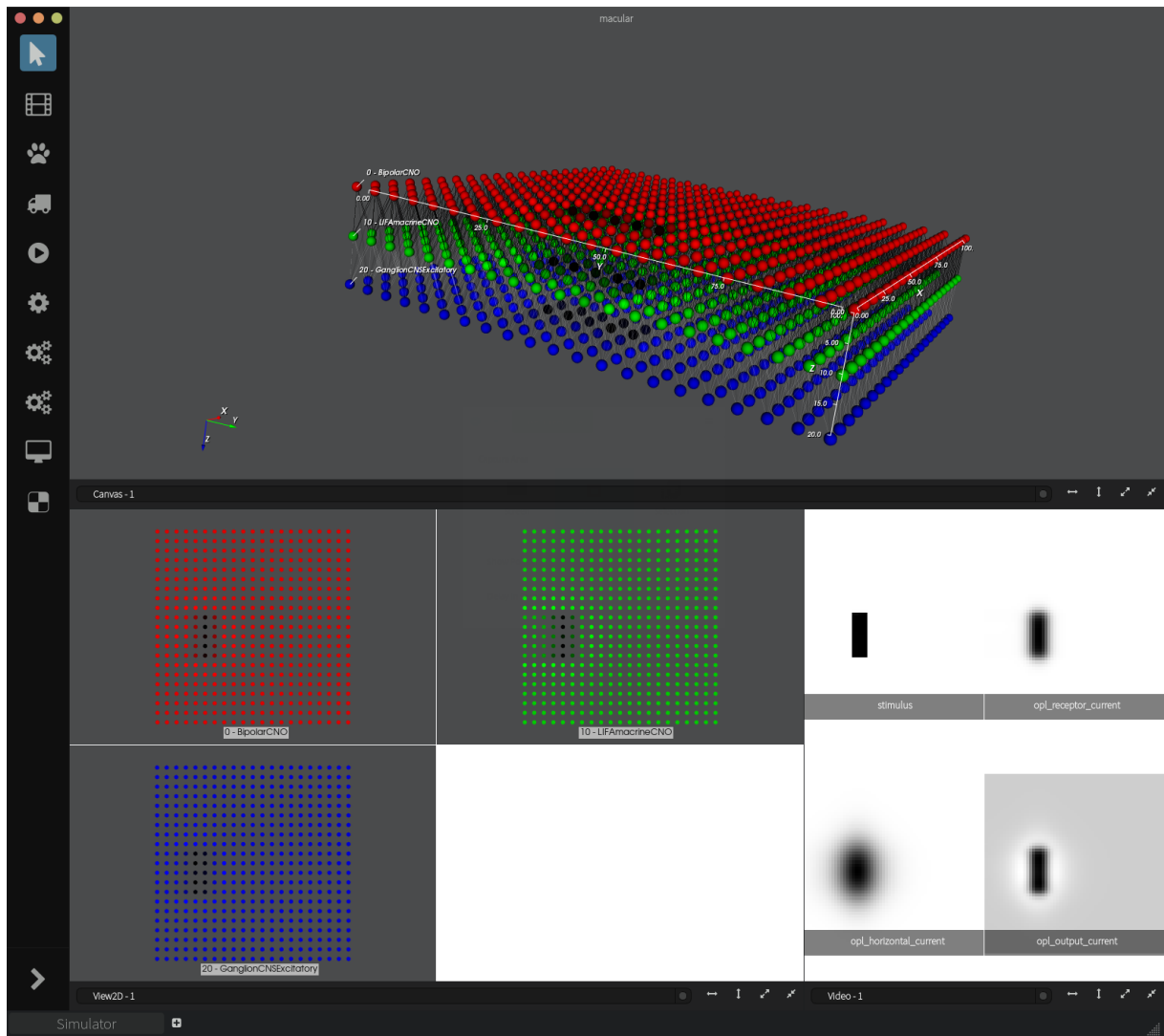


Figure 5.4. Simulator workspace in action. A simulation of the model of Fig. 5.2 with a moving bar stimulus. Bottom right panel shows the different stages of the OPL output as computed by the Virtual Retina module.

here is not to re-describe our model, but rather to provide an example of how Macular can be used for modelling and simulating the retina.

1. Graph generator: create the graph model according to Chapter 4. There are three Cell layers: BCs, ACs and RGCs. Each layer is connected to the others as illustrated in Fig. 4.1 and explained in section 4.6.2. The resulting graph can be then generated and saved in a *.mac* file (Fig. 5.2).
2. Simulator: load the graph model and open both the 2D and 3D views (Fig. 5.3). Using the 2D view, we can save the response of any cell on the grid of any Cell layer. In addition, we can customise all the model parameters and fit them to match the profiles of specific RGCs.

3. Simulator: load different stimulus files in the form of videos and run simulations (Fig. 5.4). There is the possibility to act independently on cells, modify the CNO action and measure the resulting change in activity.

5.4 Simulation Results

Having described how to deploy our model in Macular, we now attempt to probe retinal function in CTL and CNO condition with various 2D stimuli. Using Macular, we attempt to follow the logic of an electrophysiological experiment with the difference that we can inspect and modify the state and properties of each neuron and each synaptic connection at any time during a simulation.

5.4.1 Physiological reproductions

As a first test, similar to Section 4.8.1, we reproduce the physiological difference between monophasic and biphasic cell types in CTL condition. This is to ensure that Macular is able to capture the basic response features of the data, before moving on to more complex stimuli. Figure 5.5 shows the simulated responses of the OPL, BC and AC (top panel) and the simulated response of the RGC vs the experimental temporal STAs (bottom panel), for an ON-monophasic cell (left) and an ON-biphasic cell (right). Keep in mind that here we are in 2D, in contrast to Section 4.8.1.

As we have noted earlier, the main difference between the two types can be potentially attributed to the different time scales of the responses of the presynaptic cells (especially the ACs) onto the RGCs.

Varying the CNO parameter Next, we perform simulations where we vary the CNO parameters in ACs and RGCs, modelled as a conductance, first separately and then simultaneously. In the first case, we expect that when ACs are excited we will observe a stronger inhibition on RGCs response, whereas the opposite effect is expected when RGCs are excited via CNO activation. However, when both cell types are excited by CNO, the final effect on RGC output will depend on the balance between inhibitory (ACs) and excitatory drives. Figure 5.6 illustrates these simulations on the monophasic (top) and biphasic (bottom) cells presented earlier. Each figure compares the response of the RGC when there is no CNO activation (ref - purple line), when CNO acts only at the RGC level (gcno - green dotted line), when CNO acts only at the AC level (acno - blue dotted line) and finally, when CNO acts at both levels (orange and yellow lines). Comparing the purple to the blue and green, we observe a clear effect of CNO on the RGCs response, in line with the anticipated mechanism of CNO activation. However, when CNO acts on both types, we observe diverse response patterns. The RGCs response may increase (orange line) or decrease (yellow line) or even remain the same (response not shown in this figure). This agrees with the 1D simulations shown in Section 4.8.3.

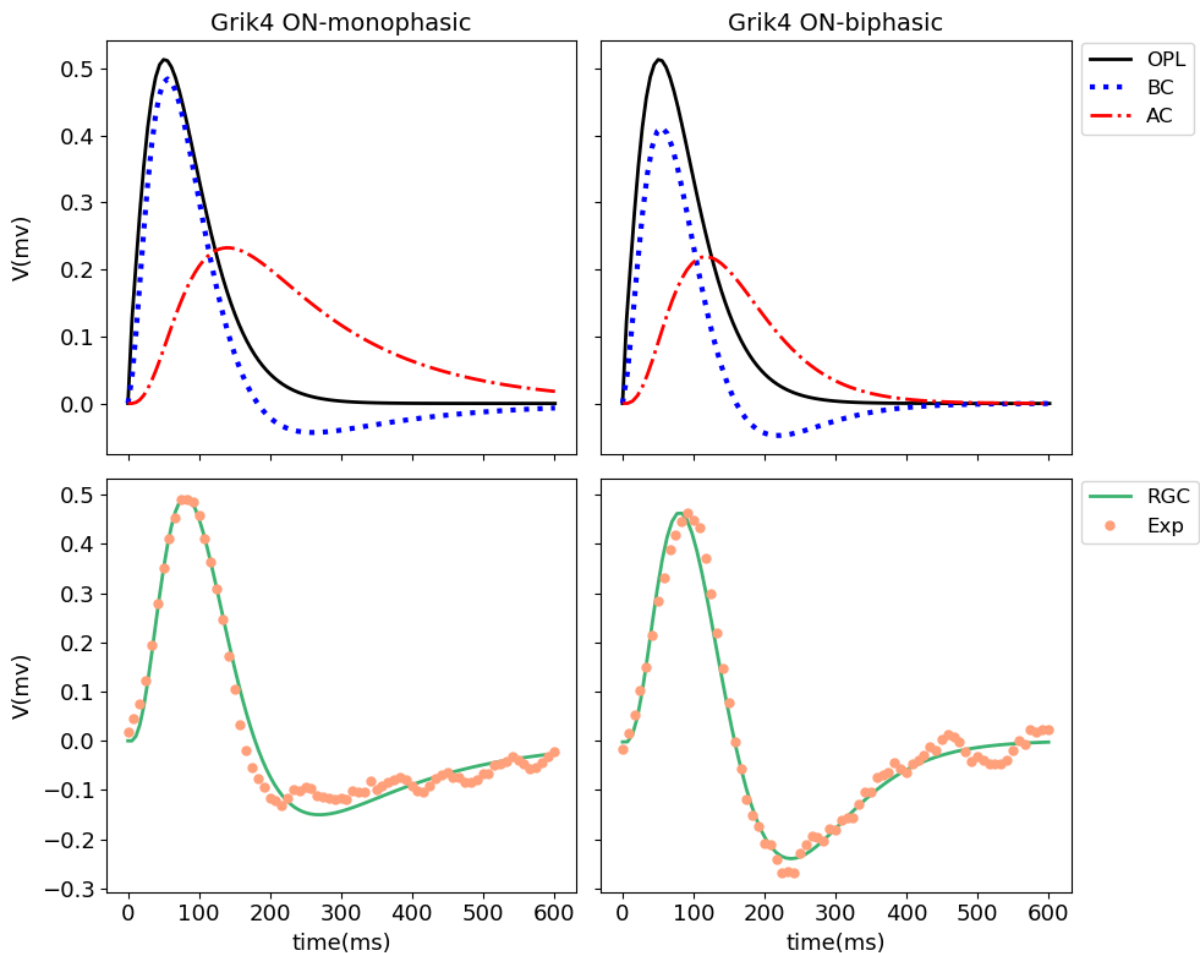


Figure 5.5. Physiological reproductions with Macular. *Top*. Simulated response of the OPL, BC and AC. *Bottom*. Simulated RGC response (green) and experimental temporal STA (orange dotted) for an ON-monophasic cell (*left*) and an ON-biphasic cell (*right*).

Chirp stimulus To further evaluate Macular’s performance in reproducing experimental responses, we simulated the responses to the chirp stimulus for the monophasic and biphasic cells. In addition, we also fit the data with the LN model presented in Chapter 3, in order to provide a baseline for comparison with our model’s performance. We remind that the LN model is built with a training set (responses to SWN) and the response to a test set (response to the chirp stimulus) is predicted. Then, to assess the performance of both models, we compare the predicted response to the real one. This is given by the peristimulus time histogram (PSTH), defined as the spike count per time bin averaged over the available trials (here 5 trials) and divided by the bin length (a measure of the mean firing rate of the neuron). The models performance is then quantified by computing the correlation coefficient (PCC) and the mean squared error (MSE) between the predicted and measured firing rate response.

Figures 5.7 and 5.8 show the results of the simulations for the monophasic and biphasic cell respectively. Each figure compares from top to bottom the LN model to Macular, the LN model to data and finally, Macular to data. In each case, the computed MSE and PCC are displayed on

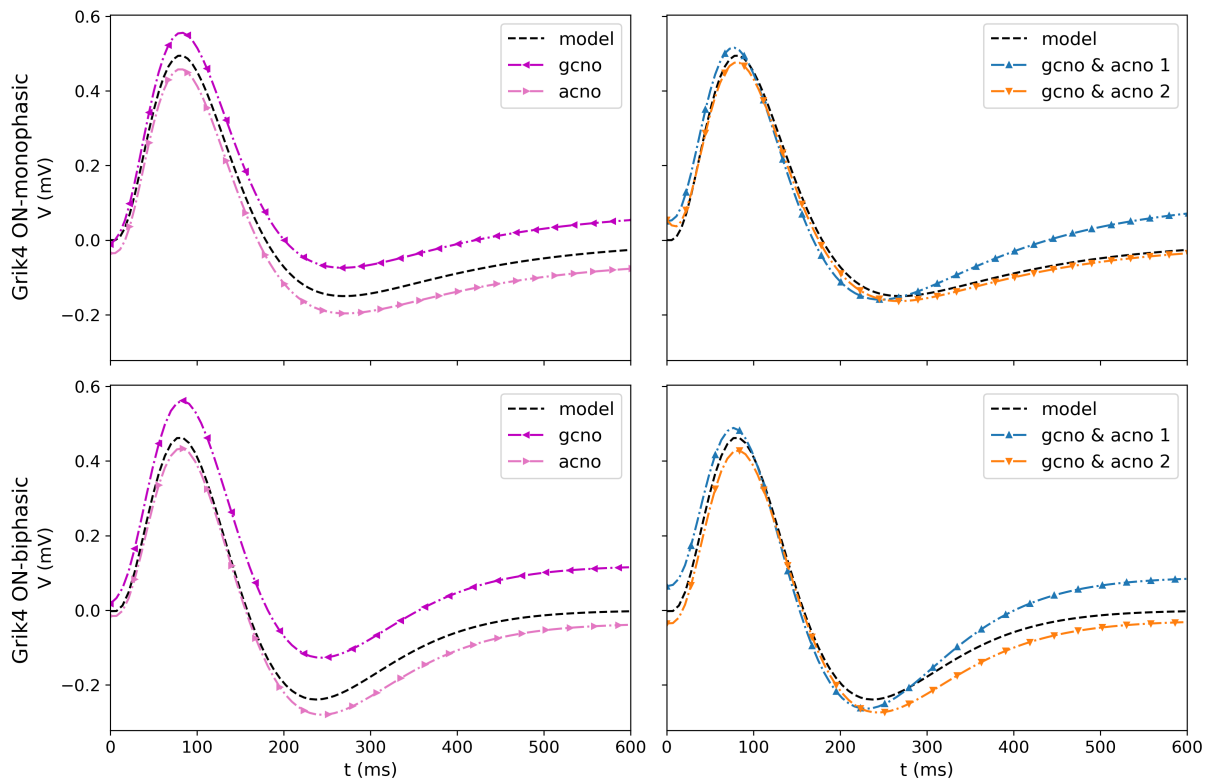


Figure 5.6. CNO effect at the individual cell level. Simulated responses of an ON-monophasic (*top*) and an ON-biphasic (*bottom*) cell in the following cases : when there is no CNO activation (model - black dashed line), when CNO acts only at the RGC level (gcno - purple line), when CNO acts only at the AC level (acno - pink line) and finally, when CNO acts at both levels (blue and orange lines).

top of each panel.

For the monophasic cell (Fig. 5.7), both the LN model and Macular seem to perform in a similar way, with the latter performing slightly better. When compared against each other, there is almost an 80% of match (PCC) and a very low MSE. However, in comparison with the data, Macular has 57% of fit (PCC) and the LN model has slightly lower (53%). For the biphasic cell (Fig. 5.8), there exists a significant and positive relationship between Macular and the LN model (90% PCC and 0.01 MSE). However, when compared to the data, the LN model seems to outperform Macular, despite the low performance of both (28% and 19% PCC correspondingly).

In both cases, it is not compelling to what extent Macular and the LN model are able to predict the RGCs responses and this can be justified. On one hand, the LN model is quite simple and condenses all the complex retinal processing in a linear function followed by a nonlinearity. Our model builds upon that and encapsulates cell dynamics per layer and synaptic connectivity. This can be reflected on its potential to capture response features that the LN model cannot, e.g at the part of the chirp stimulus where the frequency increases very fast (25-35s). The LN model responds almost uniformly, whereas the Macular model appears to adapt. Nevertheless, as the connectivity patterns considered here are quite simple, it is still not able to fully capture the

experimental responses. On the other hand, the existence of noise in the available data might be contributing to the inadequate model performance. Possible solutions would be to have more repetitions (here we had only 5 trials), or to do experiments with other stimuli that would serve as the training dataset of the model. For example, some studies claim that fitting the LN model with full-field white noise yields better prediction results.

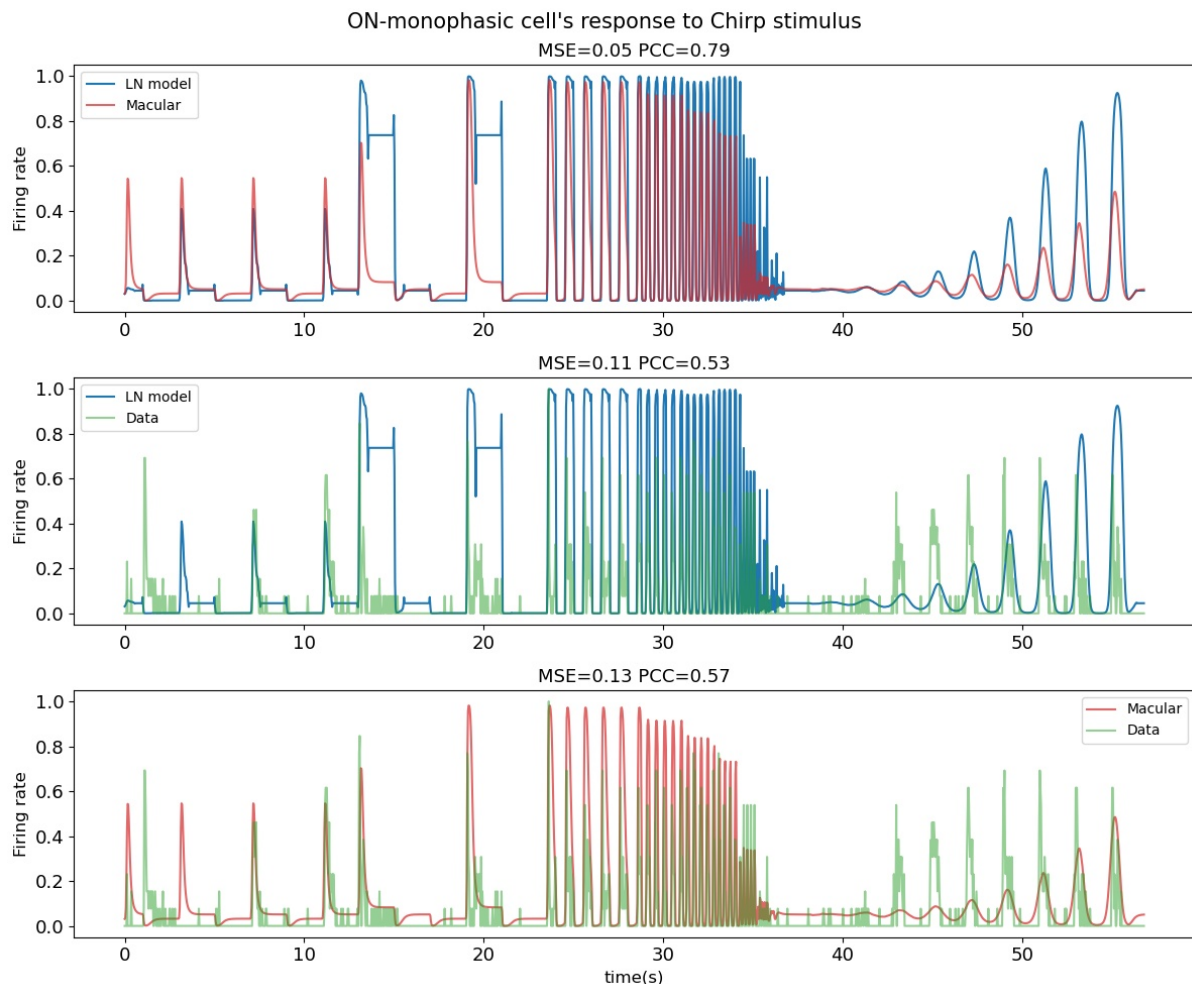


Figure 5.7. ON monophasic cell's response to Chirp stimulus. Each panel compares from top to bottom the LN model to Macular, the LN model to data and finally, Macular to data. In addition, the mean squared error (MSE) and the Pearson correlation coefficient (PCC) are computed in each case.

5.4.2 Complex stimuli

Finally, we tested Macular with stimuli with a spatio-temporal structure, such as a moving bar, in CTL and CNO conditions. We expect that under CNO influence, the cascading effect induced by lateral connectivity will trigger a wave of activity at the RGCs level, which propagates ahead of the stimulus (Souihel et al., 2021).

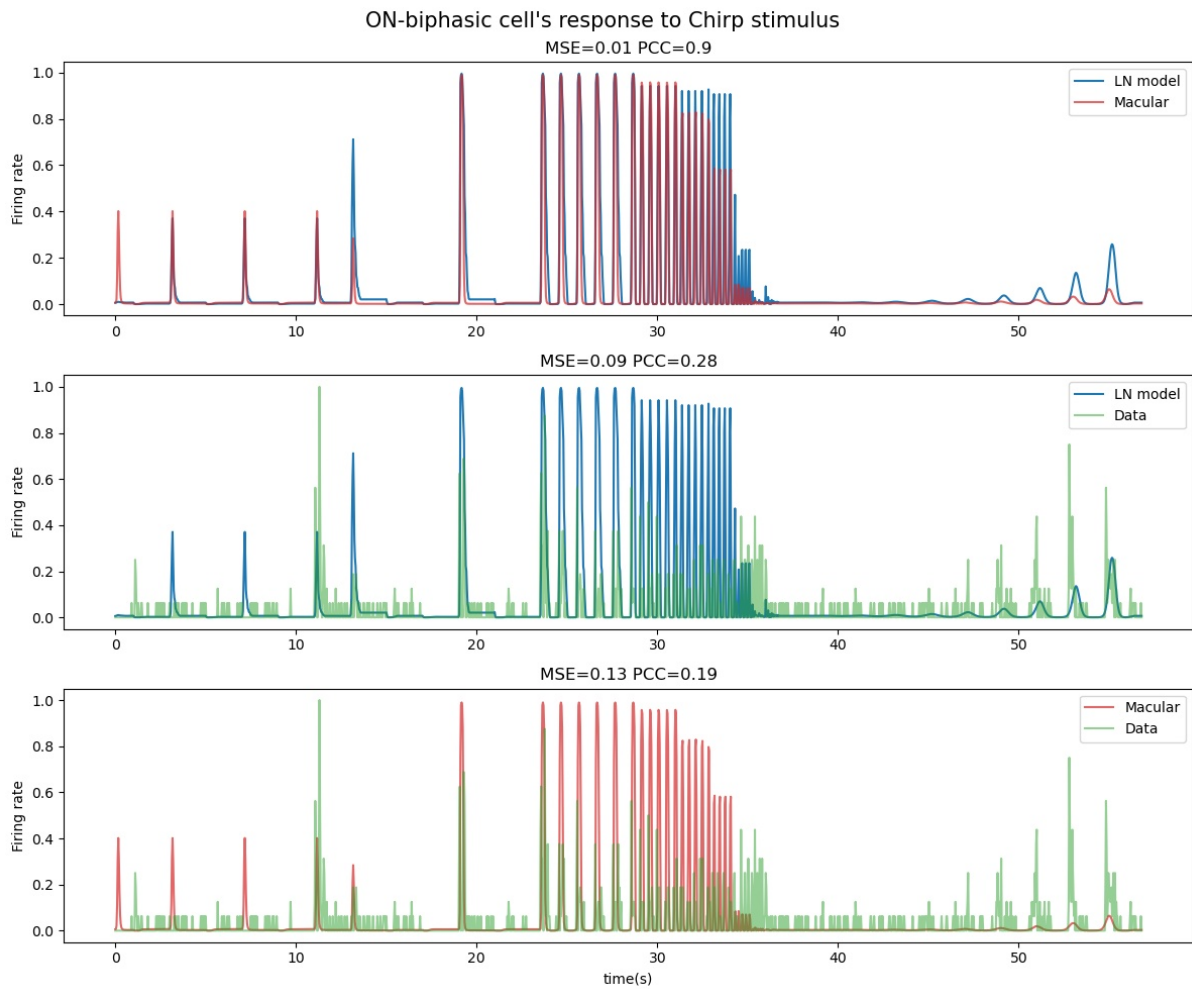


Figure 5.8. ON biphasic cell's response to Chirp stimulus. Same as Fig. 5.7

We ran simulations of our model, and we recorded the response of 10 cells located next to each other horizontally. We examined the following cases: (1) Full connectivity model; (2) Remove the connectivity from ACs to BCs ($w_{AB}=0$); (3) Remove the connectivity from ACs to RGCs ($w_{AG}=0$); (4) Remove the ACs connectivity completely (w_{AB} and $w_{AG} = 0$); (5) Increase the CNO conductance on RGCs (g_{CNO}); (6) Increase the CNO conductance on ACs (a_{CNO}); (7) & (8) Increase both conductances simultaneously (different values). We then compared four response characteristics; namely, the peak time (Fig. 5.9), the trough time (Fig. 5.11), the peak amplitude (Fig. 5.12) and the trough amplitude (Fig. 5.13), in all of these cases.

Figure 5.9 illustrates the response trajectory in each case and compares it with the expected trajectory of the moving bar. The response trajectory is computed as the time that each cell actually responded to the moving bar, while the expected trajectory is computed based on the moving bar's speed and the cell spacing (a straight line whose slope is the bar's speed). In this figure, we compare the trajectories in terms of the boundaries, the cells that by convention, do not receive the same input as the cells in the middle, the acceleration of the trajectories, on the

basis of the curvature, and the shift in time, that is the divergence from the expected trajectory.

First, we investigate the top four subplots that illustrate the network role on the RGCs peak response time. When the moving bar arrives at the first cell (left boundary), we observe that in the first four cases there is a delay of response that can be justified by the fact that the cell does not connect with the same number of presynaptic neurons. In particular, we notice that when there are no ACs (cyan) its response is even more delayed. Then, as the moving bar propagates, cells belonging to the lateral network become recruited, resulting in the network effect that leads to temporal changes in the response. In the full model (blue), the response trajectory already coincides with the predicted at the level of the second cell, and it even accelerates, with the last two cells responding earlier. However, this is not the case when we remove elements of the lateral network. When there are no ACs (cyan), the RGCs response is only driven by BCs (pooling) and thus, the trajectory slows down significantly and it takes longer before reaching the actual speed of the bar (towards the few last cells). Connecting ACs to BCs (red) slightly ameliorates the response trajectory, in contrast to when we re-enable the connectivity from ACs to RGCs (green), when the response trajectory considerably approaches the expected one. These two cases point out the ability of RGCs to respond faster and sooner to a moving stimulus due to lateral connectivity via ACs. Notably, the effect is enhanced when ACs interact directly with RGCs, compared to the indirect case via BCs.

Next, we explored what happens in the last four cases (bottom four subplots); namely, when we increase the CNO conductance in ACs and/or RGCs. When we increase the CNO conductance only at the level of RGCs (purple), we expect to have an effect both on their response time (decreasing) and peak amplitude (increasing). Yet, here we do not notice any major change on their response time, as the response trajectory is following the predicted one. On the other hand, increasing the CNO conductance only at the level of ACs (pink) should slow down the RGCs substantially. However, here as well, we do not observe any significant effect. Further simulations with a wider range of the CNO conductance are needed to reach firmer conclusions. Lastly, when we increase the CNO conductance at both levels (blue and orange - different values), we notice diverse effects. In the left panel, the excitatory effect of CNO at the level of RGCs seems to cancel out with the enhanced inhibitory effect of ACs and consequently, the net effect is negligible. However, the right panel clearly demonstrates that CNO activation might induce an anticipatory effect, where cells respond even before the bar arrives at their RF.

To further quantify the network role and CNO effect on the response time, we computed the shift in time (ms), that is the divergence of the predicted from the expected trajectory. Figure 5.10 presents the time shift in each case and for each cell. Each grey line represents a specific cell and shows how the shift evolves across the different cases, while the blue line presents the average time shift for all cells. A positive shift indicates a delayed response, whereas a negative shift is a sign of anticipation. This figure clearly points out that removing elements of the lateral network leads to a delayed response (around 50ms), while increasing CNO conductance in ACs and/or RGCs can make cells respond ahead of time (around 50ms). Moreover, in cases 5, 6 and

7, there is a subtle incline towards the right, not clearly shown here. This further highlights how DREADD activation on ACs can potentially enhance the anticipatory mechanisms provided by lateral connectivity.

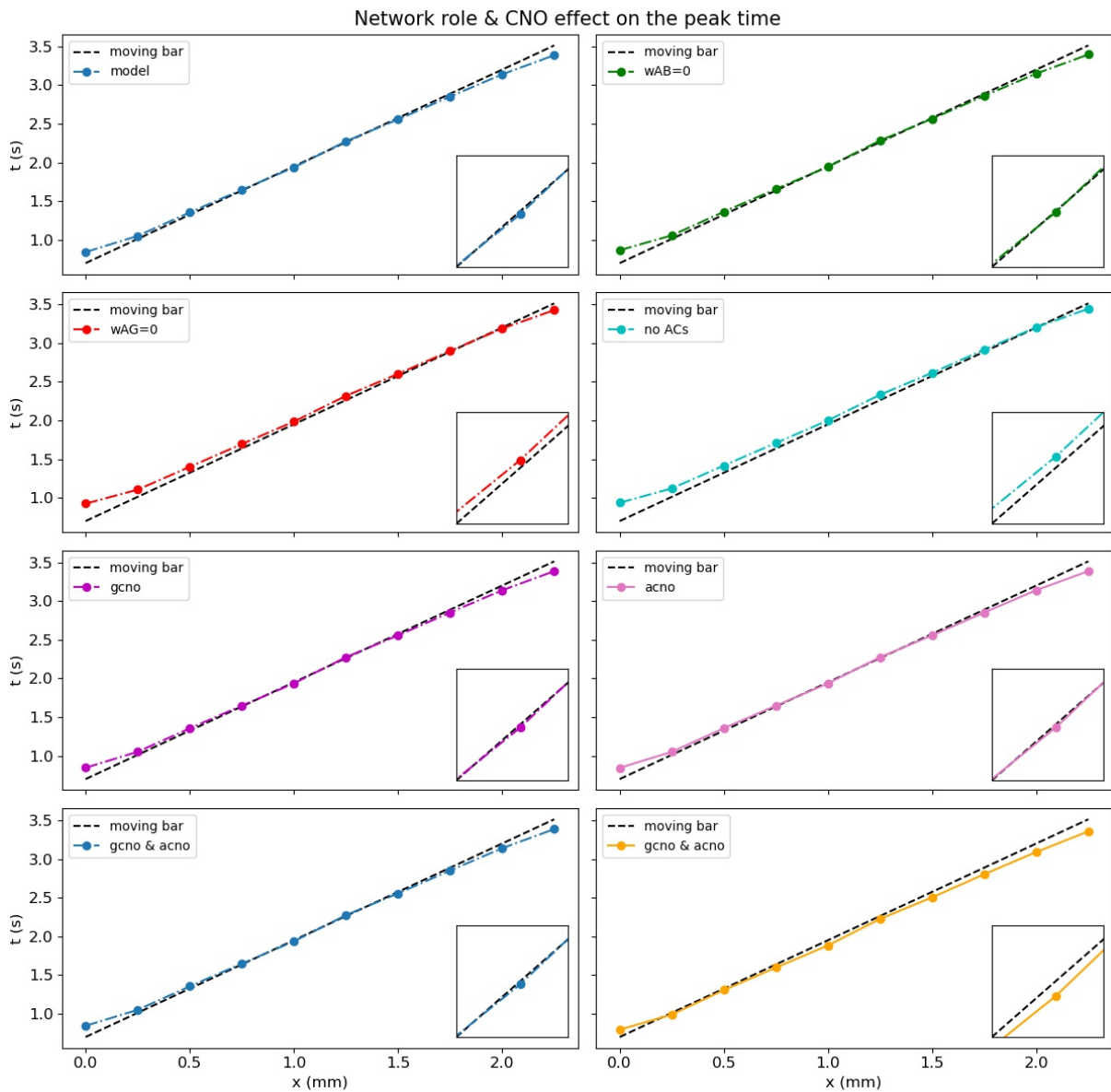


Figure 5.9. Network role and CNO effect on the response peak time. Each figure compares the response trajectory (line in colour), computed as the time that each cell actually responded to the moving bar, with the expected trajectory (black dashed line), computed based on the moving bar’s speed and the cell spacing, in each of the following cases: (1) Full connectivity model (model); (2) Remove the connectivity from ACs to BCs ($w_{AB}=0$); (3) Remove the connectivity from ACs to RGCs ($w_{AG}=0$); (4) Remove the ACs connectivity completely (w_{AB} and $w_{AG} = 0$); (5) Increase the CNO conductance on RGCs (gCNO); (6) Increase the CNO conductance on ACs (aCNO); (7) & (8) Increase both conductances simultaneously (gCNO & aCNO).

Figure 5.11 shows the network role and CNO effect on the trough time. Here, we take as a reference the full model (black dashed line). The top panel first compares how the trough time



Figure 5.10. Time shift. The divergence of the predicted from the expected trajectory in ms for each case of Fig. 5.9.

changes when we remove elements of the lateral network. Similarly to the peak time, uncoupling ACs and RGCs (red), slows down the response sufficiently. Moreover, disconnecting ACs from BCs (green), has a similar effect, though more subtle. Finally, when there are no ACs, the trough almost vanishes. This finding is in agreement with the results presented in Chapter 4, where we showed how the lateral connectivity can control the biphasic shape of RGCs. Next, we study the effect of increasing the CNO conductance only on RGCs (purple) or only on ACs (pink), on the trough time (middle panel). As in the peak time, we did not observe any significant effect, so further simulations are needed to draw a conclusion. Lastly, we explore how the trough time changes, when we increase the CNO conductance at ACs and RGCs simultaneously (bottom panel). Depending on the CNO conductance range of values, these two antagonistic effects might cancel each other out (blue) or induce an anticipatory effect (orange).

Figures 5.12 and 5.13 present the network role and CNO effect on the peak and trough amplitude correspondingly. Here, we first explore the network role (top panels), and then, we assess the effect of increasing the CNO conductance on RGCs or ACs (middle panels), and finally, on both levels (bottom panels). As before, we take as a reference the full model responses. For both response characteristics, removing elements of the lateral network, results in an increase of the RGCs activity. This is justified as ACs provide an inhibitory input to BCs and RGCs. It is also worth noting that uncoupling ACs and RGCs increases the RGCs response significantly more than uncoupling ACs to BCs.

Turning now to the impact of CNO on the response amplitude, we first remind the reader that

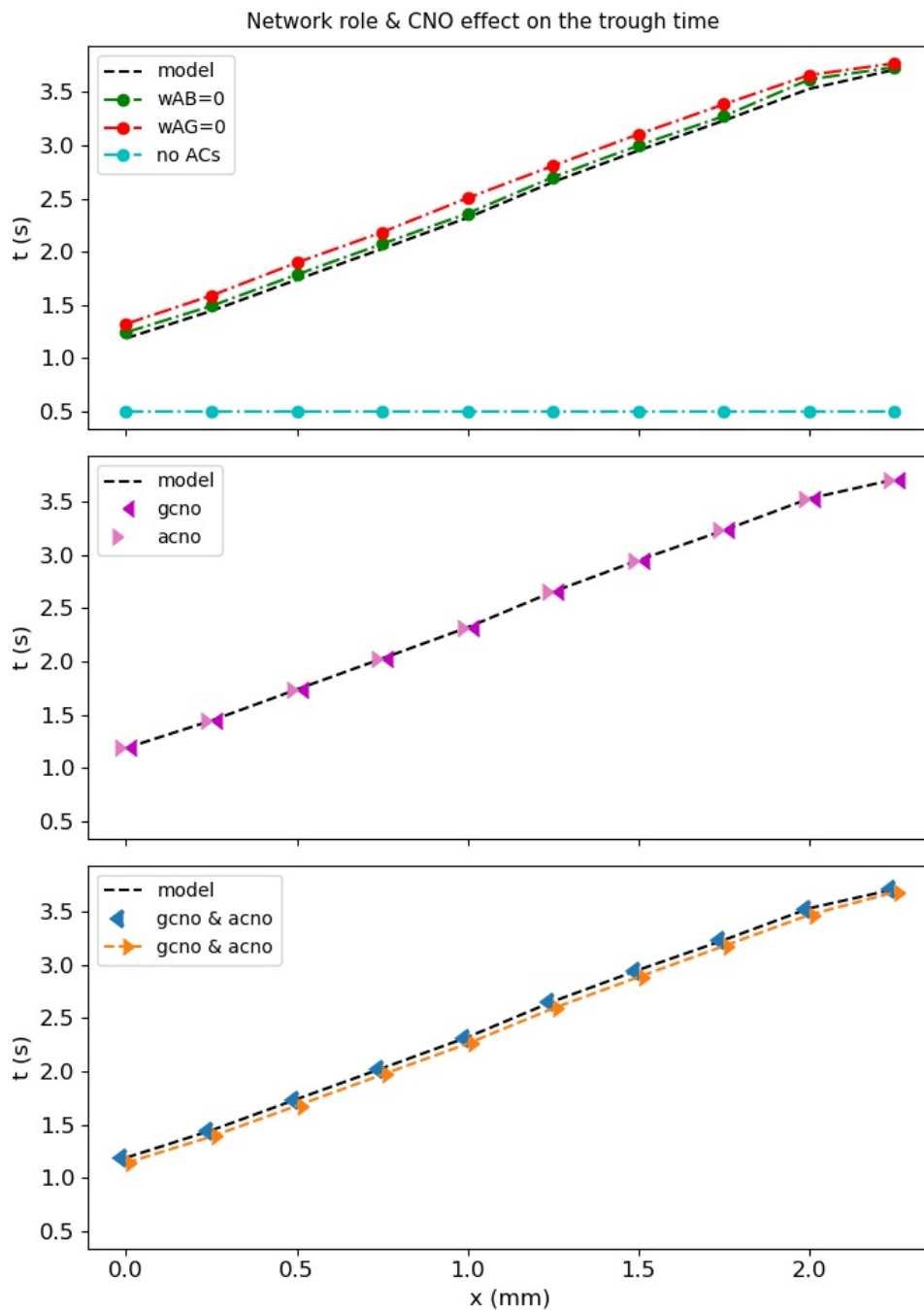


Figure 5.11. Network role and CNO effect on the response trough time. *Top*. Compares how the trough time changes when we remove elements of the lateral network. Model (black dashed line) corresponds to the fully connected model, wAB=0 (green line) corresponds to no connectivity from ACs to BCs, wAG=0 (red line) corresponds to no connectivity from ACs to RGCs, no ACs (cyan line) corresponds to no ACs in the model. *Middle & Bottom*. Compares how the trough time changes when we increase the CNO conductance on RGCs and/or ACs. gcno (purple arrows) corresponds to increasing the CNO conductance on RGCs, while acno (pink arrows) corresponds to increasing the CNO conductance on ACs. gcno & acno (blue and orange arrows - different values) corresponds to increasing the CNO conductance on RGCs and ACs simultaneously.

we expect a depolarisation of the RGC, when CNO acts only on RGCs, and a hyperpolarisation of the RGC, when CNO acts only on ACs, thereby reinforcing their inhibitory input. In the middle panels of figures 5.12 and 5.13, we observe exactly these effects. Note that cells on the boundaries differ from the other cells, as they do not receive the same excitatory (BCs) and inhibitory (ACs) inputs as the cells in the middle. However, the simultaneous increase of CNO conductance does not yield straightforward effects. Depending on the CNO conductance values, we may observe a slight increase or decrease in the peak or trough amplitude.

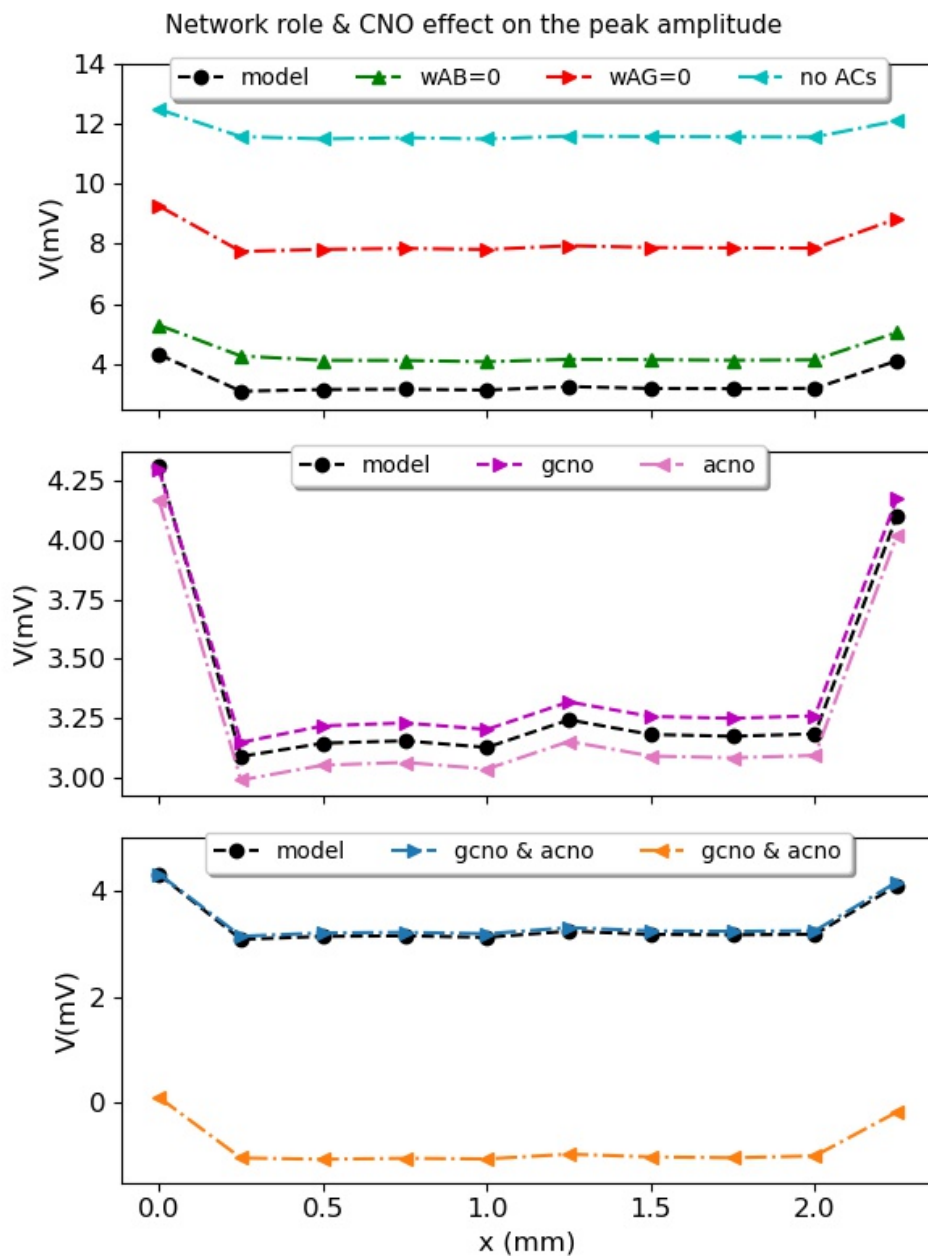


Figure 5.12. Network role and CNO effect on the response peak amplitude. Comparing how the peak amplitude changes in different cases, similarly to Fig. 5.11.

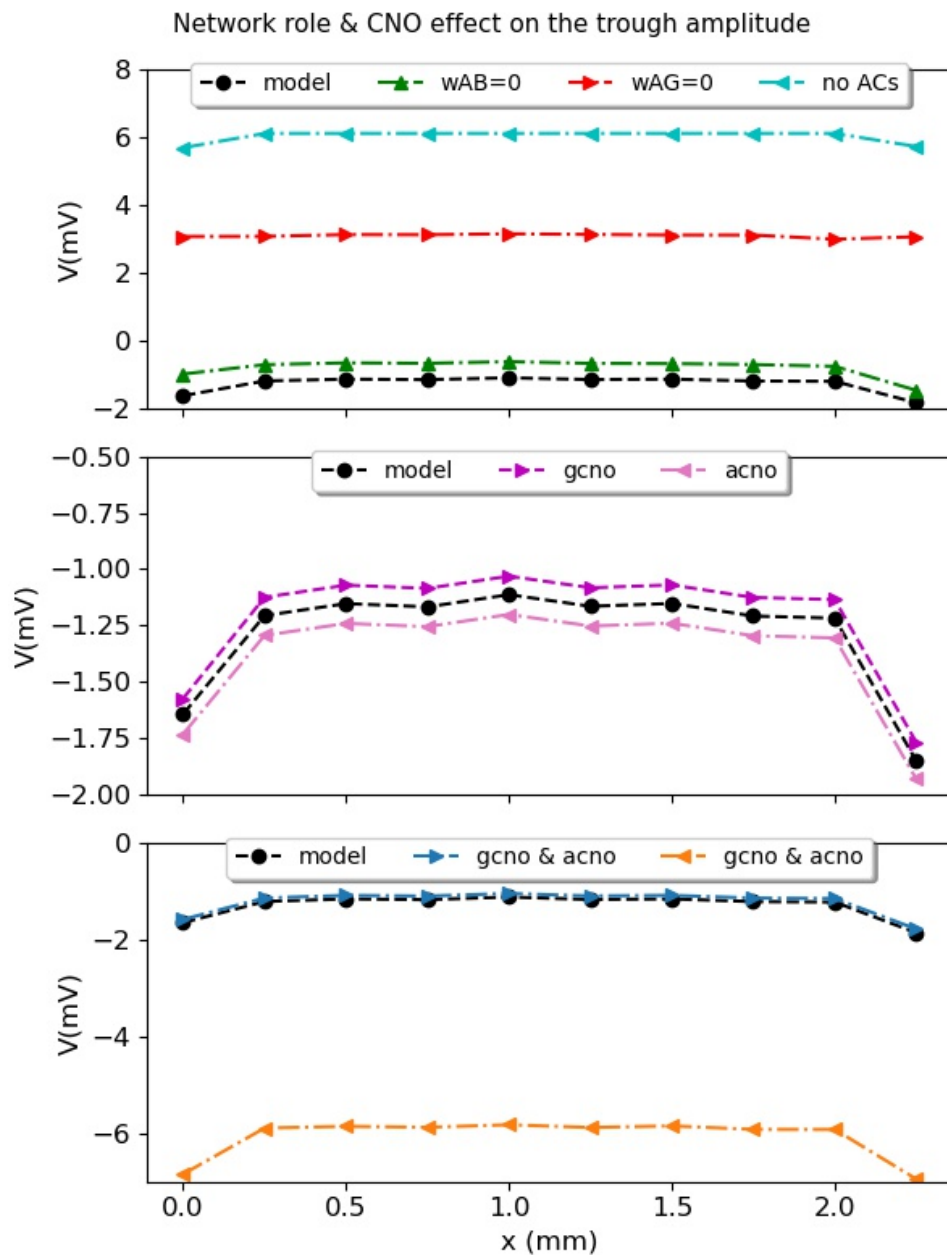


Figure 5.13. Network role and CNO effect on the response trough amplitude. Comparing how the trough amplitude changes in different cases, similarly to Fig. 5.11.

5.5 Summary and Discussion

This chapter described Macular, a flexible and extensible simulation platform for modelling and simulating the response of the early visual system. Macular has been essential for the work presented in this thesis, allowing us to implement the model presented in Chapter 4 and explore the impact of CNO on the retinal response to 2D stimuli. Numerical simulations emphasised the role of lateral connectivity in the retinal response and in particular, how it can induce anticipatory effects to moving stimuli. Based on this, CNO activation at the level of ACs and/or RGCs may

enhance or diminish the RGCs activity or even have no effect.

To further our research we are in the process of performing a quantitative analysis, based on the mathematical analysis of the model's dynamics, and propose a map of CNO induced scenarios in different situations, with a suitable space of relevant biophysical parameters.

Future work will explore a larger cell and stimuli space, in order to boost the biological plausibility of our simulations.

Chapter 6. Conclusion

This thesis set out to investigate the physiological properties of specific RGCs subgroups, sharing gene expression. Based on the ability to pharmacologically modify the level of their neural activity using pharmacogenetics, we aimed to unravel the circuit wiring underlying their functional diversity. The main idea that we sought to develop was the role of AC-mediated lateral connectivity in the single-cell and collective response of RGCs to visual stimuli. To do so, we conducted three separate, yet mutually reliant, studies on experimental, modelling, and computational grounds.

First, we analysed light responses recorded from mouse RGCs and investigated their response characteristics in control condition and when their spike firing frequency is increased using excitatory DREADDs. We observed that RGCs did not respond homogeneously to light stimuli, but showed a great diversity in their responses following DREADD activation with CNO. Surprisingly, this variability was observed not only across different RGC types, but also within the same RGC type. Thus, the results of this study suggest that there exist indirect effects competing with the direct excitatory effect, potentially originating from ACs, which are also affected by DREADD activation.

To clarify the situation, we built a model, grounded on biophysics, and studied the effects of increasing the activity of RGCs and/or ACs on the retinal output. Analytic and numerical results of this study reveal mechanisms, that explain the experimental observations and highlight the modulatory role of ACs in the functional diversity of RGCs. Therefore, by placing the problem in a modelling framework, we were able to establish a theoretical setting to explore aspects that cannot be easily achieved experimentally.

Finally, we performed *in silico* experiments using *Macular*, in diverse experimental conditions, and explored the effects of DREADD activation with CNO on the retina response to 2D stimuli. Numerical results suggest that the simultaneous excitation of RGCs and ACs (via DREADDs) can potentially enhance the anticipatory effect to moving stimuli, provided by ACs lateral connectivity.

This research supports the view that RGCs do not act independently conveying local spatio-temporal information, but they also encode visual information at a population level. We argue that this capability is due to the lateral inhibitory circuitry provided by the population of ACs, which creates a dense network connecting BCs, ACs and RGCs locally and globally. This has two implications for information processing in the retina. Firstly, RGCs diverse responses arise from a unique combination of network excitation and inhibition, which relies on the activities and interactions of upstream neurons feeding RGCs. Second, altering the activity in any one neuron might affect the activity of any other neuron belonging to this network. Consequently, disrupting the balance of excitatory and inhibitory inputs within a given circuit, using genetic-based tools,

allows to dismantle inner retinal circuits and understand how ACs shape retinal output. Our results are part of a rapidly growing body of literature, arguing that ACs hold a more universal role in retinal encoding, like parallel processing or motion anticipation (Asari et al., 2012; Franke et al., 2017a; Souihel et al., 2021; Cessac, 2021).

Our work could easily be used in future studies to explore the role of other RGCs subgroups or other retinal neurons and their interactions. In addition, it could be used to disassemble the components of other retinal circuits, by manipulating the activity of specific neurons. It could also potentially benefit research in other parts of the nervous system, as fundamental properties of the inner retina are shared with other parts of the brain.

To conclude this thesis, let us briefly discuss the perspectives of future work. Mainly, these perspectives are of three types, one for each study we conducted.

First, further data analysis could be done in order to investigate the functional properties of the specific RGC subgroups under diverse light stimuli. In addition, including RGCs that exhibited a change in their activity under DREADD activation, but did not express DREADDs, could further our understanding on the role of ACs. This could be also examined by studying the spike trains correlations in the different experimental conditions, potentially elucidating the role of network on the retinal response.

Second, the retina model could undergo few extensions towards other neural pathways or connectivity schemes. It would be also interesting to connect the RGC subtypes between them and study the impact of exciting one population on the other. For our numerical simulations, we have used cells that respond to light increments (ON cells), therefore a potential extension could be to model OFF cells.

Finally, increasing the number of simulated cells or simulating the retinal response to natural visual scenes, could be interesting extensions for our simulation platform, Macular.

Taken together, this thesis provides a framework, based on modelling and numerical simulations, to understand how specific RGCs subgroups, sharing gene expression, contribute to the encoding of visual scenes, with an emphasis on the role of lateral connectivity provided by ACs. We hope that this work will (1) contribute new knowledge on the role these RGCs subgroups play in conveying meaningful signals to the brain, leading to visual perception, and (2) propose new experimental paradigms to understand how the activation of ensembles of neurons in the retina can encode visual information.

Bibliography

- Ahn, Jungryul et al. (2020). 'New features of receptive fields in mouse retina through spike-triggered covariance'. In: *Experimental Neurobiology*. DOI: 10.5607/en.2020.29.1.38.
- Altimus, Cara M. et al. (2020). *The next 50 years of neuroscience*. DOI: 10.1523/JNEUROSCI.0744-19.2019.
- Asari, Hiroki and Markus Meister (2012). 'Divergence of visual channels in the inner retina'. In: *Nature Neuroscience*. DOI: 10.1038/nn.3241.
- Azeredo da Silveira, Rava and Botond Roska (2011). 'Cell Types, Circuits, Computation'. In: *Current Opinion in Neurobiology* 21.5, pp. 664–671. DOI: 10.1016/j.conb.2011.05.007.
- Baccus, Stephen A. (2007). 'Timing and computation in inner retinal circuitry'. In: *Annual Review of Physiology* 69, pp. 271–290. DOI: 10.1146/annurev.physiol.69.120205.124451.
- Baden, Tom (2020). 'Vertebrate vision: Lessons from non-model species'. In: *Seminars in Cell and Developmental Biology* 106.June, pp. 1–4. DOI: 10.1016/j.semcd.2020.05.028.
- Baden, Tom et al. (2016). 'The functional diversity of retinal ganglion cells in the mouse'. In: *Nature* 529.7586, pp. 345–350. DOI: 10.1038/nature16468. arXiv: 15334406.
- Baden, Tom et al. (2018). 'The Functional Organization of Vertebrate Retinal Circuits for Vision'. In: DOI: 10.1093/acrefore/9780190264086.013.68.
- Bae, J Alexander et al. (2017). *Digital museum of retinal ganglion cells with dense anatomy and physiology*. DOI: 10.1101/182758.
- Barlow, H. B. (1953). 'Summation and inhibition in the frog's retina'. In: *The Journal of Physiology*. DOI: 10.1113/jphysiol.1953.sp004829.
- Berry, Michael J. et al. (1999). 'Anticipation of moving stimuli by the retina'. In: *Nature*. DOI: 10.1038/18678.
- Bleckert, Adam et al. (2014). 'Visual space is represented by nonmatching topographies of distinct mouse retinal ganglion cell types'. In: *Current Biology*. DOI: 10.1016/j.cub.2013.12.020.
- Blundell, Inga et al. (2018). 'Code Generation in Computational Neuroscience: A Review of Tools and Techniques'. In: *Frontiers in Neuroinformatics*. DOI: 10.3389/fninf.2018.00068.
- Bower, James M and David Beeman (2003). 'The Book of Genesis - Exploring Realistic Neural Models with the GEneral NEural SIMulation System'. In: *Genesis*.
- Brette, Romain et al. (2007). *Simulation of networks of spiking neurons: A review of tools and strategies*. DOI: 10.1007/s10827-007-0038-6. arXiv: 0611089 [q-bio].
- Cajal, S.R. (1893). 'La retine des vertebres'. In: *The vertebrate retina*.

- Cessac, Bruno (2021). ‘Retinal processing: some mathematical insights’. In: URL: <https://hal.inria.fr/hal-03454859>.
- Cessac, Bruno et al. (2016). ‘ENAS : A new software for spike train analysis and simulation’. In: URL: <https://hal.inria.fr/hal-01377307>.
- Cessac, Bruno et al. (2017). ‘PRANAS: A New Platform for Retinal Analysis and Simulation’. In: *Frontiers in Neuroinformatics* 11, p. 49. DOI: 10.3389/fninf.2017.00049.
- Chen, Eric Y. et al. (2013). ‘Alert response to motion onset in the retina’. In: *Journal of Neuroscience* 33.1, pp. 120–132. DOI: 10.1523/JNEUROSCI.3749-12.2013.
- Chichilnisky, E J (2001). ‘A simple white noise analysis of neuronal light responses.’ In: *Network (Bristol, England)* 12.2, pp. 199–213. URL: <http://www.ncbi.nlm.nih.gov/pubmed/11405422>.
- Chichilnisky, E. J. and Rachel S. Kalmar (2002). ‘Functional Asymmetries in ON and OFF Ganglion Cells of Primate Retina’. In: *Journal of Neuroscience* 22.7, pp. 2737–2747. DOI: 10.1523/jneurosci.22-07-02737.2002.
- Cleland, B. G., M. W. Dubin and W. R. Levick (1971). ‘Sustained and transient neurones in the cat’s retina and lateral geniculate nucleus’. In: *The Journal of Physiology*. DOI: 10.1113/jphysiol.1971.sp009581.
- Coombs, J. et al. (2006). ‘Morphological properties of mouse retinal ganglion cells’. In: *Neuroscience*. DOI: 10.1016/j.neuroscience.2006.02.079.
- Curcio, Christine A. and Kimberly A. Allen (1990). ‘Topography of ganglion cells in human retina’. In: *Journal of Comparative Neurology*. DOI: 10.1002/cne.903000103.
- Das, Gautham P. et al. (2019). ‘Computational modelling of salamander retinal ganglion cells using machine learning approaches’. In: *Neurocomputing*. DOI: 10.1016/j.neucom.2018.10.004.
- Dayan, Peter and L F Abbott (2001). *Theoretical Neuroscience: Computational and Mathematical Modeling of Neural Systems*.
- Demb, Jonathan B. and Joshua H. Singer (2012). *Intrinsic properties and functional circuitry of the AII amacrine cell*. DOI: 10.1017/S0952523811000368.
- (2015). *Functional Circuitry of the Retina*. Vol. 1, pp. 263–289. DOI: 10.1146/annurev-vision-082114-035334.
- Demb, Jonathan B. et al. (1999). ‘Functional circuitry of the retinal ganglion cell’s nonlinear receptive field’. In: *Journal of Neuroscience*. DOI: 10.1523/jneurosci.19-22-09756.1999.
- Deriche, Rachid (1987). ‘Using Canny’s criteria to derive a recursively implemented optimal edge detector’. In: *International Journal of Computer Vision*. DOI: 10.1007/BF00123164.
- Destexhe, Alain, Zachary F. Mainen and Terrence J. Sejnowski (1994). ‘Synthesis of models for excitable membranes, synaptic transmission and neuromodulation using a common kinetic formalism’. In: *Journal of Computational Neuroscience*. DOI: 10.1007/BF00961734.

- DeVries, Steven H. and Denis A. Baylor (1997). ‘Mosaic arrangement of ganglion cell receptive fields in rabbit retina’. In: *Journal of Neurophysiology*. DOI: 10.1152/jn.1997.78.4.2048.
- Diamond, Jeffrey S. (2017). ‘Inhibitory Interneurons in the Retina: Types, Circuitry, and Function’. In: *Annual Review of Vision Science* 3, pp. 1–24. DOI: 10.1146/annurev-vision-102016-061345.
- Enciso, Germán A. et al. (2010). ‘A model of direction selectivity in the starburst amacrine cell network’. In: *Journal of Computational Neuroscience*. DOI: 10.1007/s10827-010-0238-3.
- Enroth-Cugell, Christina and J. G. Robson (1966). ‘The contrast sensitivity of retinal ganglion cells of the cat’. In: *The Journal of Physiology*. DOI: 10.1113/jphysiol.1966.sp008107.
- Euler, Thomas, Peter B. Detwiler and Winfried Denk (2002). ‘Directionally selective calcium signals in dendrites of starburst amacrine cells’. In: *Nature*. DOI: 10.1038/nature00931.
- Euler, Thomas et al. (2014). *Retinal bipolar cells: Elementary building blocks of vision*. DOI: 10.1038/nrn3783.
- Famiglietti, E. V. and Helga Kolb (1976). ‘Structural basis for ON- and OFF-center responses in retinal ganglion cells’. In: *Science*. DOI: 10.1126/science.959847.
- Faugeras, Olivier, Jonathan Touboul and Bruno Cessac (2009). ‘A constructive mean-field analysis of multi-population neural networks with random synaptic weights and stochastic inputs’. In: *Frontiers in Computational Neuroscience*. DOI: 10.3389/neuro.10.001.2009. arXiv: 0808.1113.
- Franke, Katrin and Tom Baden (2017a). ‘General features of inhibition in the inner retina’. In: *Journal of Physiology* 595.16, pp. 5507–5515. DOI: 10.1113/JP273648.
- Franke, Katrin et al. (2017b). ‘Inhibition decorrelates visual feature representations in the inner retina’. In: *Nature* 542.7642, pp. 439–444. DOI: 10.1038/nature21394.
- Geffen, Maria Neimark, Saskia E.J. De Vries and Markus Meister (2007). ‘Retinal ganglion cells can rapidly change polarity from off to on’. In: *PLoS Biology*. DOI: 10.1371/journal.pbio.0050065.
- Gewaltig, Marc-Oliver and Markus Diesmann (2007). ‘NEST (NEural Simulation Tool)’. In: *Scholarpedia*. DOI: 10.4249/scholarpedia.1430.
- Gollisch, Tim (2013). ‘Features and functions of nonlinear spatial integration by retinal ganglion cells’. In: *Journal of Physiology Paris* 107.5, pp. 338–348. DOI: 10.1016/j.jphysparis.2012.12.001.
- Gollisch, Tim and Markus Meister (2008). ‘Modeling convergent ON and OFF pathways in the early visual system’. In: *Biological Cybernetics* 99.4-5, pp. 263–278.
- (2010). ‘Eye Smarter than Scientists Believed: Neural Computations in Circuits of the Retina’. In: *Neuron* 65.2, pp. 150–164. DOI: 10.1016/j.neuron.2009.12.009.
- Goodman, Dan F.M. and Romain Brette (2009). *The brian simulator*. DOI: 10.3389/neuro.01.026.2009.

- Graupner, Michael, Frido Eerler and Michael Meyer-Hermann (2005). 'A theory of plasma membrane calcium pump stimulation and activity'. In: *Journal of Biological Physics*. DOI: 10.1007/s10867-005-4472-2.
- Guo, Tianruo et al. (2014). 'Understanding the retina: A review of computational models of the retina from the single cell to the network level'. In: *Critical Reviews in Biomedical Engineering* 42.5, pp. 419–436. DOI: 10.1615/CritRevBiomedEng.2014011732.
- Hartline, H. K. (1938). 'The response of single optic nerve fibers of the vertebrate eye to illumination of the retina'. In: *American Journal of Physiology-Legacy Content*. DOI: 10.1152/ajplegacy.1938.121.2.400.
- Herz, Andreas V.M. et al. (2006). 'Modeling single-neuron dynamics and computations: A balance of detail and abstraction'. In: *Science* 314.5796, pp. 80–85. DOI: 10.1126/science.1127240.
- Hilgen, Gerrit et al. (2017a). 'Pan-retinal characterisation of Light Responses from Ganglion Cells in the Developing Mouse Retina'. In: *Scientific Reports* 7. DOI: 10.1038/srep42330.
- Hilgen, Gerrit et al. (2017b). 'Unsupervised Spike Sorting for Large-Scale, High-Density Multielectrode Arrays'. In: *Cell Reports* 18.10, pp. 2521–2532. DOI: 10.1016/j.celrep.2017.02.038.
- Hilgen, Gerrit et al. (2019). 'A novel approach to the functional classification of retinal ganglion cells'. In: *F1000Research* 2019, 8:1608 (poster). DOI: <https://doi.org/10.7490/f1000research.1117478.1>.
- Hilgen, Gerrit et al. (2021). 'A novel approach to the functional classification of retinal ganglion cells'. In: *bioRxiv*. DOI: <https://doi.org/10.1101/2021.05.09.443323>.
- Hines, M. L. and N. T. Carnevale (1997). *The NEURON Simulation Environment*. DOI: 10.1162/neco.1997.9.6.1179.
- Jeon, Chang Jin, Enrica Strettoi and Richard H. Masland (1998). 'The major cell populations of the mouse retina'. In: *Journal of Neuroscience*. DOI: 10.1523/jneurosci.18-21-08936.1998.
- Johnston, Jamie and Leon Lagnado (2015). 'General features of the retinal connectome determine the computation of motion anticipation'. In: *eLife*. DOI: 10.7554/eLife.06250.
- Jouty, Jonathan et al. (2018). 'Non-parametric physiological classification of retinal ganglion cells in the mouse retina'. In: *bioRxiv* 14. DOI: 10.1101/407635.
- Karamanlis, Dimokratis and Tim Gollisch (2021). 'Nonlinear spatial integration underlies the diversity of retinal ganglion cell responses to natural images'. In: *Journal of Neuroscience*. DOI: 10.1523/JNEUROSCI.3075-20.2021.
- Kong, Jee-Hyun et al. (2005). 'Diversity of ganglion cells in the mouse retina: Unsupervised morphological classification and its limits'. In: *The Journal of Comparative Neurology* 489.3, pp. 293–310. DOI: 10.1002/cne.20631.

- Kreuz, Thomas et al. (2011). 'Time-resolved and time-scale adaptive measures of spike train synchrony'. In: *Journal of Neuroscience Methods*. DOI: 10.1016/j.jneumeth.2010.11.020.
- Kreuz, Thomas et al. (2013). 'Monitoring spike train synchrony'. In: *Journal of Neurophysiology*. DOI: 10.1152/jn.00873.2012. arXiv: 1209.6604.
- Kuffler, S. W. (1953). 'Discharge patterns and functional organization of mammalian retina'. In: *Journal of neurophysiology*. DOI: 10.1152/jn.1953.16.1.37.
- Laboissonniere, Lauren A. et al. (2019). 'Molecular signatures of retinal ganglion cells revealed through single cell profiling'. In: *Scientific Reports* 9.1, pp. 1–15. DOI: 10.1038/s41598-019-52215-4.
- Levenberg, Kenneth (1944). 'A method for the solution of certain non-linear problems in least squares'. In: *Quarterly of Applied Mathematics*. DOI: 10.1090/qam/10666.
- London, Anat, Inbal Benhar and Michal Schwartz (2013). *The retina as a window to the brain - From eye research to CNS disorders*. DOI: 10.1038/nrneuro1.2012.227.
- Maccione, Alessandro et al. (2014). 'Following the ontogeny of retinal waves: pan-retinal recordings of population dynamics in the neonatal mouse'. In: *The Journal of Physiology* 592.Pt 7, pp. 1545–1563. DOI: 10.1113/jphysiol.2013.262840. URL: <http://www.ncbi.nlm.nih.gov/pubmed/24366261>.
- Manvich, Daniel F. et al. (2018). 'The DREADD agonist clozapine N-oxide (CNO) is reverse-metabolized to clozapine and produces clozapine-like interoceptive stimulus effects in rats and mice'. In: *Scientific Reports*. DOI: 10.1038/s41598-018-22116-z.
- Markram, Henry (2013). 'Seven challenges for neuroscience'. In: *Functional Neurology*. DOI: 10.11138/FNeur/2013.28.3.145.
- Marquardt, Donald W. (1963). 'An Algorithm for Least-Squares Estimation of Nonlinear Parameters'. In: *Journal of the Society for Industrial and Applied Mathematics*. DOI: 10.1137/0111030.
- Martínez-Cañada, Pablo et al. (2016). 'A Computational Framework for Realistic Retina Modeling'. In: *International Journal of Neural Systems* 26.7. DOI: 10.1142/S0129065716500301.
- Masland, R. H. (2001). *The fundamental plan of the retina*. DOI: 10.1038/nm0901-877.
- Masland, Richard H. (2012a). *The Neuronal Organization of the Retina*. DOI: 10.1016/j.neuron.2012.10.002.
- Masland, Richard H (2012b). 'The tasks of amacrine cells.' In: *Visual neuroscience*.
- Meister, Markus and Toshihiko Hosoya (2001). 'Are retinal ganglion cells independent encoders'. In: *Nature*, pp. 0–2.
- Nirenberg, S. et al. (2001). 'Retinal ganglion cells act largely as independent encoders'. In: *Nature*. DOI: 10.1038/35079612.
- Ozawa, Hitoshi (2019). 'Principles and basics of immunohistochemistry'. In: *Folia Pharmacologica Japonica*. DOI: 10.1254/fpj.154.156.

- Pamplona, Daniela et al. (2021). ‘Large visual neuron assemblies receptive fields estimation using a super-resolution approach’. In:
- Paninski, Liam (2003). ‘Convergence properties of three spike-triggered analysis techniques’. In: *Network: Computation in Neural Systems* 14.3, pp. 437–464. DOI: 10.1088/0954-898X_14_3_304.
- Paninski, Liam, Jonathan W. Pillow and Eero P. Simoncelli (2004). ‘Maximum likelihood estimation of a stochastic integrate-and-fire neural encoding model.’ In: *Neural computation* 16.12, pp. 2533–61. DOI: 10.1162/0899766042321797.
- Pillow, Jonathan W. and Eero P. Simoncelli (2006). ‘Dimensionality reduction in neural models: An information-theoretic generalization of spike-triggered average and covariance analysis’. In: *Journal of Vision* 6.4, pp. 414–428. DOI: 10.1167/6.4.9.
- Pillow, Jonathan W. et al. (2008). ‘Spatio-temporal correlations and visual signalling in a complete neuronal population’. In: *Nature* 454.7207, pp. 995–999. DOI: 10.1038/nature07140.
- Pisano, Filippo et al. (2017). ‘Large scale matching of function to the genetic identity of retinal ganglion cells’. In: *Scientific Reports* 7.1, pp. 1–12. DOI: 10.1038/s41598-017-15741-7.
- Portelli, G. et al. (2016). ‘Rank Order Coding: a Retinal Information Decoding Strategy Revealed by Large-Scale Multielectrode Array Retinal Recordings’. In: *eNeuro* 3.3. DOI: 10.1523/ENEURO.0134-15.2016.
- Purves, Dale et al. (2001). ‘The Retina’. In: *Neuroscience. 2nd edition*. Sinauer Associates. URL: <https://www.ncbi.nlm.nih.gov/books/NBK10885/>.
- Remtulla, S. and P. E. Hallett (1985). ‘A schematic eye for the mouse, and comparisons with the rat’. In: *Vision Research*. DOI: 10.1016/0042-6989(85)90076-8.
- Rheume, Bruce A. et al. (2018). ‘Single cell transcriptome profiling of retinal ganglion cells identifies cellular subtypes’. In: *Nature Communications* 9.1. DOI: 10.1038/s41467-018-05134-3.
- Rieke, F. et al. (1997). *Spikes: Exploring the Neural Code*.
- Ringach, D and R Shapley (2004). ‘Reverse correlation in neurophysiology’. In: *Cognitive Science* 28.2, pp. 147–166. DOI: 10.1016/j.cogsci.2003.11.003.
- Roberts, Paul A. et al. (2016). ‘Mathematical and computational models of the retina in health, development and disease’. In: *Progress in Retinal and Eye Research* 53, pp. 48–69. DOI: 10.1016/j.preteyeres.2016.04.001.
- Rockhill, R. L., T. Euler and R. H. Masland (2000). ‘Spatial order within but not between types of retinal neurons’. In: *Proceedings of the National Academy of Sciences* 97.5, pp. 2303–2307. DOI: 10.1073/pnas.030413497.
- Rodieck, R. W. (1965). ‘Quantitative analysis of cat retinal ganglion cell response to visual stimuli’. In: *Vision Research*. DOI: 10.1016/0042-6989(65)90033-7.
- Rosa, Juliana M. et al. (2016). ‘Crossover Inhibition Generates Sustained Visual Responses in the Inner Retina’. In: *Neuron*. DOI: 10.1016/j.neuron.2016.03.015.

- Roth, Bryan L. (2016). 'DREADDs for Neuroscientists'. In: *Neuron* 89.4, pp. 683–694. DOI: 10.1016/j.neuron.2016.01.040. URL: <http://dx.doi.org/10.1016/j.neuron.2016.01.040>.
- Sanes, Joshua R. and Richard H. Masland (2015). 'The Types of Retinal Ganglion Cells: Current Status and Implications for Neuronal Classification'. In: *Annual Review of Neuroscience* 38.1, pp. 221–246. DOI: 10.1146/annurev-neuro-071714-034120.
- Sarrabezolles, Louise et al. (2017). 'Dual field combination for unmanned video surveillance'. In: *Real-Time Image and Video Processing 2017*. Ed. by Nasser Kehtarnavaz and Matthias F. Carlsohn, 102230A. ISBN: 9781510609471. DOI: 10.1117/12.2262696.
- Schreyer, Helene Marianne (2018). 'Nonlinearities in bipolar cells and their role for encoding visual signals'. In: *Doctoral thesis*.
- Schreyer, Helene Marianne and Tim Gollisch (2020). 'Nonlinearities in retinal bipolar cells shape the encoding of artificial and natural stimuli'. In: pp. 1–40. DOI: 10.1101/2020.06.10.144576.
- Schwartz, Gregory W. et al. (2012). 'The spatial structure of a nonlinear receptive field'. In: *Nature Neuroscience* 15.11, pp. 1572–1580. DOI: 10.1038/nn.3225.
- Schwartz, Odelia et al. (2006). 'Spike-triggered neural characterization'. In: *Journal of Vision* 6.4, pp. 484–507. DOI: 10.1167/6.4.13.
- Segev, Ronen, Jason Puchalla and Michael J. Berry (2006). 'Functional organization of ganglion cells in the salamander retina'. In: *Journal of Neurophysiology*. DOI: 10.1152/jn.00928.2005.
- Seung, H. Sebastian and Uygur Sümbül (2014). 'Neuronal Cell Types and Connectivity: Lessons from the Retina'. In: *Neuron* 83.6, pp. 1262–1272. DOI: 10.1016/j.neuron.2014.08.054.
- Shi, Qing et al. (2018). 'Functional characterization of retinal ganglion cells using tailored nonlinear modeling'. In: *bioRxiv*. DOI: 10.1101/421396.
- Simoncelli, Eero P et al. (2004). 'Characterization of Neural Responses with Stochastic Stimuli'. In: *The cognitive neurosciences*, p. 20.
- Souihel, Selma and Bruno Cessac (2021). 'On the potential role of lateral connectivity in retinal anticipation'. In: *Journal of Mathematical Neuroscience*. DOI: 10.1186/s13408-020-00101-z. arXiv: 2009.02081.
- Sterratt, David et al. (2011). *Principles of computational modelling in neuroscience*. ISBN: 9780511975899. DOI: 10.1017/CB09780511975899.
- Sümbül, Uygur et al. (2014). 'A genetic and computational approach to structurally classify neuronal types'. In: *Nature Communications* 5. DOI: 10.1038/ncomms4512. arXiv: NIHMS150003.
- Sun, Wenzhi, Ning Li and Shigang He (2002). 'Large-scale morphological survey of mouse retinal ganglion cells'. In: *Journal of Comparative Neurology* 451.2, pp. 115–126. DOI: 10.1002/cne.10323.

- Tchumatchenko, Tatjana et al. (2011). ‘Spike Correlations – What Can They Tell About Synchrony?’ In: *Frontiers in Neuroscience* 5. DOI: 10.3389/fnins.2011.00068.
- Tran, Nicholas M. et al. (2019). ‘Single-Cell Profiles of Retinal Ganglion Cells Differing in Resilience to Injury Reveal Neuroprotective Genes’. In: *Neuron* 104.6, 1039–1055.e12. DOI: 10.1016/j.neuron.2019.11.006.
- Tukker, John J., W. Rowland Taylor and Robert G. Smith (2004). ‘Direction selectivity in a model of the starburst amacrine cell’. In: *Visual Neuroscience*. DOI: 10.1017/S0952523804214109.
- Urban, Daniel J. and Bryan L. Roth (2015). ‘DREADDs (Designer Receptors Exclusively Activated by Designer Drugs): Chemogenetic Tools with Therapeutic Utility’. In: *Annual Review of Pharmacology and Toxicology* 55.1, pp. 399–417. DOI: 10.1146/annurev-pharmtox-010814-124803. eprint: NIHMS150003.
- Vaney, David I. and W. Rowland Taylor (2002). ‘Direction selectivity in the retina’. In: *Current Opinion in Neurobiology* 12.4, pp. 405–410. DOI: 10.1016/S0959-4388(02)00337-9.
- Völgyi, Béla, Samir Chheda and Stewart A. Bloomfield (2009). ‘Tracer coupling patterns of the ganglion cell subtypes in the mouse retina’. In: *Journal of Comparative Neurology*. DOI: 10.1002/cne.21912.
- Wang, Jing, Roy Jacoby and Samuel M. Wu (2016). ‘Physiological and morphological characterization of ganglion cells in the salamander retina’. In: *Vision Research* 119, pp. 60–72. DOI: 10.1016/j.visres.2015.12.007.
- Wässle, Heinz (2004). *Parallel processing in the mammalian retina*. DOI: 10.1038/nrn1497. arXiv: arXiv:1408.1149.
- Wässle, Heinz and H. J. Riemann (1978). ‘The mosaic of nerve cells in the mammalian retina’. In: *Proceedings of the Royal Society of London - Biological Sciences*. DOI: 10.1098/rspb.1978.0026.
- Werblin, F. S. and J. E. Dowling (1969). ‘Organization of the retina of the mudpuppy, *Necturus maculosus*. II. Intracellular recording.’ In: *Journal of neurophysiology*. DOI: 10.1152/jn.1969.32.3.339.
- Wohrer, Adrien and Pierre Kornprobst (2009). ‘Virtual Retina: A biological retina model and simulator, with contrast gain control’. In: *Journal of Computational Neuroscience* 26.2, pp. 219–249. DOI: 10.1007/s10827-008-0108-4.
- World Health Organization (2019). *World report on vision*. ISBN: 9789241516570.
- Yan, Wenjun et al. (2020). ‘Mouse Retinal Cell Atlas: Molecular Identification of over Sixty Amacrine Cell Types’. In: *Journal of Neuroscience* 40.27, pp. 5177–5195. DOI: 10.1523/JNEUROSCI.0471-20.2020.
- Zhang, Y. et al. (2012). ‘The most numerous ganglion cell type of the mouse retina is a selective feature detector’. In: *Proceedings of the National Academy of Sciences* 109.36, E2391–E2398. DOI: 10.1073/pnas.1211547109. arXiv: arXiv:1408.1149.

Zhao, Xiwu et al. (2017). 'Mechanisms creating transient and sustained photoresponses in mammalian retinal ganglion cells'. In: *The Journal of general physiology*. DOI: 10.1085/jgp.201611720.